ACCURATE FAULT LOCATION FOR POWER TRANSMISSION LINES

A thesis submitted to

CITY UNIVERSITY

for the Degree of

DOCTOR OF PHILOSOPHY

by

SADEGH JAMALI

Power Systems Protection Laboratory
Department of Electrical, Electronic
and Information Engineering

City University
Northampton Square
London ECIV OHB
U.K.

MAY 1990

In the name of Allah,

the Merciful, the Compassionate.

This thesis is dedicated to my parents.

ABSTRACT

This thesis describes a new accurate fault location technique for power transmission lines. The technique is based on a distributed parameter line model which inherently accounts for line conductor asymmetry and shunt capacitance. The accuracy of the new technique is not significantly affected by fault resistance, source network configuration or line length. Also, in most cases no fault type identification is required.

The new fault location technique uses the current and voltage phasors at power frequency measured at the line ends. These measurements are synchronised from a knowledge of the prefault phasor data.

For a single-phase network the basic idea is to equate two equations obtained for the fault point voltage; one from the sending end phasor data and the other from the receiving end phasor data. The resultant equation is solved for the distance to fault.

For multiphase systems the idea is generalised by using the theory of natural modes which involves the evaluation of eigenvalues and eigenvectors of the lines. In this way a multiphase system is decoupled into a number of single-phase modal circuits; each circuit can be solved for fault location. For perfectly transposed lines the eigenvalues can simply be evaluated from the sequence components and a real eigenvector matrix can be defined for all the lines. For untransposed lines the new algorithm maintains its high accuracy when assuming perfect transposition to simplify the evaluation of eigenvalues and eigenvectors. Also for double-circuit applications a circuit-by-circuit fault location, without any link between the two circuits, is possible.

The test results for different fault conditions presented in this thesis show the higher accuracy in fault location achieved by the new algorithm in comparison with the algorithms used in the best commercially available fault locators.

ACKNOWLEDGEMENTS

The author wishes to express his sincere gratitude to Professor A.T. Johns, DSc, PhD, BSc, CEng, FIEE, SMIEEE, FRSA, for his guidance, invaluable advice and encouragement throughout the course of study.

He is grateful to the Ministry of Culture and Higher Education of the Islamic Republic of Iran for the opportunity to pursue his higher education. Thanks are also due to City University, London, and GEC-Alsthom Measurements, Stafford, for funding the project.

He would like to thank everyone at the Power Systems Protection Research Laboratory for their support and friendship, especially Mr S.H. Lewis and Mr M. Gasparro for their extremely helpful contribution to the preparation of the thesis. He would also like to thank the engineers at GEC-Alsthom Measurements, especially Mr S.M. Haden for very useful technical discussions.

Finally, he wishes to thank the staff of the Department of Electrical, Electronic and information Engineering, City University, particularly Mrs L. Wilkins, Dr P.J. Moore and Mr E.C. Talboys who have been extremely helpful and encouraging during the course of study.

COPYRIGHT DECLARATION

I grant powers of discretion to the University Librarian to allow this thesis (ACCURATE FAULT LOCATION FOR POWER TRANSMISSION LINES) to be copied in whole or in part without further reference to me. This covers only single copies made for study purposes, subject to normal conditions of acknowledgement.

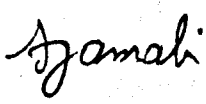

S. JAMALI

London, May 1990

LIST OF CONTENTS

LIST OF PRINCIPAL SYMBOLS

EHV	=Extra high voltage
exp	=Exponential
arg	=Argument
j	=$\sqrt{-1}$
V_S, I_S	=Sending end voltage and current
I_F	=Fault path current
Z_{SS}, Z_{SR}	=Sending and receiving end source impedances
Z_{S0}, Z_{SP}	=Zero and positive sequence source impedances
$[Z_{SS}], [Z_{SR}]$	=Sending and receiving end source impedance matrices
L	=Line length
x	=Distance to fault
p	=Distance to fault as a percentage of line length
R_f	=Fault resistance
$[R_f]$	=Fault resistance matrix
Z_L	=Line impedance
Z_{L0}, Z_{LP}	=Zero and positive sequence line impedances
Z_0, Z_P	=Zero and positive sequence line impedances per unit length
I_{Sf}	=Superimposed current at sending end
a,b,c	=Phase subscripts in single-circuit lines
a,b,c,A,B,C	=Phase subscripts in double-circuit lines
1,2,3,4,5,6	=Modal subscripts
$\overline{V}, \overline{I}$	=Vectors of phase voltages and currents
$\overline{V}_n, \overline{I}_n$	=Vectors of modal voltages and currents
[Z],[Y]	=Series impedance and shunt admittance

	matrices per unit length
$Z_{aa},\ldots,Z_{cc}$	=Elements of [Z]
$Y_{aa},\ldots,Y_{cc}$	=Elements of [Y]
A,B,C,D	=Two-port transfer matrices
[Q],[S]	=Voltage and current eigenvector matrices
$[Q_t],[S_t]$	=Transpose matrices of [Q] and [S]
Γ^2,Γ	=Eigenvalue and propagation constant
α,β	=Real and imaginary part of Γ
$[\Gamma^2],[\Gamma]$	=Diagonal matrices of Γ^2 and Γ
w	=Angular frequency
w_o	=Nominal system angular frequency
h(t)	=Unit step function
ϵ	=Permittivity
μ	=Permeability
X/R	=Reactance to resistance ratio
$[\Theta]$	$=[Q][\Gamma][Q]^{-1}$
$[\Theta_t]$	=Transpose matrix of $[\Theta]$
Z_0,Y_0	=Characteristic impedance and admittance
$[Z_0],[Y_0]$	=Characteristic impedance and admittance matrices
$[\,]^t$	=Matrix transpose
[U]	=Unit matrix
$\bar{V}_S,\bar{V}_R$	=Vectors of phase voltages at sending and receiving ends
$\bar{I}_S,\bar{I}_R$	=Vectors of phase currents at sending and receiving ends
$\bar{V}_{Sn},\bar{V}_{Rn}$	=Vectors of modal voltages at sending and receiving ends

$\bar{I}_{Sn}, \bar{I}_{Rn}$ =Vectors of modal currents at sending and receiving ends

$\bar{V}_F$ =Vector of phase voltages at fault point

$\bar{I}_F$ =Vector of fault path phase currents

$\bar{E}_{FS}, \bar{E}_{FR}$ =Vectors of phase voltages at fault point

$\bar{I}_{FS}, \bar{I}_{FR}$ =Vectors of phase currents at fault point

$\bar{I}_{FSs}, \bar{I}_{FRs}$ =Vectors of prefault phase currents at fault point

$\bar{I}_{FSf}, \bar{I}_{FRf}$ =Vectors of superimposed phase currents at fault point

$\bar{V}_{Fs}$ =Vector of prefault phase voltages at fault point

$\bar{V}_{Ff}, \bar{E}_{Ff}$ =Vectors of superimposed phase voltages at fault point

$\bar{V}_{Ss}, \bar{V}_{Rs}$ =Vectors of prefault phase voltages at sending and receiving ends

$\bar{I}_{Ss}, \bar{I}_{Rs}$ =Vectors of prefault phase currents at sending and receiving ends

$\bar{V}_{Sf}, \bar{V}_{Rf}$ =Vectors of superimposed phase voltages at sending and receiving ends

$\bar{I}_{Sf}, \bar{I}_{Rf}$ =Vectors of superimposed phase currents at sending and receiving ends

CHAPTER 1

INTRODUCTION

1.1 The Need For Accurate Fault Location

Power transmission lines require a dedicated monitoring and protection system against faults and malfunctions because of their indispensable role for electricity supply in today's highly electrified society. As they usually traverse vast areas, a good accuracy in fault location can reduce the time required to repair the damage caused by the fault and to restore the service.

Faults on transmission lines are either permanent or transient. A permanent fault is normally accompanied by mechanical damage that must be repaired to return the line to service. Even where the helicopters are immediately available for patrol following a permanent fault, fault locators perform a valuable service. Troubles cannot be found with a routine patrol unless there is some indication of where the fault occurred. For example, tree growth could reduce clearances, resulting in a flashover during severe conductor sagging. By the time the patrol arrives, the conductors have cooled, reducing the clearance to the tree, so that the weak spot is not evident. The importance of fault locators is more obvious where foot patrols are relied upon, particularly on long lines in rough terrain. Also, locators can help where maintenance jurisdiction is divided between different

companies or divisions within a company.

Fault locators are valuable even where the line has been restored either automatically or non-automatically following a transient fault. Although a transient fault will not cause interruption of the service (successful reclosing is likely), it may damage equipment, e.g. an isolator. Consequently a transient fault may cause a permanent fault in the near future. Faults in this category are those caused by cranes swinging into the line, bushfires, damaged or contaminated insulators, weather exposure, bird activity and vandalism. The locator allows rapid arrival at the site before the evidence is removed or "the trail becomes cold". Also the knowledge that faults are repeatedly occurring in the same area can be valuable in detecting the cause. Weak spots that are not obvious may be found because a more thorough inspection can be focussed in the limited area defined by the fault locator.

Although fault location has been of interest to electricity utilities for many years, in recent years it has assumed much greater importance because:

(a) The trend towards much faster fault clearance often results in there being no visual evidence of damage.

(b) The need for economy in high voltage plant is resulting in a move away from parallel feeders in long distance transmission applications. There is a consequent need to effect repairs more quickly, but

this can only be done if the fault point is accurately located. The threat to system security and the loss of revenue caused by sustained outages are important considerations in the context of fault location means.

(c) There is a global tendency towards longer transmission routes which often traverse difficult terrain.

At this point, it is worth mentioning the differences in the tasks of distance relays and fault locators. Distance relays are the essential ingredient of transmission line protection which provide a very crude indication of the general region of a fault. No accuracy in the estimate of fault location is necessary in distance protection as the primary question is whether the fault is on a particular line or not. On the other hand the decision has to be taken within a very small time interval to isolate the fault as quickly as possible. Once the fault has been cleared the fault location function is initiated using the recorded data during the fault, but in this case the time is not critical at all.

1.2 Objective of the Work

The objective of the work presented in this thesis is to find a new solution for the problem of fault location on transmission lines which meets stringent accuracy requirements and various practical and operational constraints, all of which are essential factors for the

success in its future commercial application. The technical requirements to be met by a new fault locator are described in the start of Chapter 4. They are derived from the study of the present locators in Chapter 2.

Generally it is aimed to develop a new algorithm which in most cases gives an accuracy better than ±1.5% over the total line length. Assuming the same error due to signal acquisition and processing, the total error should be smaller than ±3%. An extensive survey of the technical literature shows no locators achieving such a high accuracy under different fault conditions.

1.3 Structure of the Thesis

The main body of the thesis consists of eight Chapters. Chapter 1 is devoted to the introduction describing the objective and structure of the thesis. In Chapter 2 a thorough and extensive survey of the present techniques of fault location is given. Chapter 3 describes the theory of multiconductor and natural modes used in the simulation of transmission lines. Chapter 4 describes the theory of a new method of fault location on transmission lines. Chapters 5 to 7 are devoted to the simulation study of the new algorithm to establish its practicability and accuracy in comparison with the commercially available techniques. The synopses of Chapters 2 to 7 are given in this Chapter. Chapter 8 concludes the work and puts forward some suggestions for future work.

1.3.1 Chapter 2 Synopsis

There has been quite considerable research into fault location on two-ended transmission lines. The advent of microprocessor-based relaying has provided considerable analytical capabilities to implement more accurate fault location techniques. Basically there are two approaches in fault location; many techniques use power frequency based measurements at one or both ends of a line, while there are some techniques relying on high frequency measurements. At high frequencies, data acquisition and processing are not very reliable due to the poor fidelity of standard transducers, as well as hardware limitations, but power frequency measurements are more accurate and well established in power systems protection. This research is therefore concerned with the techniques using data at power frequency.

Study of the modern techniques is essential in the recognition of the factors affecting the accuracy in fault location. In a new technique these factors must be considered in order to improve the accuracy without impairing the practical aspects of the technique. The other important objective of such study is to ensure that no similar work has been published before. Furthermore, the literature survey should be continued during the course of the new research work.

Nearly all of the power frequency based fault location techniques presented during the last decade are studied in

Chapter 2. The commercially available fault location algorithms are mathematically described in Chapter 2 and the results of their simulation tests are given in Chapters 6 and 7 and are compared with those of a new technique.

The Chapter starts with a description of the reactance relay which shows the main problem with the techniques which use the measurements at one end of the line, a problem caused by the remote source infeed current through the fault path. In these techniques the phase angle of fault path current or voltage is required. Since there is no means, as yet, to precisely determine this angle, different methods and assumptions are employed which may reduce the accuracy. Double-end measurement fault locators are more accurate because they do not need to determine this angle.

1.3.2 Chapter 3 Synopsis

Prior to the on-site tests, which are associated with high cost and other difficulties, computer simulation is a simple and flexible method in the accuracy assessment of any algorithm. Non-algorithmic errors which are introduced by hardware limitations and incorrect settings can also be investigated in this way. However, in the simulation study of fault locators a very accurate modelling of transmission lines is required to take into account all important parameters in the real system. A very small error caused by a neglected parameter in the simulation

could lead to kilometres of error in locating the fault. For example, though the sequence component theory is an effective tool in the analysis of a faulted line for many purposes, it assumes the line is perfectly transposed, but such lines do not exist in real life. This assumption in fault location can introduce some error. A distributed parameter simulation for two-ended transmission lines was therefore developed which takes into account the effect of line asymmetry and shunt capacitance. In Chapter 3 the theory underlying this method is described and the basic equations required are derived. Also the theory of natural modes for decomposing a multiphase system into a number of uncoupled single-phase circuits is explained. In the third part of the Chapter the technique using the concept of multiconductor theory for the simulation of faulted transmission lines is given. The Chapter concludes with a description of the program structure.

1.3.3 Chapter 4 Synopsis

From the survey of Chapter 2 it is learned that the present fault location techniques have a variety of limitations in terms of system application and attainable accuracy. Most of them neglect the effect of shunt capacitance and use a sequence component model which assumes the line is perfectly transposed. Some algorithms require a representative value of the remote source impedance.

In Chapter 4 a new power frequency based algorithm is

derived from the theory of multiconductor lines and natural modes. The technique takes into account line transposition status and distributed shunt capacitance. Also it is independent of source configuration and fault path complexity. The phasor data required by the technique are measured at both ends of the line. A simple technique is used to synchronize the phasor measurements at each end with each other. There is no need for continuous data link between the two ends as only the phasor values to be transferred and this can be done by voice over a telephone link, for example. A prototype hardware description is given at the end of the Chapter.

1.3.4 Chapter 5 Synopsis

The new algorithm gives no error when the exact line parameters and phasor data are available. However, in a conventional relaying system all the required data for the new algorithm are not usually available. To adapt the new algorithm with the present system, it is necessary to test its accuracy when using the input data and simplifying assumptions utilised in conventional relaying systems. In this respect there are two main aspects to be considered: double-circuit line applications and the assumption of perfect transposition for untransposed lines.

The new algorithm in its general form requires current and voltage phasors from both circuits of a double-circuit line, but in conventional relaying systems, each circuit has its own fault locator and the effect of the other

circuit is compensated by its residual current. With this restriction in mind, in Chapter 5 the performance of the new algorithm is tested for a double-circuit line configuration using the phasor data from the faulted circuit only. It is interesting to note that the new algorithm gives no error when the line is perfectly transposed and still maintains a very high accuracy in untransposed lines using phasor data from the faulted circuit only.

In general, the new algorithm is required to evaluate eigenvalues and an eigenvector matrix for any line application. However, for all transposed lines a real eigenvector matrix can be defined and the eigenvalues are simply evaluated from the line sequence impedances. The simulation test results of Chapter 5 show an important aspect of the new algorithm; it maintains its accuracy when using transposed line eigenvalues and eigenvectors for untransposed lines. In other words, in the new algorithm any untransposed line can be assumed perfectly transposed, obviating the need for difficult mathematical operations involved in evaluating the eigenvalues and the eigenvector matrix. Moreover, in untransposed double-circuit line applications there is a good accuracy even when using the transposed parameters and data from the faulted circuit only.

1.3.5 Chapter 6 Synopsis

As part of the performance evaluation of the new fault

location algorithm a number of tests were carried out to establish its accuracy in comparison with the best commercially available algorithms. The test results given in Chapter 6 reveal the accuracy achieved by the new algorithm compared to that of the commercial algorithms under the same fault conditions.

A very favourable test circuit is chosen in 6.3 such that any algorithm can accurately locate the fault. Some parameters affect the accuracy of algorithms, e.g. fault resistance, source impedances, etc. In order to evaluate the effect of each parameter independently, in most cases one or two parameters are varied from the reference conditions. When all parameters have been tested, a typical test case compounding different parameters is given. In 6.4 test cases are for transposed lines, while in 6.5 the same cases are repeated for untransposed lines. It is worth emphasising that in the simulation studies for all the algorithms perfect transposition was assumed for untransposed lines as this is the normal practice in real systems.

1.3.6 Chapter 7 Synopsis

As the input data from the line simulation program contains no error and perfect setting was also assumed, test results of Chapter 6 reveal the algorithmic error associated with different locators. In practice this will not be the case and some non-algorithmic errors due to incorrect setting and data acquisition and processing are

inevitable. These errors must be considered in any overall accuracy assessment of the locators. In Chapter 7 the errors introduced by incorrect setting of the remote source impedance, line impedance matrix and line length are independently investigated. In 7.5 hardware errors are simulated by introducing errors into the phase angle and the magnitude of voltage and current phasors. This method reveals the sensitivity of different algorithms to the errors created during signal acquisition and processing in real systems.

CHAPTER 2

PRESENT FAULT LOCATION TECHNIQUES

2.1 Introduction

The need for very accurate fault location has long been the incentive for numerous research activities carried out in this field. With the advent of the microprocessor-based relaying devices (and the analytical capabilities provided by such devices), electricity utilities have shown increased interest in implementing accurate fault location techniques. Consequently in recent years, several microprocessor-based approaches to the problem of fault location have been developed and, to varying degrees, implemented. It should be noted that small computers can also be used as the fault location calculations can be done off-line once the fault has been cleared and the required data have been recorded.

Before commencing new research work in this area, the study and analysis of modern fault location algorithms is helpful in the recognition of their deficiencies and sources of inaccuracy. From such study the objectives to be achieved by a new algorithm can be outlined. While the new research is being conducted, it is important to continue monitoring modern fault location research to be sure that no similar work has been published.

From the frequency point of view, fault location

algorithms involve two main approaches. Most techniques employ power frequency evaluation of the system based on the phasor measurements at one or both ends of a line. Some other techniques rely on high frequency measurements, e.g. to inject an electrical pulse into the faulted line segment and take recordings of subsequent reflected voltage and current signals. Due to the poor fidelity of the standard transducers, as well as the inaccuracy associated with data recording and processing at high frequencies, the latter approach is not very popular. On the other hand, power frequency measurements are more accurate and well established in power systems protection. This thesis is therefore concerned with studies of power frequency based fault location.

In this Chapter the inaccuracy of most fault location techniques published since 1979 is discussed and some encouraging methods are described. Simulation studies were also performed on commercially available fault locators and these were compared with a new technique which is described in Chapter 4. An independent simulation test was therefore avoided as it would be easier to make judgment on the performances of different algorithms under the same fault conditions. Comparative simulation test results are given in Chapters 6 and 7.

2.2 Reactance Measurement Fault Location

The technique used in reactance relaying is to measure the apparent impedance of the line. This is a simple technique

which is usually used in distance protection. Its description reveals the main problem caused by the fault infeed current from the remote source in a single-end measurement fault location. Under fault conditions, the idea is that the apparent impedance should equal that of the line to the fault point plus the fault impedance. Given that the transmission line is predominantly reactive, and that the fault impedance tends to be resistive, the reactance component of the apparent impedance is proportional to distance to fault. For example, using the single-phase line shown in Fig. 2-1, the voltage drop at the sending end (relaying point) is:

$$V_S = I_S \cdot p \cdot Z_L + I_F \cdot R_f \qquad (2\text{-}1)$$

Dividing both sides of Eq. (2-1) by I_S and taking the imaginary part yields the apparent reactance, that is:

$$X_r = \mathrm{Im}\left[\frac{V_S}{I_S}\right] = \mathrm{Im}[p \cdot Z_L] + R_f \cdot \mathrm{Im}\left[\frac{I_F}{I_S}\right] \qquad (2\text{-}2)$$

From the apparent reactance presented to the relay, the exact location of the fault can be found, provided that the phase angles of I_S and I_F are equal or can be determined precisely. Otherwise there is an error which depends on the angle between I_S and I_F as shown in Fig. 2-2. The error is affected by the remote end infeed, the prefault load, and the line and source angles. An accurate estimation of the phase angle of I_F (or V_F) is the main concern of any fault location algorithm which uses phasor data only from one end of the line. In this Chapter

different approaches to solve this problem will be shown.

2.3 The ASEA Algorithm

This fault location technique introduced by Eriksson et. al. [1], is in commercial use in the ASEA RANZA equipment. The authors use the sequence component concept and ignore the effect of shunt capacitance. The input data to the algorithm is collected from the near end data acquisition system and a representative value for the remote end source impedance is applied. Prefault load current samples are stored to determine the change in line current caused by the fault (superimposed current).

2.3.1 Basic Equations

Considering the single-phase faulted line shown in Fig. 2-1, Eq. (2-1) can be rewritten as:

$$V_S = I_S \cdot p \cdot Z_L + \frac{I_{Sf}}{D_A} \cdot R_f \qquad (2\text{-}3)$$

where I_{Sf} is the sending end superimposed current and D_A is the current distribution factor given by:

$$D_A = \frac{I_{Sf}}{I_F} = \frac{(1-p)Z_L + Z_{SR}}{Z_{SS} + Z_L + Z_{SR}} \qquad (2\text{-}4)$$

Substituting Eq. (2-4) in Eq. (2-3) and rearranging, yields:

$$p^2 - p \cdot K_1 + K_2 - K_3 \cdot R_f = 0 \qquad (2\text{-}5)$$

where: $K_1 = \frac{V_S}{I_S Z_L} + 1 + \frac{Z_{SR}}{Z_L}$

$$K_2 = \frac{V_S}{I_S Z_L}\left(1 + \frac{Z_{SR}}{Z_L}\right)$$

$$K_3 = \frac{I_{Sf}}{I_S Z_L}\left(1 + \frac{Z_{SR}+Z_{SS}}{Z_L}\right)$$

The complex expression of Eq. (2-5) contains the unknowns p and R_f. However, Eq. (2-5) can be separated into two simultaneous equations, one real and one imaginary. By eliminating R_f a single expression results with the single unknown p. This is solved by the program, using the phasor values, taken from the Fourier analysis routine which yields the fundamental components of the signals.

In order to use Eq. (2-5) for multiphase systems, the sequence components are employed. The algorithm assumes the current distribution factor for the positive and negative sequence networks are the same. As the zero sequence current distribution factor is not known as reliably as that for the positive sequence, the zero sequence current has been extracted from the superimposed current at the sending end for single-phase-to-earth faults. Therefore for all types of fault on multiphase systems, the positive sequence current distribution factor is used and consequently the positive sequence line and source impedances are used in Eq. (2-4) for locating the fault. However, depending on the fault type, the voltage and current values in Eq. (2-5) should be defined. For single-phase-to-earth faults, say, involving phase 'a',

the voltage and current values to be used are:

$$\left.\begin{aligned} V_S &= V_{Sa} \\ I_S &= I_{Sa} + \frac{Z_{L0}-Z_{LP}}{3Z_{L0}} . I_{Sa} \\ I_{Sf} &= \frac{3}{2}(I_{Sfa}-I_{S0}) \end{aligned}\right\} \qquad (2\text{-}6)$$

where Z_{L0} and Z_{LP} are zero and positive sequence line impedances and I_{S0} is the sending end zero sequence fault current component. The factor 3/2 in Eq. (2-6) for evaluating I_{Sf} provides a heavier weighting to compensate for the removal of the zero sequence current.

For inter-phase faults including double-phase-to-earth and 3-phase faults, the voltage and current expressions to be used in Eq. (2-5), say, involving phases 'a' and 'b' are:

$$\left.\begin{aligned} V_S &= V_{Sa} - V_{Sb} \\ I_S &= I_{Sa} - I_{Sb} \\ I_{Sf} &= (I_{Sfa} - I_{Sfb}) \end{aligned}\right\} \qquad (2\text{-}7)$$

The algorithm can be modified for double-circuit or parallel line applications. Assuming an identical parallel line, the positive sequence network is completely described by redefining Eq. (2-4) as:

$$D_A = \frac{(1-p)(Z_{SS}+Z_{LP}+Z_{SR})+Z_{SR}}{2Z_{SS}+Z_{LP}+2Z_{SR}} \qquad (2\text{-}8)$$

Using Eq. (2-5) for a double-circuit or parallel line, the values for K_1, K_2 and K_3 are:

$$K_1=\frac{V_S}{I_S Z_{LP}}+1+\frac{Z_{SR}}{Z_{SS}+Z_{LP}+Z_{SR}}$$

$$K_2=\frac{V_S}{I_S Z_{LP}}\left(1+\frac{Z_{SR}}{Z_{SS}+Z_{LP}+Z_{SR}}\right)$$

$$K_3=\frac{I_{Sf}}{I_S Z_{LP}}\left(1+\frac{Z_{SR}+Z_{SS}}{Z_{SS}+Z_{LP}+Z_{SR}}\right)$$

It should be noted that in using the above equations the positive sequence source impedances must be applied. Zero sequence mutual coupling between the two circuits can be compensated for by interconnecting two fault locators. With a fault locator on the parallel line its residual current reading can be input to its companion locator; the mutual resistance and reactance are required as additional input settings. For example, it can be shown that for an 'a'-earth fault, I_S is defined as:

$$I_S=I_{Sa}+\frac{Z_{L0}-Z_{LP}}{3Z_{LP}}I_{SN1}+\frac{Z_M}{Z_{LP}}I_{SN2} \qquad (2\text{-}9)$$

where Z_M is the mutual impedance between the two circuits and I_{SN1} and I_{SN2} are the sending end residual currents of circuits 1 and 2 respectively. V_S and I_{Sf} in Eq. (2-6) remain unchanged for double-circuit lines.

2.3.2 Comments on the ASEA Algorithm

It is obvious from the foregoing that the ASEA algorithm neglects the effect of shunt capacitance. The field test

results given in the paper are for a short line (76 km) where the line capacitance current is not significant. Also the algorithm uses the sequence components which are necessarily applicable to perfectly transposed lines. The locator is therefore prone to large errors when applied to untransposed lines. The remote end impedance setting required by the ASEA algorithm can be another source of error as the source configuration may change from time to time by switching operations. It is apparent that errors can occur if the remote source impedance differs from the set value. The computer simulation test results given in Chapters 6 and 7 show that any of the above sources of error could lead to significant inaccuracy in fault location.

2.4 The Toshiba Algorithm

The technique was first presented by Takagi, et. al. [2] and is used commercially in the Toshiba SEL-121 fault locator equipment. The technique basically neglects the effect of shunt capacitance; however after the first estimate of fault location the effect of shunt capacitance is compensated. The major novelty introduced by this scheme is the use of a phase network instead of the sequence component networks for modelling the faulted line. Also, by assuming that the fault path current is in phase with the superimposed current at the sending end, the technique requires data from one end only.

2.4.1 Basic Equations

If the shunt capacitance is ignored then the voltage vector of a faulted line at the sending end is obtained from:

$$\overline{V}_S = x.[Z].\overline{I}_S + \overline{V}_F \qquad (2\text{-}10)$$

The fault point voltage vector can be written as:

$$\overline{V}_F = [R_f].\overline{I}_F \qquad (2\text{-}11)$$

In Eq. (2-11), $\overline{I}_F$ is the fault path current consisting of the sending and receiving end superimposed currents, and $[R_f]$ is a diagonal matrix of required values of fault resistance in each phase. If it is assumed that both fault path infeed currents from the sources are in phase, then the fault point voltage will be in phase with the sending end superimposed current, i.e.:

$$\overline{V}_F = ç.\overline{I}_{Ff} \qquad (2\text{-}12)$$

where ç is a real value. Putting Eq. (2-12) in (2-10), yields:

$$\overline{V}_S = x.[Z].\overline{I}_S + ç.\overline{I}_{Sf} \qquad (2\text{-}13)$$

For simplicity, consider an 'a'-earth fault. Then Eq. (2-13) can be written as:

$$V_{Sa} = x.\sum_k Z_{ak}.I_{Sk} + ç.I_{Sfa} \qquad (2\text{-}14)$$

where k=a,b,c for single-circuit lines and k=a,b,c,A,B,C for double-circuit lines. Multiplying both sides of Eq.

(2-14) by the conjugate of I_{Sfa}, i.e. I^*_{Sfa}, and equating the imaginary part of the equation gives the distance to fault, x, as:

$$x=Im[V_{Sa}\cdot I^*_{Sfa}]/Im[(\Sigma_k Z_{ak}\cdot I_{Sk})\cdot I^*_{Sfa}] \qquad (2\text{-}15)$$

Eq. (2-15) is valid for any single-phase-to-earth fault by using the corresponding phase voltages and currents. For a phase-to-phase fault, say, involving phases 'a' and 'b' on a double-circuit line, the fault location expression has the following form:

$$x=Im[V_{Sab}\cdot I^*_{Sfab}]/Im[V_{SLab}\cdot I^*_{Sfab}] \qquad (2\text{-}16)$$

where $V_{Sab}=V_{Sa}-V_{Sb}$

$I^*_{Sfab}=I^*_{Sfa}-I^*_{Sfb}$

$V_{SLab}=(Z_{aa}-Z_{ab})I_{Sa}-(Z_{bb}-Z_{ab})I_{Sb}+(Z_{ca}-Z_{cb})I_{Sc}$
$+(Z_{aA}-Z_{bA})I_{SA}+(Z_{aB}-Z_{bB})I_{SB}+(Z_{aC}-Z_{bC})I_{SC}$

In Eq. (2-16) double-phase-to-earth and 3-phase faults are included.

The authors suggest the following formula to compensate for the error caused by neglecting shunt capacitance for line lengths more than 100km:

$$x_1=x-\beta^2.x^3/3 \qquad (2\text{-}17)$$

where x_1 is the compensated fault location and β is the imaginary part of the line propagation constant.

2.4.2 Comments on the Toshiba Algorithm

The algorithm uses data from one end and assumes the fault

point infeed currents from the sources are in phase. However, in practice there could be cases where a significant discrepancy between these phase angles exists. The difference between the phase angles generally varies with the distance to fault. When the remote end source is stronger, the main contribution of the fault path current is from the remote end source, particularly for faults nearer to the remote end. In this case the fault current phase angle is governed by the infeed from the remote end.

The effect of shunt capacitance is neglected in the first estimation of the fault point. A compensated fault point estimate is then obtained from the first estimation. It is apparent from Eq. (2-17) that in compensating for the shunt capacitance effect, a value is subtracted from the first estimate of fault location, i.e. it considers that because of the capacitance current the locater always overreaches the fault point. However, it is shown in Chapter 6 that there are cases for untransposed lines where the relay underreaches in its first estimate and hence the compensation method will actually increase the error.

The algorithm can be used for untransposed lines if the self and mutual impedances of each phase are available. In practice the average values of all phases are set for each phase, assuming the line is perfectly transposed. In Ref. 3 which also gives details of the Toshiba algorithm, the authors accept that when the line

parameters are represented by the averaged values, a substantial error will occur due to asymmetry amongst the phases. There is a good example of line asymmetry in Table 2 of Ref. 3 which shows a dispersion of about 5% to 10% in the loop impedance with respect to the averaged impedance, depending on the faulted phase(s).

The field test results given in Ref. 3 also show some cases where the equipment did not satisfactorily locate the fault. The comparative simulation test results of this locator are given in Chapters 6 and 7.

2.5 Modification of the Toshiba Algorithm by Schweitzer

2.5.1 Basic Equations

In Eq. (2-12) suppose there is a phase difference T between the sending end superimposed current and the fault point voltage. Then Eq. (2-12) can be written, say, for an 'a'-earth fault as:

$$V_{Fa}=ç.I_{Sfa}.e^{jT} \qquad (2\text{-}18)$$

Hence Eq. (2-15) takes the general form of:

$$x=Im[V_{Sa}.I^{*}_{Sfa}.e^{-jT}]/Im[(\Sigma_{k} Z_{ak}.I_{Sk}).I^{*}_{Sfa}.e^{-jT}] \qquad (2\text{-}19)$$

In the Toshiba algorithm, T is set equal to zero. Schweitzer [4] suggests that T can be determined from the circuit model. It is obtained from the following expression:

$$T=\arg\{\frac{Z_{SS}+Z_L+Z_{SR}}{Z_{SS}+(1-p)Z_L}\} \quad (2\text{-}20)$$

The angle T is zero if all impedances share the same angle and T is constant if Z_{SR} and Z_L have equal angles. The improvement Schweitzer offers is to use Eq. (2-19) and to provide an estimate of the angle, instead of setting it equal to zero as assumed by the Toshiba algorithm. Two estimations are possible, and the choice depends on the knowledge and variability of the system parameters:

(a) Set T equal to a constant. This approach is particularly effective when the second condition above is met, i.e. when Z_{SR} and Z_L are of equal angle.

(b) Determine T from a function of the first fault location estimate using Eq. (2-19) and the expression for T given in Eq. (2-20). Other choices include a linear approximation or piecewise linear approximation.

2.5.2 Comments on the Schweitzer Modification

The phase angle T used by the Schweitzer modification is derived from the concept of current distribution factor given by Eq. (2-4) for the ASEA algorithm. However, here it is not clear which sequence component is used in Eq. (2-20) for estimating T. The zero sequence current distribution factor is quite indeterminate which leads to inaccuracy in determining the phase angle T for earth faults. The error will be higher for untransposed lines as

the expression for T is not valid.

The simulation test results of Chapters 6 and 7 show that the modification improves the accuracy of the Toshiba algorithm for transposed lines provided that the phase angle T is equal for all the sequence networks and therefore the positive sequence impedances can be used in Eq. (2-20). However, there are cases for untransposed lines where the modification reduces the accuracy of the Toshiba algorithm quite substantially. The requirement for setting the remote source impedance in the Schweitzer modification can itself be another source of error as the remote source impedance may change from the value set into the locator. The test results for this effect are shown in Chapter 7.

2.6 The Cook Algorithms

In his paper, V. Cook [5] presents three fault location methods based on the sequence components. He also neglects the effect of shunt capacitance in his methods. Two of the methods use the impedances measured by the protective relays at both ends of a line, while the third one uses impedance data from one end. Considerable attention has been given to the influence of prefault current as the author assumes this as the major source of error. The impedance presented to a relaying point is a function of distance to the fault, fault resistance and current distribution factor, i.e.:

$$Z_r=\frac{V_r}{I_r}=p.Z_L+K_r.R_f \qquad (2\text{-}21)$$

In Eq. (2-21) V_r and I_r are the voltage and current signals input to the relay depending on fault type. The complex coefficient K_r is a function of the network current distribution factor, fault location and fault type. For example, for a phase-to-phase fault K_r is given by:

$$K_r=0.5/D_A \qquad (2\text{-}22)$$

where D_A is the current distribution factor given by Eq. (2-4). The effect of prefault load current is considered in Eq. (2-22) by multiplying the coefficient K_r by the ratio of the superimposed relay current to the total fault current. Using the measured faulted phase impedance at each end of the line, the unknown distance to fault is obtained by solving a quadratic equation. The second algorithm which uses data from both ends is a simplified form of the quadratic algorithm. However, in the second method, the relay current magnitudes at both ends are also required. A different routine is presented when these current magnitudes are equal.

The author also presents an algorithm using the impedance measured at one end. However, in order to evaluate the current distribution factor, an assumed value is used for the remote source impedance which inevitably introduces an error in fault location. But it is claimed that the error is negligible as only the argument of the

current distribution factor is used and the major error appears in the magnitude of the current distribution factor.

2.6.1 Comments on the Cook Algorithms

In the conclusion of the paper the author states that the fault location estimates are influenced by the system being non-homogeneous; nevertheless it is not shown how the algorithms account for this source of error. By using the sequence components the algorithms cannot be used for untransposed lines. The effect of line shunt capacitance has also been neglected. The simulation study results given in the paper are for very simple cases where the fault resistance is quite small (2.9Ω) and the line length is very short (10 miles). In these simple cases any locater is expected to perform very well.

In a simulation study of the simplified two-ended algorithm it has been observed that the algorithm is prone to high errors for fault positions in the vicinity of a point on the line where the magnitudes of the infeed currents from the sources are equal. For example, for an 'a'-earth fault at 140km of a 250km transposed single-circuit line, more than 5% error (over the total line length) was recorded. The fault resistance was 10Ω and both source capacities were 1MVA. In this case the magnitudes of the currents from both sides are equal at the mid-point (125km) as the sources are identical. It has also been observed that the error is increased in

proportion to the fault resistance.

The algorithm using data from one end is based on the same idea as that by the Toshiba algorithm, i.e. it assumes a very small value for the argument of the current distribution factor; the Toshiba algorithm assumes this argument is zero.

Overall, the proposed algorithms are based on assumptions which have already been used in previous work (though the fault location equations look different). On this basis no improvement in the accuracy of fault location is expected. The paper, however, considers some fundamental problems in the analysis of distance protection and fault location which are therefore useful as a tutorial study.

2.7 The Yang and Morrison Algorithm

The authors present a method in their paper [6] for high resistance fault distance protection to calculate fault distance independent of fault resistance. The method uses the sequence components and neglects the effect of shunt capacitance.

The basic principle of the proposed algorithm is that it is not necessary to actually find the fault current; any current proportional to it will suffice. If such a current can be found that is measurable from the relaying point, a number of basic problems will be overcome. The fault path current may be expressed as a sum of zero,

positive and negative sequence components, and each component may be broken into two contributions, one from the near end of the line and the other from the remote end. Only the superimposed currents need to be considered, as the prefault quantities may be simply extracted. As stated in the paper, the appropriate sequence networks show that while the zero sequence current on the relay side may not be in phase with the fault path current, the positive and negative sequence fault currents flowing from the relay side must be virtually in phase with the same components of fault path current, because the arguments of positive and negative sequence impedances for high voltage transmission lines are almost the same as those of generators. Noting further that all sequence components of the fault path current are in phase, it is concluded that the sum of the positive and negative sequence superimposed currents at the relaying point is approximately in phase with the fault path current. This analysis suggests that the current obtained by subtracting the zero sequence current from the superimposed current at the relaying point will be a current proportional to the fault path current.

Once the proportional current has been found, the fault equation based on the instantaneous current and voltage at the relaying point is written which contains two unknowns, one of which is the distance to fault. The equation is evaluated at two different times, and can then be solved for the unknowns. The authors suggest that the

accuracy will improve if a measuring time close to the zero-crossing of the superimposed current is chosen. This is because of a reduction in the effect of the non-linearity of arc resistance due to smaller voltage drop across the fault resistance near zero current [7].

Although the algorithm has been proposed for high resistance earth fault distance protection, its study could be useful for the analysis of problems associated with accurate fault location. The authors make a more reasonable assumption than the Toshiba algorithm by assuming the fault path current is in phase with the sending end superimposed current when its zero sequence current is extracted. This can result in smaller errors as the zero sequence network is quite indeterminate. However, the technique has been proposed only for earth faults and test results given in the paper show high errors in some cases. Overall, the method has some good features which can be used as a basis for evolving a new fault location technique.

2.8 Other Fault location Algorithms

Nearly all the possible simplifying assumptions for an accurate fault location have been discussed in the foregoing Sections. There is other published work which derives other algorithms of essentially the same type. It is not therefore expected that these methods significantly increase the attainable accuracy. They are, however, briefly described here to complete the survey.

Sachdev and Agarwal [8] suggest a technique in which use is made of a local digital impedance relay and its current data plus the corresponding data from the remote end. An estimate of the fault location is first obtained by neglecting the shunt capacitance. The estimate is then compensated for the effect of shunt capacitance. The technique uses the sequence components and does not require synchronized measurements at the two line terminals. The procedure should result in a precise estimate of fault location as it uses data from both ends of the line, but appreciable errors have been reported in the paper for certain fault locations. Also, the technique does not consider line asymmetry by using the sequence components. The proposed compensation for the effect of shunt capacitance, though improving the accuracy for perfectly transposed lines, can increase the error for untransposed lines as is shown in Chapter 6 for the Toshiba algorithm, which uses essentially the same technique. Like the Cook algorithm, considerable error has been reported in Ref. 9 for faults at the points on the line where the fault current contributions from the sources have similar magnitudes.

Wiszniewsky [10] considers fault resistance as the reason for errors in the fault location technique based on reactance measurement from one end. He states that fault resistance is comparatively small during interphase faults while for earth faults it may be substantial. By using the remote source impedance, a correction is proposed for the

apparent reactance measured during high resistance faults. The correction is based on an estimation of the phase difference between the total fault current at one end of the line and the fault path current. It also assumes that the phase angle of the measured impedance can be considered equal to the angle of the line impedance. No test results have been given in the paper. However, it is obvious that in terms of attainable accuracy no improvement is expected over the previously described algorithms which use the same assumption, e.g. the ASEA algorithm.

The paper by Jeyasura and Rahman [11] gives a method which uses the phasor voltage and current measured at the line terminals. These measurements are not required to be synchronized as the algorithm uses the apparent impedance measured by the faulted phase impedance relays at both ends to evaluate the phase shift between the sending and receiving end measurements. The sequence components are used by the method and the effect of shunt capacitance is neglected.

Sant and Paithankar [12] propose a fault location technique that uses data from one end of the line. But this technique assumes the line is connected to a source at one end only. The fault location estimate obtained by this approach is not therefore accurate if fault current is contributed by both sources in the presence of fault resistance.

Richards and Tan [13] propose an iterative technique which estimates the impedance to a fault as seen from the line terminals, and convert the estimate to a line length. This approach is also sensitive to fault resistance, particularly if the fault is fed from both terminals. The technique uses a sequence component approach that treats both the fault location and fault resistance as unknown quantities. Shunt capacitance is also neglected.

A recent paper by Lawrence and Waser [14] uses a time domain rather than a frequency domain representation of voltage and current. The phase network model of the line is used, permitting explicit treatment of self and mutual impedance effects for multiphase systems. This method permits the inclusion of unbalanced system impedances associated with untransposed lines. A lumped model of shunt capacitance may also be included. The analysis procedure employed in the fault location algorithm is based on the Z-transform technique to model the system response to a fault. As shown for a simplified single-phase circuit in the paper, the remote end source voltage is evaluated from the prefault condition, i.e. it assumes the remote source voltage does not change during the fault. Knowing that the effective source impedance of synchronous machines, for example, changes during the fault conditions, the use of prefault source voltages during fault conditions could be a major source of error. Another major problem with this technique is that it requires an experienced engineer to view the faulted

waveform and select prefault and fault data windows and execute the fault location program. Even though the control dispatch or control centre is manned 24 hours a day, the technical personnel necessary to do the analysis may not be available if immediate fault location is required. It is claimed by the authors that the estimated errors are within 3 to 4 percent of the actual fault location.

2.9 Summary

In this Chapter most of the fault location algorithms which utilise phasor measurement at one or both ends of a line have been studied. These employ power frequency waveform evaluation and then use an iterative or non-iterative technique to solve a set of non-linear equations containing the distance to fault as a variable.

Those algorithms which use phasor data from one end should solve the problem of the remote source current contribution to the fault path current. Sant and Paithankar propose an algorithm which assumes the line is connected to a source at one end only. In the Toshiba algorithm it is assumed that fault path current infeeds from remote and near ends are in phase. Eriksson, et. al. (the ASEA algorithm), Cook and Wiszniewsky propose methods which use fault current distribution factors determined from a knowledge of the remote end source impedance. Also Schweitzer modifies the Toshiba algorithm to form an iterative method by using the remote source impedance.

Richards and Tan put forward an iterative method which estimates the impedance to fault, and converts the estimate to a line length. Lawrence and Waser use a time domain representation of voltage and current and assume the remote source voltage remains unchanged after the occurrence of fault.

Sachdev and Agarwal, Jeyasura and Rahman, and Cook propose algorithms which use the data from both ends of a line. These techniques are much the same and require the apparent impedance measured by distance relays at the line ends and the amplitude of the voltage and/or current from the remote end. These techniques do not require synchronized measurement at the line ends.

All algorithms, except the Toshiba algorithm and the algorithm proposed by Lawrence and Waser which use a phase network, use a sequence network representation of the faulted line, i.e. they cannot consider the effect of line asymmetry. The sequence components are only applicable to perfectly transposed lines. Only the algorithms by Toshiba, and Sachdev and Agarwal consider the effect of shunt capacitance by using a lumped model of it.

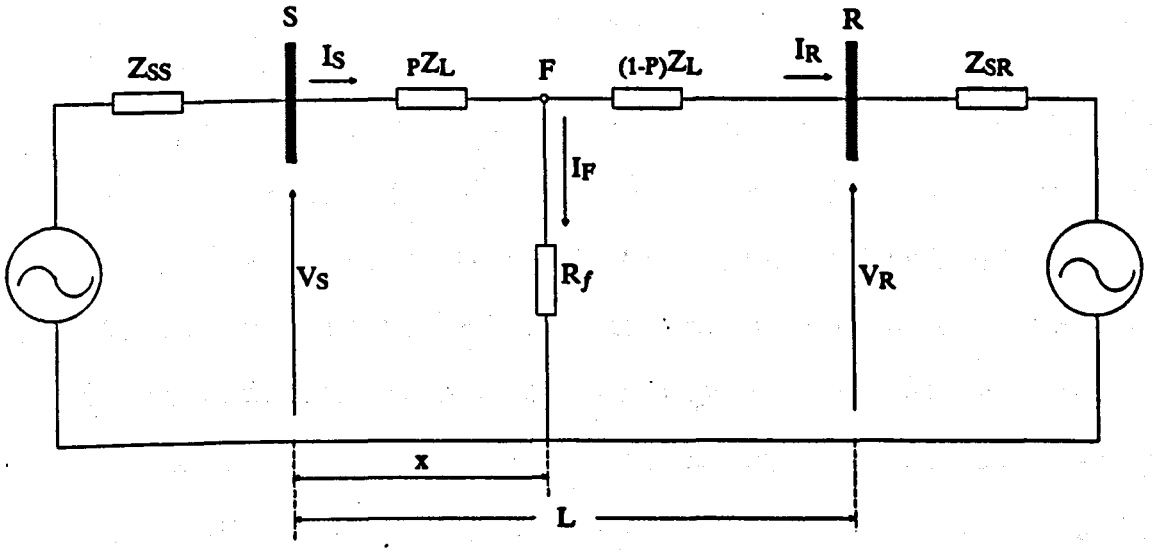

Fig. 2-1 Faulted single-phase line

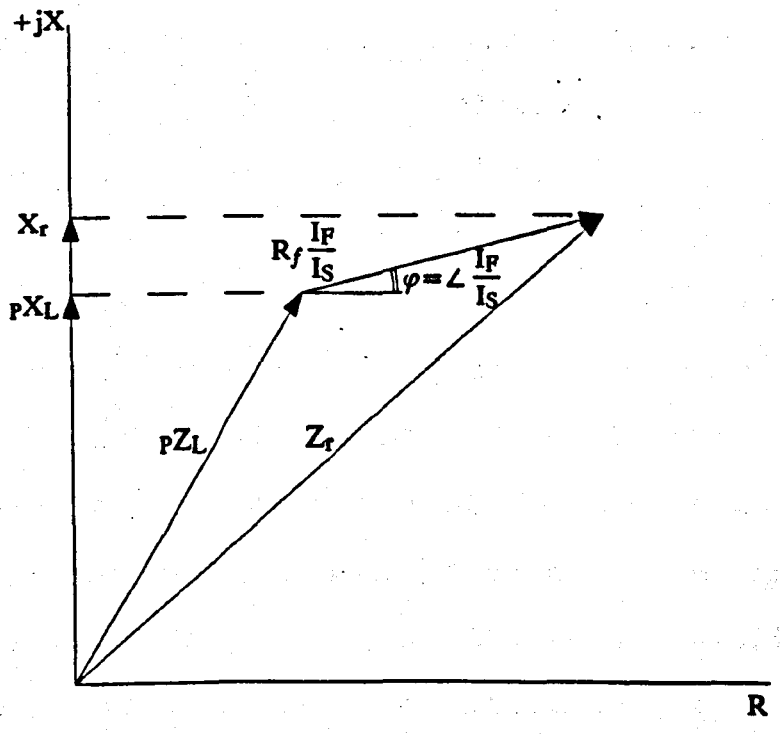

Fig. 2-2 Impedance presented to the relay at S-end of Fig. 2-1

CHAPTER 3

TRANSMISSION LINE SIMULATION

3.1 Introduction

The performance evaluation of the fault location algorithms for different fault conditions necessitates an accurate simulation of the transmission line. The algorithmic errors of the locators can then be tested and by introducing errors in the input data and settings their sensitivity to non-algorithmic errors can also be evaluated. The non-algorithmic errors are mainly produced by non-ideal performance of the transducers, signal processing inaccuracies and incorrect settings.

In order to study the effect of line unbalance and shunt capacitance on accuracy, a distributed model of the line is needed for the simulation. It should be noted that even with balanced generation, the asymmetrical position of the phase conductors with respect to the surface of the earth leads to line becoming unbalanced and hence the sequence component theory is not a reliable tool for the purpose of this study. The theory underlying the distributed simulation study, known as the theory of multiconductor lines, is mainly developed by Wedepohl [15]. In this Chapter the theory is briefly explained and the basic equations required for studying the fault locators are derived. Also the theory of natural modes for decomposing a multiphase system into a number of uncoupled

single-phase circuits is described. Then the technique for the simulation of faulted transmission lines at power frequency is given. In the last part the structure of the simulation program is given.

3.2 Theory of Multiconductor Lines

Any a.c. transmission or distribution line consists of at least three phase conductors. In some cases EHV lines may comprise two 3-phase circuits; strung or suspended from the same tower structure as in double-circuit lines having a vertical configuration (Fig. 3-1) or two circuits running in parallel, as in a twin-circuit line with horizontal configuration. Other conductors may also be present in the form of earth wires for the purpose of shielding the phase conductors from lightning strokes, and these are usually bonded to ground at each tower. An important part is also played by the ground over which the line runs as this can also be considered as an additional lossy conductor having a complex distributed characteristic.

Thus it may be seen that the practical transmission line is a complex arrangement of conductors, all of which are mutually coupled not only to each other but also to earth. Even with balanced generation, the earth path plays a part since the asymmetrical positions of the phase conductors with respect to the surface of the earth leads to line unbalance and hence to currents flowing in the earth return path. Thus unbalanced conductor geometry may

also lead to voltage unbalance at supply points. As a result it is often the practice to minimise the effects of line unbalance by transposing the phase conductors at regular intervals in order to achieve some averaging of the line parameters. At frequencies which a line can be considered electrically short (e.g. line lengths less than a quarter of the wavelength), the net unbalance may be considered as though it was averaged out and ignored. Hence at power frequencies, the line may be considered short so that line unbalance is relatively unimportant. As a result, for most applications the sequence component theory has long been a useful tool for the analysis of balanced power systems under both operational and fault conditions. However, consideration of a very accurate fault location technique requires that mutual effects between the phases must be represented more accurately, as the distance to fault evaluated by a locator clearly depends upon line unbalance. It is shown in Chapter 6 that the fault location techniques which use the sequence components produce erroneous values of fault position, even for short untransposed lines.

The aim of this Section and the following Section is to consider and apply the concepts of multiconductor line theory in which phase variable relationships are derived for distributed parameter lines and to illustrate the theory and applications of natural modes of propagation to overhead transmission circuits.

3.2.1 Basic Equations

Any multiconductor line section is defined by its series impedance matrix per unit length [Z] and its shunt admittance matrix per unit length [Y]. Consider a homogeneous line containing n conductors and taking an element of infinitesimal length δx, when current I_j flows in the jth conductor (where j=1,2,..,n), the voltage developed in length δx of the kth conductor is:

$$\delta V_k = -\sum_{j=1}^{n} Z_{kj} I_j \delta x \qquad (3\text{-}1)$$

where k goes from 1 to n to include all conductors and Z_{kj} is the mutual impedance per unit length of the kth conductor for current in the jth conductor. The negative sign appears because the change in voltage is negative for increasing x. Similarly, there is a shunt displacement current due to the potential applied to the jth conductors which is:

$$\delta I_k = (-Y_{kk} V_k + \sum_{j=1 \text{ (except k)}}^{n} Y_{kj} V_j) \delta x \qquad (3\text{-}2)$$

Alternatively in matrix form and for $\delta x \to 0$ the following definitive equations are appropriate:

$$d\bar{V}/dx = -[Z]\bar{I} \qquad (3\text{-}3)$$

$$d\bar{I}/dx = -[Y]\bar{V} \qquad (3\text{-}4)$$

From Eqs. (3-3) and (3-4) can be obtained:

$$d^2\bar{V}/dx^2 = [Z][Y]\bar{V} \qquad (3\text{-}5)$$

$$d^2\bar{I}/dx^2=[Y][Z]\bar{I} \tag{3-6}$$

If $[\Theta]=([Z][Y])^{\frac{1}{2}}$, then $[\Theta_t]=([Y][Z])^{\frac{1}{2}}$ because [Z] and [Y] are symmetrical, but in general $[\Theta]$ and $[\Theta_t]$ are not equal. The solutions to Eqs. (3-5) and (3-6) for a point at a distance x along the line are:

$$\bar{V}_x=\exp(-[\Theta]x)\bar{V}_i+\exp([\Theta]x)\bar{V}_r \tag{3-7}$$

$$\bar{I}_x=\exp(-[\Theta_t]x)\bar{I}_i+\exp([\Theta_t]x)\bar{I}_r \tag{3-8}$$

Eqs. (3-7) and (3-8) may be interpreted on the basis of forward and reverse travelling waves where $\bar{V}_i$, $\bar{V}_r$, $\bar{I}_i$ and $\bar{I}_r$ are vectors required to satisfy conditions at the boundaries. In practice the suffices i and r refer to incident and reflected values. By differentiating Eq. (3-7) and substituting in Eq. (3-3), Eq. (3-8) can be expressed in a different form as:

$$\bar{I}_x=[Y_0][\exp(-[\Theta]x)\bar{V}_i-\exp([\Theta]x)\bar{V}_r] \tag{3-9}$$

where $[Y_0]$ is the characteristic admittance matrix and is defined as:

$$[Y_0]=[Z]^{-1}[\Theta] \tag{3-10}$$

i.e., the input admittance of the semi-infinite homogeneous line. Conversely the characteristic impedance matrix (or surge impedance matrix) is formulated by inversion as:

$$[Z_0]=[\Theta]^{-1}[Z] \tag{3-11}$$

Also by using Eq. (3-9) in Eq. (3-4):

$$[Y_0]=[Y][\Theta]^{-1} \tag{3-12}$$

and

$$[Z_0]=[\Theta][Y]^{-1} \tag{3-13}$$

Alternatively by using Eq. (3-8) in Eq. (3-4), the voltage may be expressed in terms of the current to give:

$$\bar{V}_x=[Z_0][\exp(-[\Theta_t]x)\bar{I}_i-\exp([\Theta_t]x)\bar{I}_r] \tag{3-14}$$

where the characteristic impedance matrix is:

$$[Z_0]=[Y]^{-1}[\Theta_t] \tag{3-15}$$

But this can be shown to be the transpose of Eq. (3-13), from which it follows the $[Z_0]$ and $[Y_0]$ are symmetrical matrices even though $[\Theta]$ in general is not.

3.2.2 Two-Port Equations

In order to evaluate voltage and current values at the line terminals or sections it is often more convenient to formulate a solution in terms of the two-port equations. For a homogeneous multiconductor line of length L (Fig. 3-2), putting x=L in Eqs. (3-7) and (3-9) yields:

$$\bar{V}_R=\exp(-[\Theta]L)\bar{V}_i+\exp([\Theta]L)\bar{V}_r \tag{3-16}$$

$$\bar{I}_R=[Y_0][\exp(-[\Theta]L)\bar{V}_i-\exp([\Theta]L)\bar{V}_r] \tag{3-17}$$

For x=0

$$\bar{V}_S=\bar{V}_i+\bar{V}_r \tag{3-18}$$

$$\bar{I}_S=[Y_0](\bar{V}_i-\bar{V}_r) \qquad (3\text{-}19)$$

In these equations subscripts S and R stand for sending end and receiving end quantities. From Eq. (3-19) we obtain:

$$[Z_0]\bar{I}_S=\bar{V}_i-\bar{V}_r \qquad (3\text{-}20)$$

Solving Eqs. (3-18) and (3-20) for $\bar{V}_i$ and $\bar{V}_r$, yields:

$$\bar{V}_i=(\bar{V}_S+[Z_0]\bar{I}_S)/2 \qquad (3\text{-}21)$$

$$\bar{V}_r=(\bar{V}_S-[Z_0]\bar{I}_S)/2 \qquad (3\text{-}22)$$

Substituting Eqs. (3-21) and (3-22) in Eq. (3-16) and rewriting the equations we have:

$$\bar{V}_R=A\bar{V}_S-B\bar{I}_S \qquad (3\text{-}23)$$

where $A=(\exp(-[\Theta]L)+\exp([\Theta]L))/2=\cosh([\Theta]L)$

$B=(\exp([\Theta]L)-\exp(-[\Theta]L))[Z_0]/2=\sinh([\Theta]L)[Z_0]$

Similarly using Eqs. (3-21) and (3-22) in Eq. (3-17) it can be shown:

$$\bar{I}_R=-C\bar{V}_S+D\bar{I}_S \qquad (3\text{-}24)$$

where $C=[Y_0]\sinh([\Theta]L)$ and $D=[Y_0]\cosh([\Theta]L)[Z_0]$

Or in matrix form:

$$\begin{bmatrix}\bar{V}_R\\-\bar{I}_R\end{bmatrix}=\begin{bmatrix}A & B\\C & D\end{bmatrix}\begin{bmatrix}\bar{V}_S\\-\bar{I}_S\end{bmatrix} \qquad (3\text{-}25)$$

For the homogeneous line Eq. (3-25) can be written, for the same A, B, C and D constants, in the following form:

$$\begin{bmatrix} \bar{V}_S \\ \bar{I}_S \end{bmatrix} = \begin{bmatrix} A & B \\ C & D \end{bmatrix} \begin{bmatrix} \bar{V}_R \\ \bar{I}_R \end{bmatrix} \qquad (3\text{-}26)$$

The current directions must be considered in constructing the ABCD-matrix. In the above equations, the direction of currents flowing from S to R is assumed positive.

An advantage of this form of transfer function matrix is the ease with which a number of line sections with different constants can be combined, e.g. for a line consisting of three different line sections we can write:

$$\begin{bmatrix} \bar{V}_S \\ \bar{I}_S \end{bmatrix} = \begin{bmatrix} A_1 & B_1 \\ C_1 & D_1 \end{bmatrix} \begin{bmatrix} A_2 & B_2 \\ C_2 & D_2 \end{bmatrix} \begin{bmatrix} A_3 & B_3 \\ C_3 & D_3 \end{bmatrix} \begin{bmatrix} \bar{V}_R \\ \bar{I}_R \end{bmatrix} \qquad (3\text{-}27)$$

3.2.3 Evaluation of [Z] and [Y] Matrices

Representation of the homogeneous multiconductor line in phase variable terms in the foregoing requires the numerical evaluation of the [Z] and [Y] matrices. The calculation methods of these matrices are briefly described in Appendix 3A, though a more detailed description can be found in Ref. 16. Generally the calculation of [Z] and [Y] is based on the data from the line geometry, electrical parameters and earth path resistivity. Also in Appendix 3A the effect of the earth wire on the [Z] matrix and the single-conductor equivalent

of the bundled conductors are explained.

3.2.4 Calculation Methods of the [Z][Y] Functions

In order to use the transfer function equations, it is required to evaluate A, B, C and D constants which are in turn determined from the matrix product [Z][Y]. This is not undertaken readily and in order to resolve the numerical difficulties a linear transformation is introduced such that the eigenvalues and eigenvectors of the matrix product [Z][Y] must be determined.

Taking $[\Gamma^2]$ as the diagonal eigenvalue matrix it follows from :

$$[Z][Y]=[Q][\Gamma^2][Q]^{-1} \qquad (3\text{-}28)$$

that the relevant matrices used in the two-port equations for example can be evaluated by the theory of matrix functions leading to:

$$[\Theta]=[Q][\Gamma][Q]^{-1} \qquad (3\text{-}29)$$

[Q] being a matrix of eigenvectors in which each column corresponds to an eigenvalue of the [Z][Y] product.

Since $[Z_0]=[\Theta]^{-1}[Z]$ and $[Y_0]=[Y][\Theta]^{-1}$ the following may be written:

$$
\left.
\begin{aligned}
[Z_0] &= [Q][\Gamma]^{-1}[Q]^{-1}[Z] \\
[Y_0] &= [Y][Q][\Gamma]^{-1}[Q]^{-1} \\
A &= [Q]\cosh([\Gamma]L)[Q]^{-1} \\
B &= [Q]\sinh([\Gamma]L)[Q]^{-1}[Z_0] \\
C &= [Y_0][Q]\sinh([\Gamma]L)[Q]^{-1} \\
D &= [Y_0][Q]\cosh([\Gamma]L)[Q]^{-1}[Z_0]
\end{aligned}
\right\} \qquad (3\text{-}30)
$$

Methods are available for calculating the eigenvalues and eigenvectors of a matrix but the form of the solution determines which method is the most suitable, e.g. the roots may be repeated or close together, real or complex. The calculation methods of eigenvalue and eigenvector matrices used by the simulation program are described in Appendix 3B for both transposed and untransposed lines.

3.3 Natural Modes of Propagation

It has been shown how the practical multiconductor line can be represented in terms of phase variables with little difficulty provided that functions of the matrix [θ] can be evaluated. A procedure leading to the diagonalisation of [θ] has been suggested so that the functions can be obtained from the functions of the diagonal [Γ] matrix. The diagonalisation leads to the concept of natural modes of propagation and this is of benefit in obtaining a clearer insight into the nature of wave propagation on complex transmission systems. In dealing with the theory of natural modes it is perhaps useful to point out that the sequence components are in fact modes of propagation

which corresponds to the case of a perfectly balanced 3-phase line [21].

3.3.1 Modal voltages

Consider the voltage propagation equation for a semi-infinite line (i.e. a line without reflection) using Eq. (3-7):

$$\bar{V}_x=\exp(-[\theta]x)\bar{V}_i \qquad (3\text{-}31)$$

where $\bar{V}_i$ is an incident voltage vector. Furthermore finding the eigenvalues and eigenvectors of $[\theta]$:

$$\bar{V}_x=[Q]\exp(-[\Gamma]x)[Q]^{-1}\bar{V}_i \qquad (3\text{-}32)$$

and introducing the variables $\bar{V}_{xn}$ and $\bar{V}_{in}$ such that $\bar{V}_{xn}=[Q]^{-1}\bar{V}_x$ and $\bar{V}_{in}=[Q]^{-1}\bar{V}_i$ it follows that:

$$\bar{V}_{xn}=\exp(-[\Gamma]x)^{-1}\bar{V}_{in} \qquad (3\text{-}33)$$

But $\exp(-[\Gamma]x)$ is diagonal, indicating that each element of $\bar{V}_{xn}$ can be considered to the mutual exclusion of all other elements. For any such element, it is possible to think in terms of a single-phase line characterised by the corresponding element of the $[\Gamma]$ matrix, there being as many such lines as there are distinct values of Γ.

A solution in terms of each component voltage is exactly analogous to the solution of a single-phase line problem. Each component voltage is associated with its own propagation constant Γ_k where for $\Gamma_k=\alpha_k+j\beta_k$, α_k and β_k define attenuation and phase shift constants per unit

length respectively. The latter also define phase velocity such that $u_k=w/\beta_k$.

The concept of component voltages leads to the simple interpretation that at any point x the actual voltage vector may be considered as being composed of a number components, the relative distribution of voltage corresponding to a given component being defined by a particular column of [Q], known as the modal matrix. These columns in turn define natural modes of propagation. Thus if one of the natural modes is generated at one end of a multiconductor line it will propagate without changing its voltage distribution but it will of course be attenuated and shifted in phase. In general there are as many modes as there are effective conductors.

3.3.2 Modal Currents

So far only voltage modes have been considered, but equally well, current modes having the same propagation characteristic as the corresponding voltage modes can be defined. However, as a result of line unbalance the relative distributions for the current modes are not in the strictest sense equal to those for voltage. From $d^2\bar{I}/dx^2=[Y][Z]\bar{I}$ it follows that:

$$[\Theta_t]=([Y][Z])^{\frac{1}{2}}=[S][\tau][S]^{-1} \qquad (3\text{-}34)$$

Hence corresponding to the voltage equations it may be seen that $[\tau]$ defines propagation constants for the natural modes of current defined by the columns of matrix

[S], the modal matrix for current. However, as the determinant of a matrix and its transpose are equal, it follows that the eigenvalues of [θ] and $[\theta_t]$ are equal, i.e. τ=Γ. Considering this results and $[\theta_t]^t=[\theta]$, it is seen that $[\theta]=[S_t]^{-1}[\Gamma][S_t]$ which can be compared with the matrix $[\theta]=[Q][\sigma]^{-1}[\Gamma][\sigma][Q]^{-1}$; where the arbitrary diagonal matrix [σ] is introduced for generality. By comparison, the relationship $[S_t][Q]=[\sigma]$ can be obtained. In particular, suitable normalisation can be used to set [σ]=[U] in which case the current eigenvector matrix can be considered to be defined in such a way that $[S]=[Q_t]^{-1}$ and not as [S]=[Q] unless it is a perfectly balanced system which would give $[\theta]=[\theta_t]$. It may be shown that a particular voltage mode will only produce currents of the same mode and vice versa.

3.3.3 Decomposition of Two-Port Equations

As an example of the application of the theory of natural modes in the analysis of transmission lines, consider the two-port equation given by Eq. (3-25) from which the receiving end voltage vector can be obtained:

$$\bar{V}_R=A\bar{V}_S-B\bar{I}_S \qquad (3\text{-}35)$$

In the above equation each phase voltage at the receiving end is electromagnetically coupled to the all phase voltages and currents at the sending end as A and B in general are not diagonal. Representing phase values in Eq. (3-35) by the modal ones (shown by subscript n) and putting the values for A and B from Eq. (3-30) we have:

$$[Q]\bar{V}_{Rn}=[Q]\cosh([\Gamma]L)[Q]^{-1}[Q]\bar{V}_{Sn} -[Q]\sinh([\Gamma]L)[Q]^{-1}[Z_0][S]\bar{I}_{Sn} \quad (3\text{-}36)$$

Rearranging Eq. (3-36):

$$\bar{V}_{Rn}=A_n\bar{V}_{Sn}-B_n\bar{I}_{Sn} \quad (3\text{-}37)$$

where $A_n=\cosh([\Gamma]L)$ and $B_n=\sinh([\Gamma]L)[Q]^{-1}[Z_0][S]$. Knowing that $\cosh([\Gamma]L)$ and $\sinh([\Gamma]L)$ are diagonal matrices and also $[Q]^{-1}[Z_0][S]$ is a diagonal matrix it follows that an n-phase system has been decoupled into n independent single-phase circuits. Solving each modal circuit separately, at any point on the line all modal voltages and currents can be evaluated. Having evaluated the modal values at a point on the line, the phase values at that point can be obtained using [Q] and [S] matrices. Conversely, the modal values can be evaluated from the phase ones using $[Q]^{-1}$ or $[S]^{-1}$. For example, for a 3-phase perfectly transposed line comprising phases 'a', 'b' and 'c' using $[Q]^{-1}$ from Appendix 3B and $\bar{V}_n=[Q]^{-1}\bar{V}$, the modal values for voltage are:

$$\left.\begin{aligned} V_1&=V_a+V_b+V_c \\ V_2&=V_a-V_c \\ V_3&=V_a-2V_b+V_c \end{aligned}\right\} \quad (3\text{-}38)$$

where subscripts 1,2 and 3 refer to the mode numbers. The same relationships between modal and phase quantities are obtained for current as for perfectly transposed lines

[S]=[Q]. In Eq. (3-38) it is obvious that the mode-1 voltage (or current) is electromagnetically coupled to the earth while the other two modes are coupled to the phase conductors. For this reason mode-1 is called earth-mode while mode-2 and mode-3 are aerial-modes.

3.4 Simulation of Faulted Transmission Lines

In the conventional method, a faulted transmission line is solved by transforming its phase network into the sequence networks. This method is simple and effective for many purposes, but cannot take into account the line asymmetry and distributed shunt capacitance. The technique employed here is based on the multiconductor theory. The method essentially is one of superposition, i.e. when a fault occurs it effectively superimposed a voltage on the normal steady-state system voltages. The superimposing source is located at the fault point and is equal and opposite to the normal system voltage at that point. The superimposed voltages and currents thus set up can be considered as existing in their own right in an otherwise de-energised system, i.e. in a model of the system in which each source voltage is hypothetically zero.

3.4.1 Transfer Matrices of Faulted Transmission Lines

A faulted transmission system essentially consists of a network of cascaded sections as shown in Fig. 3-3. Two-port transfer matrices are particularly useful in the solution of such problems. For example, the transfer matrix representing the line section up to the point of

fault is given by Eq. (3-39), and this can be used in combination with the corresponding matrices representing the fault discontinuity and the fault section between the fault and the receiving end busbar, to yield a relationship between the currents and voltages at each end of the line. Eq. (3-40) shows the multiplication process involved to yield the latter relationship.

$$\begin{bmatrix} \bar{V}_S \\ \bar{I}_S \end{bmatrix} = \begin{bmatrix} A_1 & B_1 \\ C_1 & D_1 \end{bmatrix} \begin{bmatrix} \bar{E}_{Fs} \\ \bar{I}_{Fs} \end{bmatrix} \qquad (3\text{-}39)$$

where A_1, B_1, C_1 and D_1 are found from Eq. (3-30) for the length x.

$$\begin{bmatrix} \bar{V}_S \\ \bar{I}_S \end{bmatrix} = \begin{bmatrix} A_1 & B_1 \\ C_1 & D_1 \end{bmatrix} \begin{bmatrix} A_f & B_f \\ C_f & D_f \end{bmatrix} \begin{bmatrix} A_2 & B_2 \\ C_2 & D_2 \end{bmatrix} \begin{bmatrix} \bar{V}_R \\ \bar{I}_R \end{bmatrix} \qquad (3\text{-}40)$$

The submatrices A_2, B_2, C_2 and D_2 defining the transfer matrix representing the line section beyond the fault are found by substituting the length (L-x) involved, and the matrix defining the fault discontinuity is formulated according to the type of fault simulated. The source side network is similarly represented and incorporated in the system equations as detailed later [17].

3.4.2 Fault-Transient Model

As mentioned the fault-transient model is based on the superposition method which hinges upon representing the voltage at the fault point by the sum of two voltages;

steady-state prefault voltage, $\bar{V}_{Fs}$, and superimposed voltage, $\bar{V}_{Ff}$ as shown in Fig. (3-4). $\bar{V}_{Ff}$ is a suddenly applied voltage, which when added to $\bar{V}_{Fs}$ represents the postfault voltage. A solution may thus be obtained by performing two separate calculations in which the desired voltages and currents are evaluated when $\bar{V}_{Fs}$ is applied to the energised system, and the superimposed voltage $\bar{V}_{Ff}$ is applied to the line with all source voltages set at zero. It should be noted that the steady-state voltage vector $\bar{V}_{Fs}$ can be evaluated from a knowledge of the prefault voltages and currents at the terminating busbars. In fact, the vector $\bar{V}_{Fs}$ is only needed insofar as it enables the value of $\bar{V}_{Ff}$ to be evaluated as a prerequisite to the second part of the computational process.

3.4.3 Formulation for Two-Ended System

The prefault voltage at the fault point, $\bar{V}_{Fs}$, is easily evaluated from a knowledge of the prefault voltages at the terminating busbars. It should be noted that before the fault the sending and receiving end current and voltage vectors are related by Eq. (3-41).

$$\begin{bmatrix} \bar{V}_{Ss} \\ \bar{I}_{Ss} \end{bmatrix} = \begin{bmatrix} A_1 & B_1 \\ C_1 & D_1 \end{bmatrix} \begin{bmatrix} A_2 & B_2 \\ C_2 & D_2 \end{bmatrix} \begin{bmatrix} \bar{V}_{Rs} \\ \bar{I}_{Rs} \end{bmatrix} = \begin{bmatrix} A & B \\ C & D \end{bmatrix} \begin{bmatrix} \bar{V}_{Rs} \\ \bar{I}_{Rs} \end{bmatrix} \qquad (3\text{-}41)$$

The sending and receiving end currents before the fault are thus given by:

$$\bar{I}_{Ss}=(C-DB^{-1}A)\bar{V}_{Rs}+DB^{-1}\bar{V}_{Ss} \quad (3\text{-}42)$$

$$\bar{I}_{Rs}=-B^{-1}A\bar{V}_{Rs}+B^{-1}\bar{V}_{Ss} \quad (3\text{-}43)$$

and

$$\bar{V}_{Fs}=(A_2-B_2B^{-1}A)\bar{V}_{Rs}+B_2B^{-1}\bar{V}_{Ss} \quad (3\text{-}44)$$

Each of the above equations are evaluated at power frequency because the prefault condition is essentially a steady-state one, irrespective of the postfault frequency domain of interest. For the purpose of the work presented in this thesis the postfault equations are also evaluated at power frequency.

3.4.4 Sound Phase Voltage Problem

In order to complete the solution, it is necessary to establish the response of the unenergised circuit to the superimposed voltage $\bar{V}_{Ff}$. A value is required for both faulted and sound phases. In the case of a faulted phase or phases no difficulty exists. For example, if we consider a single-phase-to-earth fault on phase 'a', then the superimposed voltage is simply equal and opposite to the prefault voltage at the point of fault, i.e.:

$$V_{Ffa}=-V_{Fsa}\sin(w_o t+\phi)h(t) \quad (3\text{-}45)$$

For the unfaulted phases, there is no such direct means of knowing the appropriate values of superimposed voltage. However, it is shown in Appendix 3C that the currents due to the application of the superimposed voltage are related by Eq. (3-46):

$$\bar{V}_{Ff}=-\{[(C_1+D_1[Z_{SS}]^{-1})(A_1+B_1[Z_{SS}]^{-1})^{-1}+(C_2+D_2[Z_{SR}]^{-1})$$

$$(A_2+B_2[Z_{SR}]^{-1})^{-1}]^{-1}+[R_f]\}(\bar{I}_{FSf}-\bar{I}_{FRf}) \qquad (3\text{-}46)$$

It should be noted that because in double-circuit lines both circuits are normally connected to the same busbar, the extensive source impedance matrix for double-circuit lines is singular and therefore cannot be inverted, so that Eq. (3-46) is not applicable. To solve this problem a matrix partitioning technique is used in Appendix 3D to find the relationship between $\bar{V}_{Ff}$ and $(\bar{I}_{FSf}-\bar{I}_{FRf})$ for double-circuit lines.

The above mentioned relationships involve a 3x3 matrix for single-circuit lines and 6x6 matrix for double-circuit lines. Taking the former case first, Eq. (3-46) will take the form:

$$\begin{bmatrix} V_{Ffa} \\ V_{Ffb} \\ V_{Ffc} \end{bmatrix} = \begin{bmatrix} Z_{11} & Z_{12} & Z_{13} \\ Z_{21} & Z_{22} & Z_{23} \\ Z_{31} & Z_{32} & Z_{33} \end{bmatrix} \begin{bmatrix} I_{FSfa}-I_{FRfa} \\ I_{FSfb}-I_{FRfb} \\ I_{FSfc}-I_{FRfc} \end{bmatrix} \qquad (3\text{-}47)$$

Consider now an 'a'-earth fault, the currents $\bar{I}_{FSf}$ and $\bar{I}_{FRf}$ will be equal in the 'b' and 'c' phases because they are healthy and Eq. (3-47) takes the simplified form:

$$\begin{bmatrix} V_{Ffa} \\ V_{Ffb} \\ V_{Ffc} \end{bmatrix} = \begin{bmatrix} Z_{11} \\ Z_{21} \\ Z_{31} \end{bmatrix} (I_{FSfa}-I_{FRfa}) \qquad (3\text{-}48)$$

With reference to Eq. (3-48), the voltage V_{Ffa} is known so that the superimposed voltages in the sound phases are easily evaluated.

Appendix 3E shows the routines for solving the sound phase voltage problem for the other types of fault, including faults on double-circuit lines and inter-circuit faults.

3.4.5 Superimposed Voltages and Currents at Busbars

Having calculated the vectors of superimposed voltage, $\bar{V}_{Ff}$, and current, $\bar{I}_{FSf}$-$\bar{I}_{FRf}$, using one of the routines given in 3.4.4 or Appendix 3E, then the superimposed voltage vector, $\bar{E}_{Ff}$, is obtained from:

$$\bar{E}_{Ff}=\bar{V}_{Ff}+R_f(\bar{I}_{FSf}-\bar{I}_{FRf}) \qquad (3\text{-}49)$$

With reference to Fig. 3-4, if homogeneous line sections are assumed, two principal relationships emerge:

$$\begin{bmatrix} \bar{E}_{Ff} \\ -\bar{I}_{FSf} \end{bmatrix} = \begin{bmatrix} A_1 & B_1 \\ C_1 & D_1 \end{bmatrix} \begin{bmatrix} \bar{V}_{Sf} \\ -\bar{I}_{Sf} \end{bmatrix} \qquad (3\text{-}50)$$

$$\begin{bmatrix} \bar{E}_{Ff} \\ \bar{I}_{FRf} \end{bmatrix} = \begin{bmatrix} A_2 & B_2 \\ C_2 & D_2 \end{bmatrix} \begin{bmatrix} \bar{V}_{Rf} \\ \bar{I}_{Rf} \end{bmatrix} \qquad (3\text{-}51)$$

The voltages and currents at each end are related to the source impedance matrix by:

$$\bar{V}_{Sf}=-[Z_{SS}]\bar{I}_{Sf} \qquad (3\text{-}52)$$

$$\bar{V}_{Rf}=[Z_{SR}]\bar{I}_{Rf} \quad (3\text{-}53)$$

From these equations voltages and currents at the sending and receiving ends are evaluated by:

$$\bar{V}_{Sf}=(A_1+B_1[Z_{SS}]^{-1})^{-1}\bar{E}_{Ff} \quad (3\text{-}54)$$

$$\bar{V}_{Rf}=(A_2+B_2[Z_{SR}]^{-1})^{-1}\bar{E}_{Ff} \quad (3\text{-}55)$$

$$\bar{I}_{Sf}=-[Z_{SS}]^{-1}\bar{V}_{Sf}=-[Z_{SS}]^{-1}(A_1+B_1[Z_{SS}]^{-1})^{-1}\bar{E}_{Ff} \quad (3\text{-}56)$$

$$\bar{I}_{Rf}=[Z_{SR}]^{-1}\bar{V}_{Rf}=[Z_{SR}]^{-1}(A_2+B_2[Z_{SR}]^{-1})^{-1}\bar{E}_{Ff} \quad (3\text{-}57)$$

Again it should be noted that these equations are valid for single-circuit lines. Appendix 3D gives the expressions for double-circuit lines.

3.5 Structure of the Program

As mentioned the program is concerned with the simulation of two-ended faulted transmission lines at power frequency. It can be used for single- and double-circuit lines, and different types of fault, including simultaneous earth fault on both circuits and inter-circuit faults, can be applied. Different values of fault resistance can be included for any type of fault. The program also can be run for perfectly transposed lines and lines without shunt capacitance. The following steps summarize the routine used for the simulation.

(a) The input data are read in. These include the physical geometry of the line, stranding factors appropriate to the bundling arrangements, earth

resistivity, conductor permeability and resistivity.

(b) Shunt admittance matrix [Y] and series impedance matrix [Z] are constructed using the methods explained in Appendix 3A.

(c) If the line is untransposed the matrix product [Z][Y] is formed to evaluate the diagonal eigenvalue matrix $[\Gamma^2]$ and eigenvector matrix [Q]. If the line is perfectly transposed separate routine is used to calculate eigenvalue and eigenvector matrices. The calculation methods for these matrices are shown in Appendix 3B. From these matrices the characteristic impedance and admittance matrices, $[Z_0]$ and $[Y_0]$, are formed. Then the transfer function sub-matrices A,B,C,D can be constructed for any section of the line. If the line is considered capacitance-free, i.e. [Y]=0, then A=C=[U] ([U] is unit matrix), D=0 and B=[Z].L where L is the line section length.

(d) Having calculated the A,B,C,D matrices for different sections of the line, the prefault phasors of current and voltage are evaluated.

(e) Depending on fault type it has been shown in Section 3.4 how the program uses superposition technique to find postfault voltage and current vectors at the busbars. Total postfault values are simply evaluated by adding superimposed values to the steady-state ones.

Details and order of the input data to run the program are given in Appendix 3F entitled "Program User Manual".

3.6 Summary

In this Chapter, two-port equations have been derived from the theory of multiconductor lines. These equations account for line unbalance and shunt capacitance. Using the theory of natural modes, it has been shown that a multiphase system can be decoupled into a number of single-phase networks. A simulation program has been developed to model faulted transmission lines at power frequency by using two-port equations and the concept of natural modes. The program is used for the study of power frequency based fault locators.

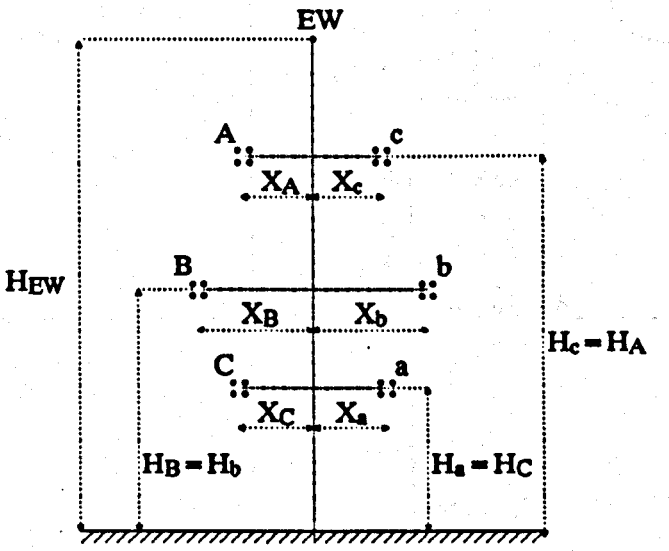

Fig. 3-1 Double-circuit line vertical configuration

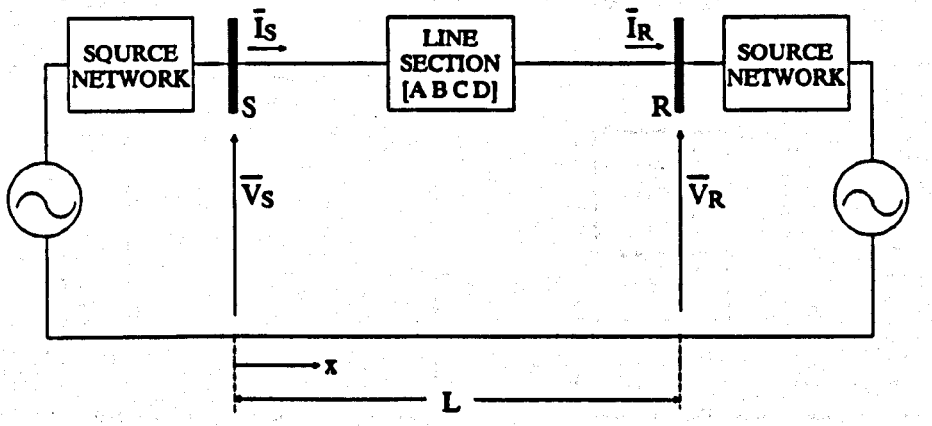

Fig. 3-2 Basic two-ended multiconductor line

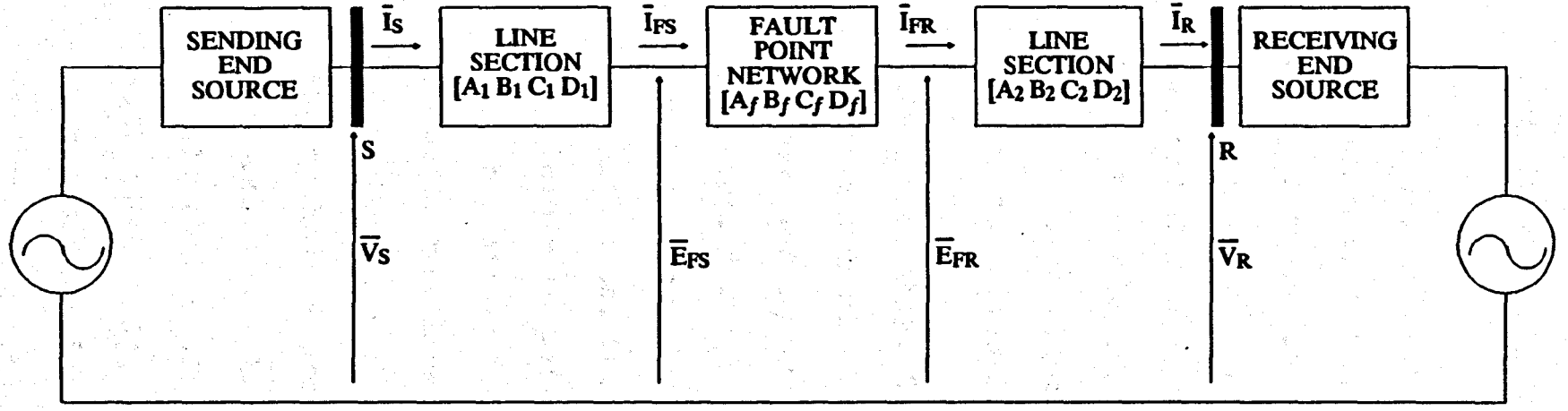

Fig. 3-3 Faulted transmission line model

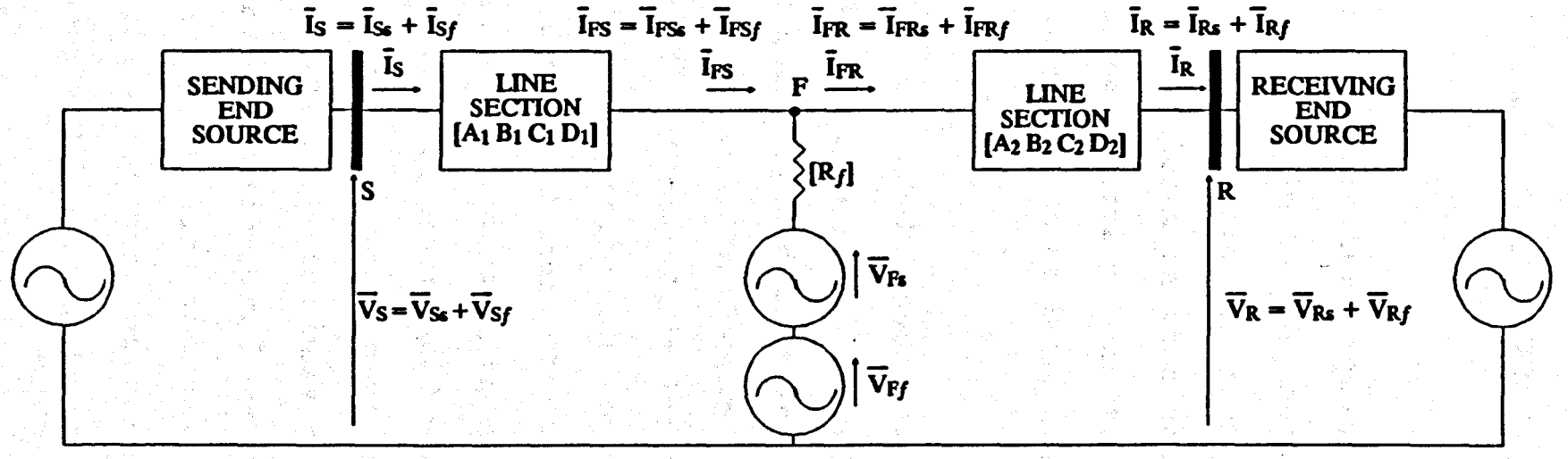

Fig. 3-4 Fault-transient model utilising superimposed fault voltage

CHAPTER 4

NEW APPROACH TO TRANSMISSION LINE FAULT LOCATION

4.1 Introduction

At the present time, fault location techniques are generally subject to a variety of limitations both in terms of the system applications to which they can be applied and the accuracy of fault location that can be obtained. Such limitations derive primarily from the use of fault location algorithms that neglect at least one or more of the following sources of error:

(a) Line asymmetry: The self and mutual impedances and admittances of each phase of transmission lines are determined by the line geometry and they are not identical for all phases as reasoned in Chapter 3. It has been shown in Chapter 2 that most fault location techniques use the sequence components which are only applicable to perfectly transposed lines. There are some techniques which can be applied to untransposed lines if the impedances for each phase can be set, otherwise they give substantial errors. For example, the technique proposed in Ref. 2 which uses phase networks, gives large errors when the mean impedances of all phases of an untransposed line are used for each phase [3], i.e. the assumption of perfect transposition for untransposed lines should not be used for such algorithms.

(b) Shunt capacitance: Capacitance current for long lines, particularly under high resistance fault conditions, can be comparable with the current in the fault path. Most algorithms do not consider shunt capacitance and the vast majority of those that do, use a lumped model for shunt capacitance [2,8]; this in turn is not an exact representation of the line and does not permit very high accuracy in fault location. In Ref. 2 the effect of shunt capacitance is compensated after the first estimation of the fault location. However, it is shown in Chapter 6 that this method can aggravate the error for untransposed lines.

(c) Fault resistance: Unknown fault resistance and the phase difference between the fault current contribution from the local and remote sources introduces error. Hence the reactance measurement technique, as used in distance protection and some fault locators, is very prone to errors due to out of phase remote source infeed through fault resistance. Analysis of such errors has been shown in 2.2.

(d) Remote source impedance setting: Some previous fault location algorithms require a setting for the remote source impedance. In modern transmission networks normally several lines and generators are connected to the line terminals. Switching operations often change the source operating configuration from those assumed in setting the fault location equipment which

in turn can lead to a large error in fault location. The changing reactance of synchronous machines during fault conditions adds another layer of uncertainty to the source equivalent model setting.

(e) Capacitive voltage transformer: Difficulties are often encountered in the use of capacitor voltage transformers, which are generally incapable of passing higher frequency phenomena. Thus, difficulties can arise for the algorithms utilising high frequency components. An example of such algorithms is given in Ref. 22.

The new technique presented in this thesis was developed specifically with the objective of overcoming the foregoing limitations and thereby significantly improves the accuracy with which transmission system faults can be located. In doing so, many of the fundamental limitations on the accuracy achievable are revealed. The results of simulation studies to determine the basic accuracy of the new technique are given in Chapters 5,6, and 7. The technique has also the merit that it does not require a determination of the phase(s) involved in a particular fault. Previous techniques use different algorithmic routines for different types of fault, thus seriously impairing accuracy if incorrect fault identification occurs under contingency or difficult fault situations.

The new technique is essentially a narrow band method

that does not require wide band transducers and can be used in applications employing capacitor voltage transformers. It involves capturing the prefault and postfault voltage and current waveforms measured at two ends of a line, cyclically filtering the waveforms to derive the power frequency component waveforms, converting the latter to phasor form and displaying such phasor values for manual transmission between the fault locators at the line ends (automatic transmission could obviously be used where a dedicated link is available).

It is doubtful whether any particular novelty could be claimed in respect of the procedures outlined in the above paragraph since a variety of filtering arrangements could be developed to derive phasor quantities and the transmission of information between monitoring points has been used in various guises for many years. The particular novelty claimed lies in the method of processing the information derived via the above outlined procedure in order to derive a more accurate and reliable indication of the actual fault position than has hitherto been possible. This thesis is therefore primarily concerned with describing the methods of processing the derived information and the algorithms for implementing the methods.

4.2 Basic Principles

The voltages and currents measured at each end of a transmission line are filtered so as to produce a measure

of the steady-state power frequency voltage and current phasors. The latter are obtained as data described by means of postfault processing applied to data captured during the fault clearance process. A hardware description is given at the end of this Chapter.

4.2.1 Simple Single-Phase Line

Consider the two-port relationship applicable to an assumed single-phase line application. With reference to Fig. 4-1, the postfault steady-state voltage V_F across the fault at a distance x from end S is readily expressed in terms of the voltages and currents measured at the line ends:

$$V_F=\cosh(\Gamma x)V_S-Z_0\sinh(\Gamma x)I_S \qquad (4\text{-}1)$$

$$V_F=\cosh(\Gamma(L-x))V_R+Z_0\sinh(\Gamma(L-x))I_R \qquad (4\text{-}2)$$

The surge (or characteristic) impedance, Z_0, and line propagation constant, Γ, are given by $Z_0=(Z/Y)^{\frac{1}{2}}$ and $\Gamma=(ZY)^{\frac{1}{2}}$ respectively, where Z is the line series impedance and Y is the line shunt admittance per unit length. Eqs. (4-1) and (4-2) are equated so as to eliminate any necessity for defining the fault point network, thereby eliminating any uncertainties as to the precise value of the fault path impedance.

$$\cosh(\Gamma x)V_S-Z_0\sinh(\Gamma x)I_S=\cosh(\Gamma(L-x))V_R+Z_0\sinh(\Gamma(L-x))I_R \qquad (4\text{-}3)$$

$$[-Z_0\cosh(\Gamma L)I_R-\sinh(\Gamma L)V_R+Z_0I_S]\sinh(\Gamma x)+$$
$$[\cosh(\Gamma L)V_R+Z_0\sinh(\Gamma L)I_R-V_S]\cosh(\Gamma x)=0 \qquad (4\text{-}4)$$

Rearrangement of Eq. (4-4) provides an exact evaluation of the distance to the fault, x, as given in Eq. (4-5).

$$x=[\tanh^{-1}(-N/M)]/\Gamma \qquad (4\text{-}5)$$

where $M=-Z_0\cosh(\Gamma L)I_R-\sinh(\Gamma L)V_R+Z_0I_S$

$N=\cosh(\Gamma L)V_R+Z_0\sinh(\Gamma L)I_R-V_S$

A useful, but not exclusive, method of solving for the fault distance x is to use the convergent expansion given in Eq. (4-6).

$$x=[-(N/M)-(N/M)^3/3-(N/M)^5/5-(N/M)^7/7-...]/\Gamma \qquad (4\text{-}6)$$

It should be noted that Eq. (4-5) is indeterminate in any case where it is applied to a healthy line. In this case, it can be shown that M=N=0. This fact provides useful confirmation of a healthy line where the protection triggers the fault location process under, for example, remote back-up conditions.

If all relevant line parameters could be specified without error, Eq. (4-5) would lead to an exact evaluation of the distance to fault, x. In such a hypothetical case, x would be calculated as a real value. However, in practice the calculated value of x has a very small imaginary part which is ignored; the real part is thus taken to represent the fault distance. The imaginary part accounts for some errors in line parameter settings and/or measurements and data processing errors. Eq. (4-5) requires only known line data (Z and Y) and known phasor values derived from measurands at the line ends. Any fault

location estimate thereby derived is therefore independent of both the fault impedance and the source impedance. The method can of course utilise superimposed measurands of the type used in high speed directional comparison protection equipment [18]. In this respect, it is found from the simulation studies given in the following Chapters that generally the accuracy of fault location is better for most line configurations when superimposed components are used. Furthermore, the fault location algorithm relates to a distributed parameter line model, and inherently includes for the effect of shunt capacitance.

It is of interest to note that a paper by Schweitzer [4], which is primarily concerned with the fault location algorithm by Takagi [2], derives an algorithm using Eq. (4-3). However, the approach suggested is developed only for single-phase lines and there is no indicated method of extending the idea to a practical multiphase system. The indications are that the idea was dropped due to difficulties of applying the method to multiphase lines and perhaps also due to expected difficulties in choosing and selecting a suitable set of measurands to deal with various fault types. Much of the work performed and detailed in this thesis is therefore concerned with finding a method of overcoming the latter difficulties.

It should be noted that because power frequency phasor voltages and currents are extracted through the postfault

filtering process, Eqs. (4-1) and (4-2) remain linear even in the case where some degree of fault point non-linearity is present, e.g. arc non-linearity. Furthermore, provided that the fault location algorithm is derived only using the linear Eqs. (4-1) and (4-2), any source side non-linearities, e.g. shunt reactors, generator non-linearities, etc., cannot affect the accuracy of the fault location. In what follows, only those equations derived from the essentially linear equations are therefore used and it is assumed that sufficient postfault filtering is performed to ensure that the power frequency components of voltage and current are utilised within the algorithm derived.

4.2.2 Extension to Single-Circuit Lines

The method described above cannot be applied directly to a multiphase power line since a number of phases are involved. Consider a single-circuit 3-phase transmission line in which the phases are identified by a,b,c as indicated in the single-line equivalent of Fig. 4-2. In this case, the vector of the various voltages and currents ($[V_{Fa,b,c}]$, $[I_{Sa,b,c}]$, etc.) are related using the two-port matrices A_S, B_S, A_R and B_R which in turn are 3x3 matrices defined using the line series impedance matrix [Z] and the line shunt admittance matrix [Y]. With reference to Fig. 4-2, the multiphase equivalents of Eqs. (4-1) and (4-2) are:

$$[V_{Fa,b,c}]=A_S[V_{Sa,b,c}]-B_S[I_{Sa,b,c}] \qquad (4\text{-}7)$$

$$[V_{Fa,b,c}]=A_R[V_{Ra,b,c}]+B_R[I_{Ra,b,c}] \qquad (4\text{-}8)$$

where $[V_{Fa,b,c}]$, $[V_{Sa,b,c}]$, $[I_{Ra,b,c}]$, etc. are vectors defining voltages and currents for each phase, e.g. $[V_{Ra,b,c}]=[V_{Ra}\ V_{Rb}\ V_{Rc}]^t=\bar{V}_R$.

It is important to note that the two-port matrices A_S, B_S, etc. can, if necessary, be formed to include any discrete line transposition, which in turn is conductive to maintaining very high levels of measurement accuracy in long line applications. In most cases, however, it is sufficient to treat each line section as homogeneous. It is worth also noting that the two-port equations can, in the multiconductor transmission line case, include for the effect of conductor asymmetry, shunt capacitance and the effect of any composite ground return, i.e. they can include the combined effect of the earth and earth wire return as discussed in Chapter 3.

The basic fault location algorithm can be extended to multiphase transmission lines by decoupling Eqs. (4-7) and (4-8) into uncoupled or independent single-phase networks of the type shown in Fig. 4-1. This is done using the theory of natural modes and matrix function theory [15] as commonly used in the digital simulation of faulted EHV transmission systems [17]. The theory underlying such techniques has been described in Chapter 3. Briefly, it is reminded that the method involves finding the eigenvector matrices of the [Z][Y] product ([Q] say) and the [Y][Z] product ([S] say). The voltages and currents are thereby

derived from each phase a,b,c and are transformed to corresponding modal voltage and current quantities 1,2,3 by means of the corresponding [Q] and [S] eigenvector matrices:

$$\left.\begin{aligned}\bar{V}_{Sn}&=[V_{S1}\ V_{S2}\ V_{S3}]^t=[Q]^{-1}[V_{Sa}\ V_{Sb}\ V_{Sc}]^t\\ \bar{I}_{Sn}&=[I_{S1}\ I_{S2}\ I_{S3}]^t=[S]^{-1}[I_{Sa}\ I_{Sb}\ I_{Sc}]^t\end{aligned}\right\} \qquad (4\text{-}9)$$

Application of the transformation to modal quantities results in a multiphase line being decomposed into a number of single-phase uncoupled models of the type shown in Fig. 4-1. Details of the two-port equations decomposition have been given in Section 3.3.3. For each modal component, there is an equation pair of the form of Eqs. (4-1) and (4-2). Thus for a single-circuit line, there are three pairs of such equations corresponding to the modes 1,2,3 so that for mode-2, for example, the equation pair used would take the form of Eqs. (4-10) and (4-11).

$$V_{F2}=A_{S2}V_{S2}-B_{S2}I_{S2} \qquad (4\text{-}10)$$

$$V_{F2}=A_{R2}V_{R2}+B_{R2}I_{R2} \qquad (4\text{-}11)$$

Any one or more mode pair equations can be used to determine the fault location. For example, a mode-2 based evaluation given by Eq. (4-12) yields:

$$x=[\tanh^{-1}(-N_2/M_2)]/\Gamma_2 \qquad (4\text{-}12)$$

where $M_2=-Z_{02}\cosh(\Gamma_2 L)I_{R2}-\sinh(\Gamma_2 L)V_{R2}+Z_{02}I_{S2}$

$N_2=\cosh(\Gamma_2 L)V_{R2}+Z_{02}\sinh(\Gamma_2 L)I_{R2}-V_{S2}$

Eq. (4-12) and any companion equations formed using the other modes is the exact equivalent of Eq. (4-5). The appropriate modal surge impedances required are readily determined from the matrix product $[Z_{0n}]=[\Gamma]^{-1}[Q]^{-1}[Z][S]$ in which $[\Gamma]$ is a diagonal matrix of so-called modal propagation constants comprising the square root of the eigenvalues of the matrix product [Z][Y], [15,16]. Matrix $[Z_{0n}]$ thus takes the diagonal form of $[Z_{01}\ Z_{02}\ Z_{03}]$ for a 3-phase line, the individual values being the modal surge impedances.

4.2.3 Extension to Double-Circuit Lines

The fault location technique can be extended to double-circuit applications by utilising the phasor values from the second circuit e.g., $[V_{Fa,b,c,A,B,C}]$ and $[I_{Sa,b,c,A,B,C}]$ (see Fig. 3-1). In this case, the two-port matrices A_S, B_S, A_R and B_R are 6x6 matrices. Eqs. (4-10) and (4-11) can then be generalised for a double-circuit line, i.e.:

$$[V_{Fa,b,c,A,B,C}]=[A_S][V_{Sa,b,c,A,B,C}] -[B_S][I_{Sa,b,c,A,B,C}] \quad (4\text{-}13)$$

$$[V_{Fa,b,c,A,B,C}]=[A_R][V_{Ra,b,c,A,B,C}] +[B_R][I_{Ra,b,c,A,B,C}] \quad (4\text{-}14)$$

Consequently the modal form of Eq. (4-9) consists of 6 modes of current and voltage in a double-circuit line:

$$\left.\begin{aligned}
\bar{V}_{Sn} &= \begin{bmatrix} V_{S1} \\ \cdots \\ V_{S6} \end{bmatrix} = [V_{S1}\ V_{S2}\ V_{S3}\ \cdots\ V_{S6}]^t \\
&= [Q_D]^{-1}[V_{Sa}\ V_{Sb}\ V_{Sc}\ \cdots\ V_{SC}]^t \\
\bar{I}_{Sn} &= \begin{bmatrix} I_{S1} \\ \cdots \\ I_{S6} \end{bmatrix} = [I_{S1}\ I_{S2}\ I_{S3}\ \cdots\ I_{S6}]^t \\
&= [S_D]^{-1}[I_{Sa}\ I_{Sb}\ I_{Sc}\ \cdots\ I_{SC}]^t
\end{aligned}\right\} \qquad (4\text{-}15)$$

where $[Q_D]$ and $[S_D]$ are double-circuit line eigenvector matrices.

The decoupled form of Eq. (4-15) results in 6 pairs of equations, all of the basic form of Eqs. (4-7) and (4-8). The rest of fault locating routine for double-circuit lines is exactly as previously described. In this form inter-circuit faults can also be located.

4.3 Practical Aspects of the New Fault Locator

4.3.1 Eigenvalue and Eigenvector Matrix Evaluation

The eigenvalues and eigenvector matrix required by the new fault location technique are readily evaluated at power frequency and can be programmed for any application into the algorithm from a knowledge of the line geometry. Alternatively, the algorithm can be arranged to accept physical geometries and to determine eigenvalues and eigenvector matrix when a locator is installed. These techniques are general and include for the effect of line asymmetry. However, it is shown in Chapter 5 that in most cases (even for untransposed lines) an acceptable accuracy

can be achieved if perfectly line transposition is assumed. In this case, irrespective of the line geometry, the eigenvalues and eigenvector matrix take the simplified form given in Appendix 3B for any transmission line application. By doing so, the modal components can easily be evaluated.

4.3.2 Synchronisation of Sending and Receiving End Data

It is evident from Eq. (4-3) that the basic fault locating algorithm involves entering data derived from both ends of the line and this in turn requires that the relevant phasor quantities are related to a common time reference. Time synchronisation of the measurands at both ends could be achieved by means of a continuous data channel linking each end, but this approach is unwieldy. In practice, prefault voltage and current data at one end can be used to provide a common reference to relate such data to that measured at the receiving end. For example, the prefault mode-2 voltage at the sending end can be calculated in the equipment at the receiving end from the two-port network equations for an unfaulted line as given in Eq. (4-16). This approach obviates the need for data synchronisation via a communication link.

$$V_{S2}=\cosh(\Gamma_2 L)V_{R2}-Z_{02}\sinh(\Gamma_2 L)I_{R2} \qquad (4\text{-}16)$$

Evaluation of Eq. (4-16) gives the phase angle between the sending and receiving end voltages and thereby provides the time between the prefault zero-crossing of the measurands at each end. The latter time is used to

provide a common time reference which in turn relates the sampled voltage data derived at each end. A similar process is applied in respect of sampled current data, where the relevant two-port relationship used to derive a common current reference is as given in Eq. (4-17):

$$I_{S2}=\sinh(\Gamma_2 L)V_{R2}/Z_{02}-\cosh(\Gamma_2 L)I_{R2} \qquad (4\text{-}17)$$

However, for short line applications where the line capacitance current is negligible, the prefault currents at both ends of the line are the same. That is, the prefault condition is:

$$I_S=-I_R \qquad (4\text{-}18)$$

Thus observation of the prefault current yields the phase relationship between the "clocks" at the two ends with which all the voltages and currents are compared.

It is shown in Chapter 7 that the performance of the new algorithm against voltage and current phase angle errors is quite well. It maintains its high accuracy even in the presence of an error of up to $\pm 10^{o}$ in the current or voltage phase angle. In other words, for most line lengths a short line assumption to use Eq. (4-18) for the synchronisation of phasor data can be justified.

4.3.3 Hardware Description

Voltage and current waveforms are sampled in real time at both line ends. When a start signal is received this process continues until the postfault data has also been

captured. All further processing can be done off-line. The data is band pass filtered and the power frequency phasor information extracted. The modal transformation is then applied to these phasors using the previously calculated eigenvector matrix. The modal voltage and current are then exchanged with those from the equipment at the remote line end. Note that it is only the phasor values that need to be transferred and not the entire data set. This can be done automatically or by voice over a telephone link, for example. Once the values are exchanged, the modal A_n and B_n coefficients e.g. A_{S2}, B_{S2}, A_{R2} and B_{R2} of Eqs. (4-10) and (4-11) are formed using the input line parameters and the distance to fault is then determined.

Fig. 4-3 shows in block diagram form the main hardware elements required for the distance to fault locator equipment. The three phase voltage and current signals from the line transformers are fed, via isolation transformers and anti-alias filters, into a multiplexer. The output from the multiplexer is then passed through a sample and hold gate and into an analogue to digital convertor for digitisation. The resultant digitised signals are stored in a cyclic buffer in the microprocessor's random access memory (RAM), by the direct memory access unit (DMA). The input/output unit is also sampled continuously, until a start signal is received from the line protection equipment (typically a distance relay). Also required are a keypad and alpha numeric display. These are used to display and transfer the modal

voltage and current vectors, and to display the final distance to fault result. They are also used to enter the line settings for storage in the microprocessors electrically erasable PROM.

4.4 Summary

A new fault location algorithm has been described and the basic equations derived. The technique uses the phasor values of current and voltage at the line ends which are synchronised from a knowledge of prefault phasor data. For a single-phase network, the idea is to equate two equations obtained for the fault point voltage; one from the sending end phasor data and the other from the remote end phasor data. In order to generalise the idea to multiphase systems, the line eigenvalues and eigenvector matrix are used to convert a multiphase system into a number of single-phase modal networks. Each modal network can be solved for fault location, provided that the corresponding modal voltage and current are produced by the fault. In general the number of modal networks are equal to the number of phase conductors. In deriving the fault location equations, no assumptions are made in respect of fault resistance, source network, line shunt capacitance and fault type. The new technique can also take into account line conductor asymmetry. The phasor data from the remote end can be transferred by voice over a telephone link.

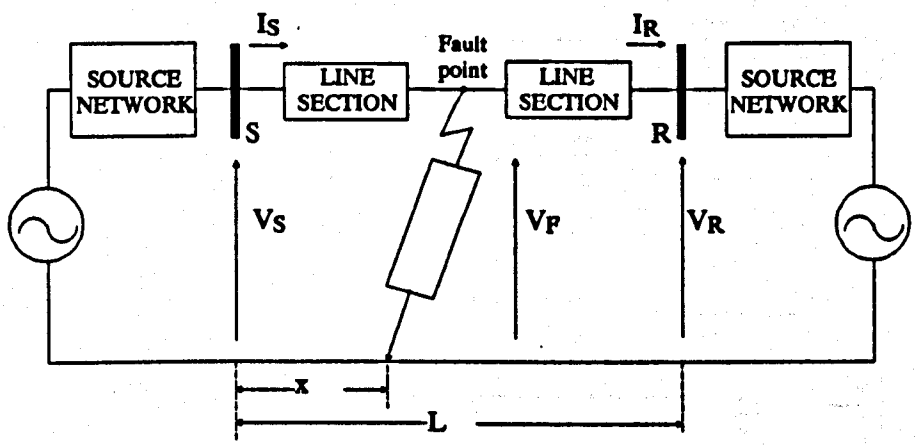

Fig. 4-1 Single-phase faulted line/source network

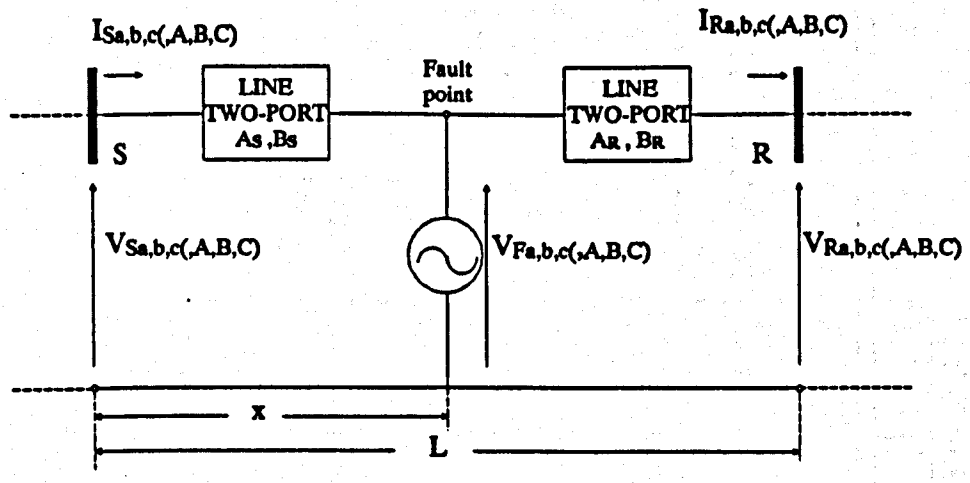

Fig. 4-2 Single-line diagram of faulted multiphase line described by two-port matrices (subscripts a, b, c, A, B, C are for double-circuit lines)

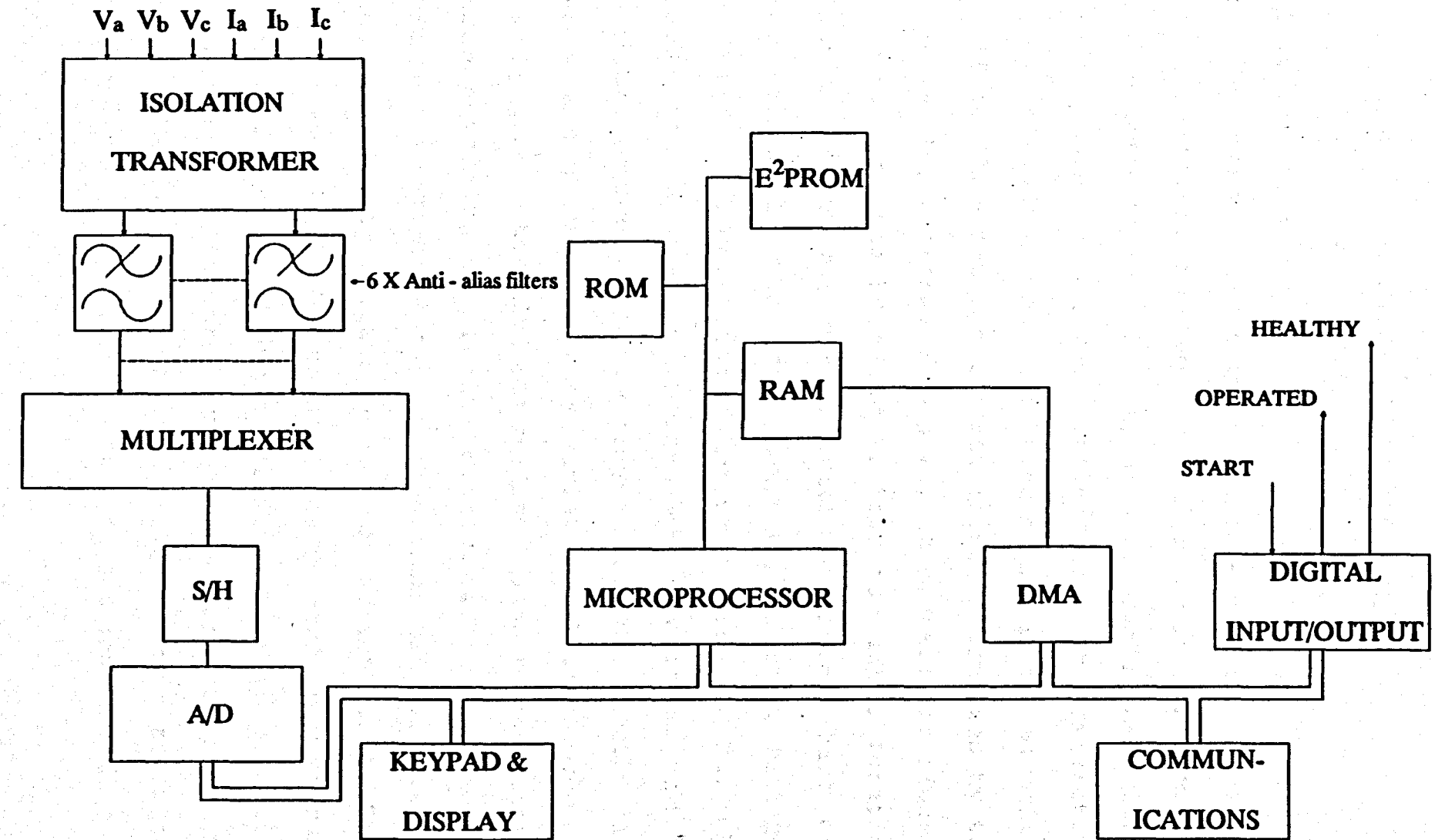

Fig. 4-3 Hardware block diagram

CHAPTER 5

PRACTICAL CONSIDERATIONS

5.1 Introduction

It is necessary to determine the accuracy of the new fault location algorithm using simulation tests prior to any on-site tests because the latter are normally associated with high cost and other difficulties. The simulation method primarily reveals the inaccuracies in the algorithm itself and does not include any errors introduced by the hardware and/or transducers i.e., it reveals the highest accuracy that can be expected from the fault location algorithm. However, non-algorithmic errors which are introduced by hardware limitations and incorrect settings can also be investigated by this method. For the simulation studies a program was developed and is described in Chapter 3. The program uses distributed line parameters to derive phase variable relationships and thereby gives a detailed and realistic line representation under operating and fault conditions. The values of voltage and current phasors at the terminating busbars are produced for any fault type and source condition. This Chapter and the following ones are devoted to different aspects of the simulation studies in order to establish the accuracy of the new algorithm. In this Chapter the simplifying aspects of the new fault location algorithm for its future commercial application are considered.

It has been ascertained that if the new locator is set using the exact parameters derived from the actual eigenvalues/eigenvectors for an untransposed line, the only errors that occur are those due to hardware i.e., the algorithmic error is zero. However, the new algorithm should maintain its accuracy for line parameters and phase quantities which are normally available in the conventional relaying system. This enables the use of the new fault locator for any type of transmission line without any need for special arrangement and setting. Two major issues of this category is investigated in the following Sections; adapting a single-circuit fault locator to a double-circuit line and using transposed line parameters for untransposed lines. It is worth mentioning that in the simulation studies presented in this thesis the term "transposed line" means a line which is perfectly transposed and balanced.

5.1.1 Test Circuits

The following line configurations were chosen for the test purpose.

(a) Single-circuit 500kV horizontally constructed line as commonly used in the USA (Fig. 5-1).

(b) Single-circuit 400kV vertically constructed line (Fig. 5-2). This line configuration is an example of maximum line conductor asymmetry. This line configuration could happen when one circuit of a double-circuit line tower is wired, and it was chosen in order to measure the maximum inaccuracy resulting

from non-transposition of the line.

(c) Double-circuit 400kV line as commonly used in the UK supergrid system (Fig. 5-3).

For all test results presented in this thesis the zero and positive sequence source impedances were assumed equal. The wiring data and earth resistivity for the line configurations were as follows:

-Phase conductor= 4x54/7/0.33cm s.c.a. with .305m bundle spacing (s.c.a=steel core aluminium conductor)

-Earth wire= 54/7/0.33cm s.c.a

-Earth resistivity, assumed homogeneous= 100Ωm.

5.1.2 Test Procedure

In this Chapter the test results are first given for unloaded short (100km), medium (250km) and long (400km) lines with identical sources and faults at positions between 1km from the sending end and 1km from the receiving end inclusive. Then for the case which gives the highest error, i.e. fault at 1km distance from the receiving end, different prefault loading conditions and source configurations are considered. A very high fault resistance (100Ω) is included in most cases.

5.1.3 Fault Resistance Arrangements

For each type of fault, an example of fault resistance arrangement used by the line simulation program is shown in Fig. 5-4. Throughout the simulation studies in this thesis, these arrangements are used, but different phase(s) may be involved. However, as mentioned in Chapter

4 the new algorithm is independent of the fault point network, e.g. the complex form of fault point network on a double-circuit line which is shown in Fig. 5-5 has no effect on the accuracy of the new algorithm.

5.2 Double-Circuit Line Application

The new fault location algorithm is general, i.e. it can be used for any multiphase system. Only the phase values at both ends of the line are required. For example, for double-circuit lines six phase voltages and six phase currents at each end are used and therefore the algorithm can locate inter-circuit as well as intra-circuit faults. However, it is a normal practice in double-circuit line relaying to deal with each circuit separately and the effect of the other circuit is considered only by its residual current and voltage.

5.2.1 Transposed Double-Circuit Lines

In order to see the effect of the sound circuit on the faulted circuit in the new algorithm, the fault location equation from Chapter 4 using an aerial mode, say mode-2, is rewritten:

$$A_{S2}V_{S2}-B_{S2}I_{S2}=A_{R2}V_{R2}+B_{R2}I_{R2} \qquad (5\text{-}1)$$

where $A_{S2}=\cosh(\Gamma_2 x)$, $B_{S2}=\sinh(\Gamma_2 x)Z_{02}$

$A_{R2}=\cosh(\Gamma_2(L-x))$, $B_{R2}=\sinh(\Gamma_2(L-x))Z_{02}$

Γ_2=mode-2 propagation constant

Z_{02}=mode-2 characteristic impedance

L=line length , x=distance to fault

As shown in Appendix 3B, for double-circuit perfectly transposed lines the mode-2 currents and voltages are evaluated from the phasor ones as follows:

$$\left.\begin{aligned} V_{S2} &= V_{Sa} - V_{Sc} + V_{SA} - V_{SC} \\ I_{S2} &= I_{Sa} - I_{Sc} + I_{SA} - I_{SC} \\ V_{R2} &= V_{Ra} - V_{Rc} + V_{RA} - V_{RC} \\ I_{R2} &= I_{Ra} - I_{Rc} + I_{RA} - I_{RC} \end{aligned}\right\} \qquad (5\text{-}2)$$

For the faults on circuit-'abc', it can be seen from Eq. (5-2) that when using mode-2 only the phase-'A' minus phase-'C' voltages and currents from circuit-'ABC' are required to be linked to the fault locator of circuit-'abc', instead of the residual current and voltage as linked conventionally. Also in using the earth-mode (mode-1) the modal currents and voltages are:

$$\left.\begin{aligned} V_{S1} &= V_{Sa} + V_{Sb} + V_{Sc} + V_{SA} + V_{SB} + V_{SC} \\ I_{S1} &= I_{Sa} + I_{Sb} + I_{Sc} + I_{SA} + I_{SB} + I_{SC} \\ V_{R1} &= V_{Ra} + V_{Rb} + V_{Rc} + V_{RA} + V_{RB} + V_{RC} \\ I_{R1} &= I_{Ra} + I_{Rb} + I_{Rc} + I_{RA} + I_{RB} + I_{RC} \end{aligned}\right\} \qquad (5\text{-}3)$$

Eq. (5-3) shows that when using mode-1 the conventional relaying scheme provides the necessary data from the sound circuit which are the residual values, e.g.:

$$V_{S1} = V_{Sa} + V_{Sb} + V_{Sc} + V_{S,residual} \text{(from circuit-'ABC')} \qquad (5\text{-}4)$$

It should be noted that the earth-mode cannot be used

for phase-to-phase and 3-phase faults as these types of fault do not produce earth-mode current and voltage. Moreover, in a transposed line the prefault earth-mode component which is produced by the asymmetry of line conductors is not present. However, an aerial-mode, e.g. mode-2, can be used for any type of fault on transposed lines.

Considering a fault on circuit-'abc', the fault location equation using mode-2 can be written in the following form:

$$A_{S2}(V_{Sa}-V_{Sc})+A_{S2}(V_{SA}-V_{SC})-B_{S2}(I_{Sa}-I_{Sc})-B_{S2}(I_{SA}-I_{SC})= A_{R2}(V_{Ra}-V_{Rc})+A_{R2}(V_{RA}-V_{RC})+B_{R2}(I_{Ra}-I_{Rc})+B_{R2}(I_{RA}-I_{RC}) \quad (5\text{-}5)$$

Knowing that in a transposed double-circuit line one circuit has the same effect on each phase of the other circuit because of identical mutual impedances, Z_M, and mutual admittances, Y_M, in the [Z] and [Y] matrices, therefore subtracting phase-'c' voltage or current from phase-'a' values in Eq. (5-5), e.g. $(V_{Sa}-V_{Sc})$, cancels out the effect of circuit-'ABC'. This means the terms associated with the data from the sound circuit, i.e. V_{SA}, I_{SA}, etc., can be ignored in a transposed double-circuit line when mode-2 is used and therefore Eq. (5-5) is reduced to the following form:

$$A_{S2}(V_{Sa}-V_{Sc})-B_{S2}(I_{Sa}-I_{Sc})=A_{R2}(V_{Ra}-V_{Rc})-B_{R2}(I_{Ra}-I_{Rc}) \quad (5\text{-}6)$$

The same discussion applies to mode-3 (the other aerial-mode) where modal values are evaluated as below:

$$\left.\begin{aligned} V_{S3} &= V_{Sa} - 2V_{Sb} + V_{Sc} + V_{SA} - 2V_{SB} + V_{SC} \\ I_{S3} &= I_{Sa} - 2I_{Sb} + I_{Sc} + I_{SA} - 2I_{SB} + I_{SC} \\ V_{R3} &= V_{Ra} - 2V_{Rb} + V_{Rc} + V_{RA} - 2V_{RB} + V_{RC} \\ I_{R3} &= I_{Ra} - 2I_{Rb} + I_{Rc} + I_{RA} - 2I_{RB} + I_{RC} \end{aligned}\right\} \quad (5\text{-}7)$$

Results of the simulation tests shown in Table 5-1 for phase-'a'-to-earth faults and in Table 5-2 for phase-'a'-to-phase-'b' faults confirm the above discussion. It can be seen that for any fault condition there is no error using the aerial-modes (modes 2 and 3). In Cases 18 to 30, different source configurations and prefault loadings are considered for the extreme case of a fault at 399km on a 400km line. Also, it is seen that there is very little error using earth-mode (mode-1) for 'a'-earth faults. This is because the line is balanced and therefore the residual current and voltage from circuit-'ABC' are insignificant which results in a very small error when the terms associated with the sound circuit are ignored. But as it has been explained earlier in this Chapter the test results given in Table 5-2 show that the earth-mode can not be used for phase-to-phase faults. Many other tests were carried out for different types of fault involving different phases of circuit-'abc' without any data from circuit-'ABC'. The results are the same as those shown in Table 5-1 for earth faults, including double-phase-to-earth faults, and Table 5-2 for phase faults, including 3-phase faults. For reasons of brevity these results are not included. Furthermore the same results are obtained

using superimposed voltages and currents or postfault total voltages and currents.

To summarize, it has been shown that for a transposed double-circuit line the new algorithm gives no error when it is used on one circuit without any data linked from the other circuit. Knowing that nearly all previously proposed algorithms assume a perfectly balanced system then this makes the job complete if the most accurate fault location algorithm for a transposed line is intended. The algorithm is simple to apply for transposed lines and one of the aerial-modes can be used for any type of fault. Irrespective of line configuration a unique eigenvector matrix can be defined for voltage and current. For example, using the eigenvector matrix defined in Appendix 3B for transposed lines, mode-2 currents and voltages can easily be derived by subtracting phase-'c' voltage and current from phase-'a' values. Given the line propagation constants and the line length, the values of cosh(ΓL) and sinh(ΓL) in the fault location equation can be pre-evaluated and set into the relay's processing unit.

5.2.2 Untransposed Double-Circuit Lines

Now we proceed to investigate the case for untransposed lines. Because of the complexity associated with untransposed lines it is difficult to discuss the effect of the sound circuit in fault location equations for different modes as has been done for transposed lines. However, the line simulation program makes it possible to

examine the accuracy of the new algorithm when the data from the faulted circuit only are available. Again, for reasons of brevity, results for 'a'-earth and 'b'-'c' faults shown in Tables 5-3 and 5-4 have been selected from the results of the tests carried out for all types of fault. The results obtained for other types of earth faults (including double-phase-to-earth faults) and those results for other phase faults (including 3-phase faults) are very similar to the results shown in Table 5-3 and 5-4 respectively. It should be noted that double-circuit line eigenvalues and eigenvectors are applied in cases of both transposed and untransposed line. However, this will not degrade the results obtained as eigenvalues and eigenvectors of a line are predetermined values from the line geometry.

Table 5-3 for 'a'-earth faults shows that for any fault condition, using mode-1 and superimposed values of voltage and current, the modulus of error is less than 0.6% of the total line length. However, for phase-to-phase faults shown in Table 5-4 the best results are achieved using mode-2 and the superimposed values of current and voltage. It can also be seen from Table 5-4 that for faults close to the stronger source the error is smaller, e.g. compare Cases 18 and 19. There are some Cases in Table 5-4 where the modulus of error is higher than 1%, but this high error occurs for the faults very close to the source. For example, in Case 19 where the fault position is at 249km of a 250km line and the source near

the fault point is 7 times weaker than the other source capacity, the error modulus is 2.4%. This Case is not a very realistic one and it cannot degrade the accuracy of the new algorithm. Other fault location algorithms cannot handle such cases as is shown in Chapter 6. From these results the overall conclusions for the untransposed double-circuit line using faulted circuit data only are:

(a) Superimposed values of current and voltage must be used as when the line is loaded before the fault, the error is very high if the total values of postfault current and voltage are used.

(b) Mode-1 (earth-mode) should be used for earth faults while mode-2 (aerial-mode) is only suitable for phase faults. However, it is shown in the following Section that by using the transposed line parameters for untransposed double-circuit lines, mode-2 will be accurate enough for all types of fault.

5.3 Simplifying the Algorithm for Untransposed Lines by Using Transposed Line Eigenvalues and Eigenvectors

As shown in Chapter 3, the line eigenvalues and eigenvector matrix are computed from the line series impedance and shunt admittance matrices ([Z],[Y]) and these are in turn computed from a knowledge of the line conductor geometry, earth plane resistivity and the conductor parameters. From the line propagation constants (which are the square roots of eigenvalues) and eigenvector matrix the line modal surge impedances are

evaluated. Propagation constants and modal surge impedances are the basic parameters set into the new locator.

Although a simple eigenvector matrix with real elements can be defined for all transposed lines irrespective of their configurations, for untransposed lines the matrix needs to be evaluated for each line application and set into the locator. Furthermore while voltage and current eigenvector matrices are different for untransposed lines, they are identical for transposed lines. The line simulation program can evaluate the eigenvalues and eigenvector matrix for any untransposed line.

In general, the eigenvector matrix and its inverse for an untransposed line have complex elements so in practice it is difficult to evaluate modal quantities from a complex combination of phasor values. For example, for the transposed single-circuit vertical line mode-2 voltage and current are evaluated from:

$$\left.\begin{aligned} V_2 &= V_a - V_c \\ I_2 &= I_a - I_c \end{aligned}\right\} \qquad (5\text{-}8)$$

but when it is untransposed we have:

$$\left.\begin{aligned} V_2 &= (-0.16+j0.08)V_a + (0.04-j0.05)V_b + (0.18-j0.05)V_c \\ I_2 &= (0.40-j0.07)I_a + (-0.16+j0.08)I_b + (-0.56)I_c \end{aligned}\right\} \qquad (5\text{-}9)$$

Owing to the complexity associated with the eigenvalues and eigenvectors evaluation and application for untransposed lines, the algorithm was tested for untransposed lines using their assumed transposed eigenvalues and eigenvectors.

If perfect line transposition is assumed, the calculation of the propagation constants and modal surge impedances is simplified since it is readily shown in Appendix 3B that, for example, using mode-2 for a single-circuit line they can be expressed directly in terms of the positive phase sequence line impedance, Z_p, and shunt admittance, Y_p, per unit length of line, i.e. $\Gamma_2=(Z_pY_p)^{\frac{1}{2}}$ and $Z_{02}=(Z_p/Y_p)^{\frac{1}{2}}$. Also, as mentioned earlier, the assumption of perfect transposition leads to eigenvector matrices for current and voltage which are equal ([S]=[Q]) and independent of the line geometry. The need to calculate the voltage and current eigenvector matrices is then avoided and they take the special form given in Eq. (5-10). It should be noted that many eigenvector matrices can be defined for transposed lines. The eigenvector matrix of Eq. (5-10) is real and simple to implement.

$$[S]=[Q]=\begin{bmatrix}1 & 1 & 1\\ 1 & 0 & -2\\ 1 & -1 & 1\end{bmatrix} \qquad (5\text{-}10)$$

The simulation test results for different line configurations are given in the following Sections. The results have been chosen for some extreme fault conditions

which give the highest errors. The accuracy of the algorithm is shown for 'a'-earth faults as examples of earth faults, and 'a'-'b' and 'b'-'c' faults as examples of phase faults. The conclusions, however, also take into consideration the results of other types of fault, involving different phase(s), which are not given for the purpose of brevity.

5.3.1 Single-Circuit Horizontal Lines

The results for 'a'-earth faults are given in Table 5-5 for mode-1 and mode-2. The results for mode-3 (not shown) are less accurate than mode-2. In addition the results are given for both the total postfault voltages and currents and the superimposed ones. It can be seen from these results that mode-1 gives more accurate results than mode-2. It is clear that the superimposed values of current and voltage should be used since the results using the total values are poor when the line is prefault loaded. The results for other types of fault involving earth confirm that mode-1 is the most accurate mode for earth faults.

The results for 'a'-'b' and 'b'-'c' faults are given in Table 5-6 for mode-2 and mode-3. For the phase faults earth-mode cannot be used as the only source of earth-mode current or voltage is unsymmetrical line conductor geometry which does not give significant earth-mode values. The superimposed values of voltage and current are used in order to suppress the effect of prefault load. It

can be seen from Table 5-6 that there is no difference between mode-2 and mode-3 for 'a'-'b' faults, but mode-3 is much better for 'b'-'c' faults. For 'a'-'c' faults much more accurate results are obtained using mode-2 while for 3-phase fault mode-3 results are marginally better than mode-2. The results for 'a'-'c' and 3-phase faults are not shown for the purpose of brevity. Therefore for phase faults on horizontal line configurations the fault type identification is required when transposed line parameters are used for untransposed lines.

It should be noted that the single-circuit horizontal line is a special case which must always be considered in the performance evaluation of the new algorithm. The above mentioned selection of the appropriate mode for a fault is not necessary in real life and the new algorithm is much simpler and more accurate when it is implemented for horizontal single-circuit lines. This is because the phase arrangement of Fig. 5-1 for the horizontal line, with phase-'c' in the middle, does not occur in real systems, which have the 'a'-'b'-'c' phase arrangement. The arrangement of Fig. 5-1 was deliberately chosen as in the simulation program the routine for evaluating the eigenvalues does not converge when phase-'b' is the middle phase conductor. However, it is important to note that the transposed lines eigenvector matrix of Eq. (5-10) is also the eigenvector matrix of the untransposed horizontal line with the 'a'-'b'-'c' phase arrangement. Therefore, the errors for untransposed horizontal lines are in practice

much lower than the simulation results given in this thesis. Even with the 'a'-'c'-'b' phase arrangement which is used in the simulation studies throughout this thesis, mode-2 current and voltage are simply evaluated from:

$$\left.\begin{aligned} V_2 &= V_a - V_b \\ I_2 &= -I_a + I_b \end{aligned}\right] \qquad (5\text{-}11)$$

Comparing Eq. (5-11) with mode-2 current and voltage of the 'a'-'b'-'c' phase arrangement which are:

$$\left.\begin{aligned} V_2 &= V_a - V_c \\ I_2 &= I_a - I_c \end{aligned}\right] \qquad (5\text{-}12)$$

it is seen that in both cases, mode-2 values are evaluated from the phasor difference between the outer phase conductors. Therefore, the mode-2 values can be simply evaluated for any type of fault on the horizontal lines giving no error irrespective of the line transposition status.

Again, it is emphasised that the simulation errors shown in this thesis for the untransposed horizontal line are higher than would occur in practice.

5.3.2 Single-Circuit Vertical Lines

From the results of Table 5-7 for 'a'-earth faults it is obvious that mode-1 and the superimposed values of voltage and current should be used. Similar result were obtained

for earth faults involving other phase(s).

The phase fault results are given in Table 5-8. From these results and the results for 'a'-'c' and 3-phase faults (not shown) it is concluded that except for 'b'-'c' faults which requires mode-3 to be applied, mode-2 must be used for higher accuracy.

5.3.3 Double-Circuit Lines

The double-circuit line test results are given in Tables 5-9 and 5-10 for earth and phase faults respectively. It should be noted that in the case of the double-circuit line, only the phasor data from the faulted circuit were used. For earth faults, it is interesting to note that mode-2 can be used, though mode-1 gives slightly better results. Also mode-2 should be used for any type of phase fault including 3-phase faults. As before, for any type of fault, superimposed values of voltage and current must be used when the untransposed line is assumed perfectly transposed.

It is important to note that, comparing Tables 5-3 and 5-9, for earth faults on untransposed double-circuit lines mode-2 gives more accurate results by using the assumed transposed parameters.

Therefore, for double-circuit lines mode-2 should be used for any type of phase faults and no fault identification is required. Also for these lines the results using mode-2 are still accurate for earth faults.

5.4 Summary

In this Chapter because of practical limitations the accuracy of the new algorithm has been evaluated for the input data only from the faulted circuit of a double-circuit line and assuming perfect transposition for untransposed lines.

It has been shown that for double-circuit lines it is possible to use only the faulted circuit voltages and currents for an accurate fault location. In this way each circuit fault location can be dealt with separately without any data linked from the other circuit. For transposed lines mode-2 (aerial-mode) can be used for any type of fault on one circuit giving no algorithmic error. However, for untransposed lines a mode selection is required to select mode-1 (earth-mode) for earth faults and mode-2 for phase faults.

Because of the difficulties in evaluating the eigenvalues and the eigenvector matrix which relate modal voltages and currents to the phasor ones, the algorithm was tested for untransposed lines using the assumed transposed line eigenvalues and eigenvector matrix. For extreme fault conditions which rarely occur in real life, acceptable accuracy has been observed from the simulation test results. Moreover, for untransposed double-circuit lines even by assuming perfect transposition as well as using only the data from the faulted circuit, very accurate results have been observed. Also it has been

shown that for any type of fault on single-circuit horizontal lines and double-circuit lines an aerial-mode can be used thereby avoiding the use of indeterminate earth path resistivity as required for earth-mode surge impedance and eigenvalue calculations.

In conclusion, when perfect transposition is assumed for untransposed lines the following points must be considered:

(a) For any type of fault and line configuration the superimposed values of current and voltage should be used.

(b) For the vertical single-circuit line configuration, mode selection is required as earth-mode must be used for earth faults and an aerial-mode for phase faults.

(c) For the horizontal line configuration with the phase arrangement of Fig. 5-1, an aerial-mode can be used for any type of fault. For the phase arrangement in practice, i.e. phase-'b' in the middle of the other phases, mode-2 can be used for any type of fault giving almost no error.

(d) For the double-circuit line using the data from the faulted circuit, mode-2 can be used for any type of fault.

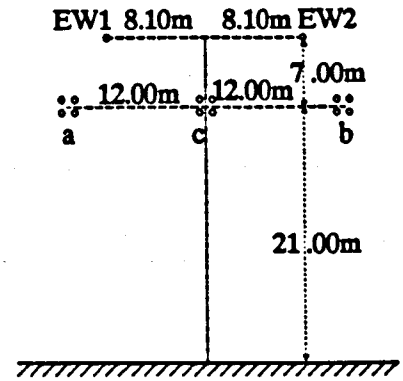

Fig. 5-1 Horizontal single-circuit line

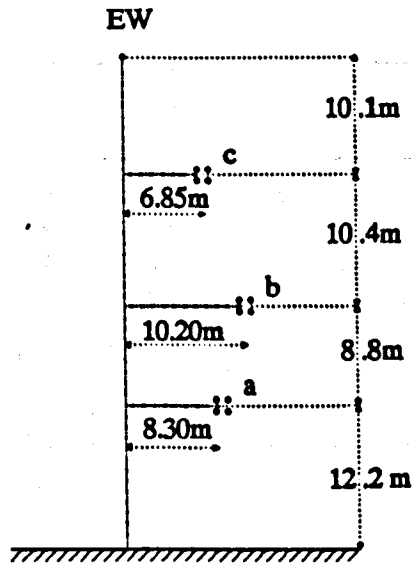

Fig. 5-2 Vertical single-circuit line

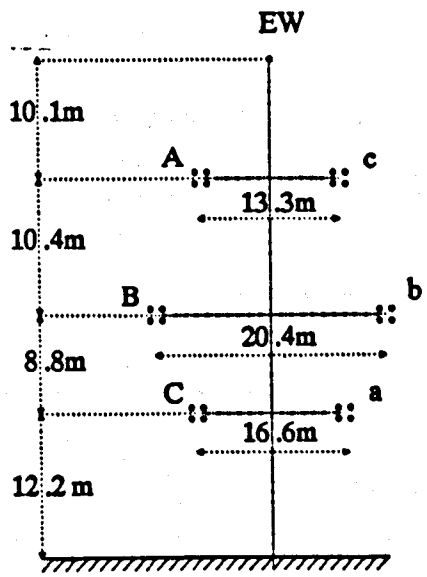

Fig. 5-3 Double-circuit line

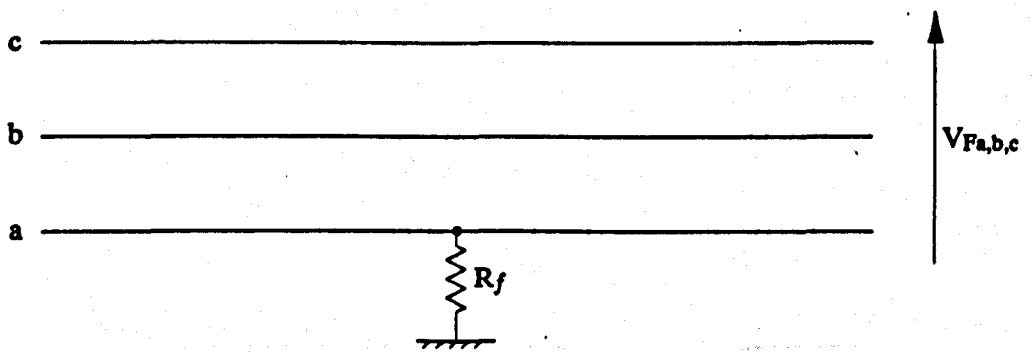

(a) 'a'-earth fault

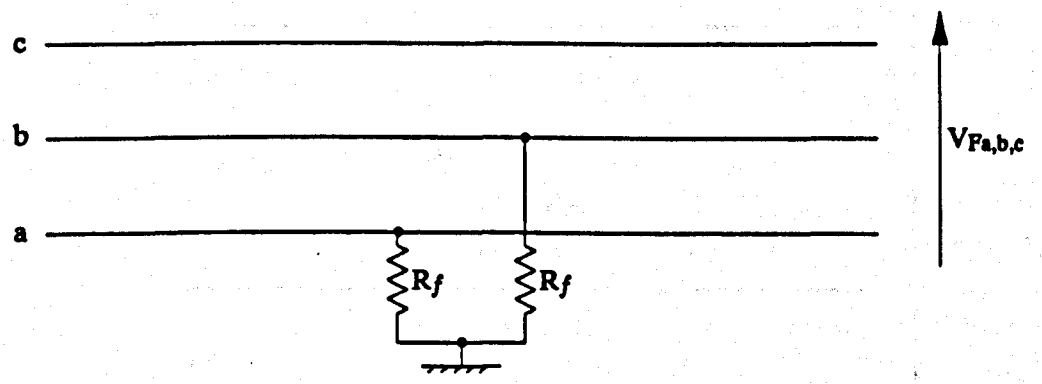

(b) 'a'-'b'-earth fault

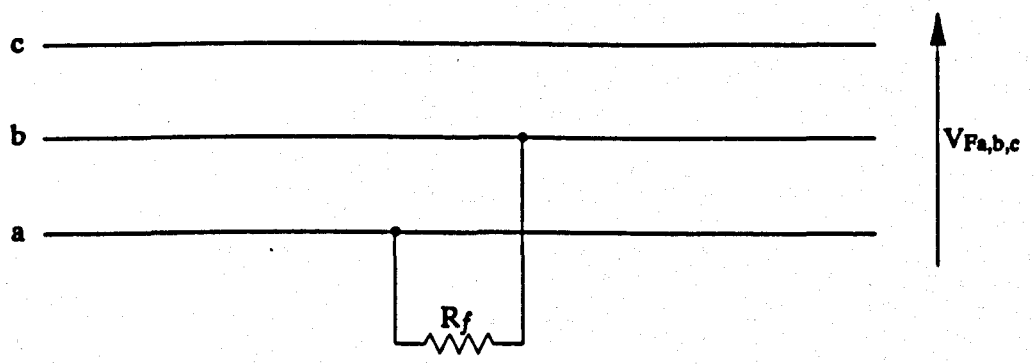

(c) 'a'-'b' fault

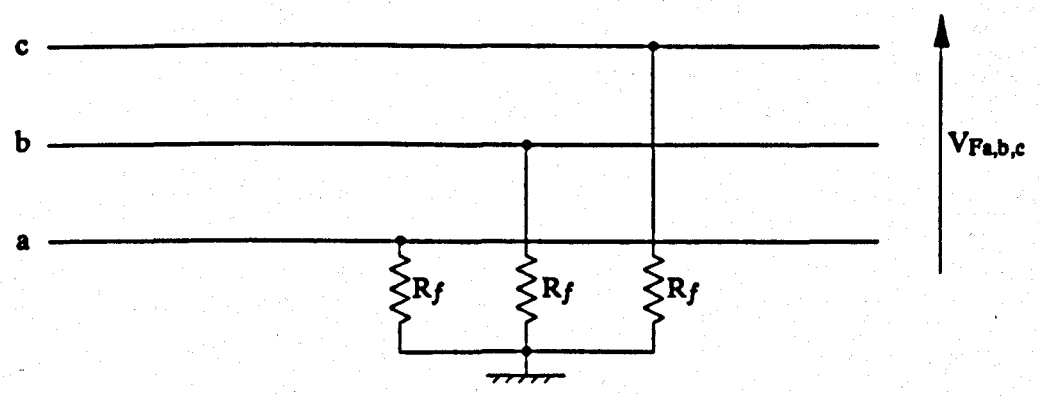

(d) 3-phase fault

Fig 5-4 Fault resistance arrangment for different types of fault

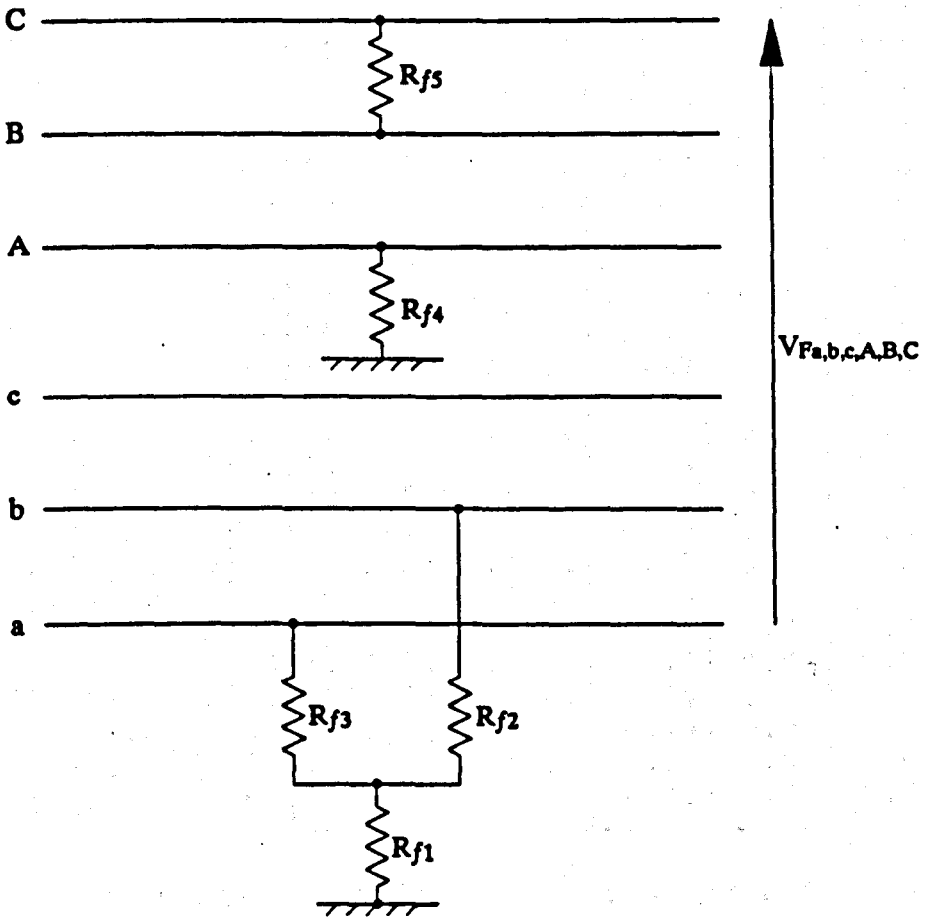

Fig 5-5 A complex fault situation

No	L	x	Source Data Cap. (GVA)		X/R ratio		R_f (Ω)	Load angle (deg.)		Error (%)		
	km	km	S	R	S	R		δ_S	δ_R	md-1	md-2	md-3
1	100	1	5	5	40	40	100	0.	0.	0.0	0.0	0.0
2	100	20	5	5	40	40	100	0.	0.	-0.01	0.0	0.0
3	100	40	5	5	40	40	100	0.	0.	-0.01	0.0	0.0
4	100	60	5	5	40	40	100	0.	0.	0.01	0.0	0.0
5	100	80	5	5	40	40	100	0.	0.	0.01	0.0	0.0
6	100	99	5	5	40	40	100	0.	0.	0.0	0.0	0.0
7	250	1	5	5	40	40	100	0.	0.	0.0	0.0	0.0
8	250	50	5	5	40	40	100	0.	0.	-0.06	0.0	0.0
9	250	100	5	5	40	40	100	0.	0.	-0.03	0.0	0.0
10	250	150	5	5	40	40	100	0.	0.	0.03	0.0	0.0
11	250	200	5	5	40	40	100	0.	0.	0.06	0.0	0.0
12	250	249	5	5	40	40	100	0.	0.	0.0	0.0	0.0
13	400	1	5	5	40	40	100	0.	0.	0.0	0.0	0.0
14	400	80	5	5	40	40	100	0.	0.	-0.17	0.0	0.0
15	400	160	5	5	40	40	100	0.	0.	-0.08	0.0	0.0
16	400	240	5	5	40	40	100	0.	0.	0.08	0.0	0.0
17	400	320	5	5	40	40	100	0.	0.	0.17	0.0	0.0
18	400	399	5	5	40	40	100	0.	0.	0.19	0.0	0.0
19	400	399	5	5	40	40	100	20.	0.	0.19	0.0	0.0
20	400	399	5	5	40	40	100	0.	20.	0.19	0.0	0.0
21	400	399	35	35	40	40	100	20.	0.	0.19	0.0	0.0
22	400	399	35	35	40	40	100	0.	20.	0.19	0.0	0.0
23	400	399	5	35	40	40	100	20.	0.	0.19	0.0	0.0
24	400	399	35	5	40	40	100	0.	20.	0.19	0.0	0.0
25	400	399	5	5	40	40	10	20.	0.	0.19	0.0	0.0
26	400	399	5	5	10	40	100	20.	0.	0.19	0.0	0.0
27	400	399	5	5	40	10	100	20.	0.	0.19	0.0	0.0
28	400	399	35	35	40	10	100	20.	0.	0.19	0.0	0.0
29	400	399	5	35	40	10	100	20.	0.	0.19	0.0	0.0
30	400	399	35	5	40	10	100	20.	0.	0.19	0.0	0.0

Table 5-1 Computed results for 'a'-earth faults on a <u>transposed</u> double-circuit line using the faulted circuit phasor data only.

<u>Key to Table</u>

S,R=near end source and remote end source, respectively

L=line length, x=actual distance to fault from S

δ_S, δ_R=phase relationship of voltage at busbar-S and busbar-R, respectively. E.g. if $\delta_S=20^o$ and $\delta_R=0^o$ then power transfer is from S to R and vice versa.

md-1=mode-1, md-2=mode-2, md-3=mode-3

Error(%)=100x(evaluated distance to fault – actual distance to fault)/total line length

No	L	x	Source Data Cap. (GVA)		X/R ratio		R_f (Ω)	Load angle (deg.)		Error (%)		
	km	km	S	R	S	R		δ_S	δ_R	md-1	md-2	md-3
1	100	1	5	5	40	40	100	0.	0.	*	0.0	0.0
2	100	20	5	5	40	40	100	0.	0.	*	0.0	0.0
3	100	40	5	5	40	40	100	0.	0.	*	0.0	0.0
4	100	60	5	5	40	40	100	0.	0.	*	0.0	0.0
5	100	80	5	5	40	40	100	0.	0.	*	0.0	0.0
6	100	99	5	5	40	40	100	0.	0.	*	0.0	0.0
7	250	1	5	5	40	40	100	0.	0.	*	0.0	0.0
8	250	50	5	5	40	40	100	0.	0.	*	0.0	0.0
9	250	100	5	5	40	40	100	0.	0.	*	0.0	0.0
10	250	150	5	5	40	40	100	0.	0.	*	0.0	0.0
11	250	200	5	5	40	40	100	0.	0.	*	0.0	0.0
12	250	249	5	5	40	40	100	0.	0.	*	0.0	0.0
13	400	1	5	5	40	40	100	0.	0.	*	0.0	0.0
14	400	80	5	5	40	40	100	0.	0.	*	0.0	0.0
15	400	160	5	5	40	40	100	0.	0.	*	0.0	0.0
16	400	240	5	5	40	40	100	0.	0.	*	0.0	0.0
17	400	320	5	5	40	40	100	0.	0.	*	0.0	0.0
18	400	399	5	5	40	40	100	0.	0.	*	0.0	0.0
19	400	399	5	5	40	40	100	20.	0.	*	0.0	0.0
20	400	399	5	5	40	40	100	0.	20.	*	0.0	0.0
21	400	399	35	35	40	40	100	20.	0.	*	0.0	0.0
22	400	399	35	35	40	40	100	0.	20.	*	0.0	0.0
23	400	399	5	35	40	40	100	20.	0.	*	0.0	0.0
24	400	399	35	5	40	40	100	0.	20.	*	0.0	0.0
25	400	399	5	5	40	40	10	20.	0.	*	0.0	0.0
26	400	399	5	5	10	40	100	20.	0.	*	0.0	0.0
27	400	399	5	5	40	10	100	20.	0.	*	0.0	0.0
28	400	399	35	35	40	10	100	20.	0.	*	0.0	0.0
29	400	399	5	35	40	10	100	20.	0.	*	0.0	0.0
30	400	399	35	5	40	10	100	20.	0.	*	0.0	0.0

Table 5-2 Computed results for 'a'-'b' phase faults on a transposed double-circuit line using the faulted circuit phasor data only.

Key to Table

S,R=near end source and remote end source, respectively
L=line length(km), x=actual distance to fault from S(km)
δ_S, δ_R=phase relationship of voltage at busbar-S and busbar-R, respectively. E.g. if $\delta_S=20^o$ and $\delta_R=0^o$ then power transfer is from S to R and vice versa.
md-1=mode-1, md-2=mode-2, md-3=mode-3
*=more than 10% error
Error(%)=100x(evaluated distance to fault – actual distance to fault)/total line length

No	L	x	Source Data Cap. (GVA)		X/R ratio		R_f (Ω)	Load angle (deg.)		Error (%) Total V&I		Sup. V&I	
	km	km	S	R	S	R		δ_S	δ_R	md-1	md-2	md-1	md-2
1	100	1	5	5	40	40	100	0.	0.	0.3	*	0.4	*
2	100	33	5	5	40	40	100	0.	0.	0.1	-7.5	0.1	-7.5
3	100	66	5	5	40	40	100	0.	0.	-0.1	7.0	-0.1	7.0
4	100	99	5	5	40	40	100	0.	0.	-0.3	*	-0.4	*
5	100	99	5	5	40	40	100	10.	0.	-2.6	*	-0.4	*
6	100	99	5	5	40	40	100	20.	0.	-4.8	*	-0.4	*
7	100	99	5	5	40	40	100	0.	20.	4.1	*	-0.4	*
8	100	99	5	35	40	40	100	0.	20.	4.1	0.3	-0.1	3.6
9	100	99	35	5	40	40	100	0.	20.	3.8	*	-0.6	*
10	100	99	35	5	10	40	100	0.	20.	3.8	*	-0.6	*
11	250	1	5	5	40	40	100	0.	0.	0.1	*	0.3	*
12	250	83	5	5	40	40	100	0.	0.	0.0	-4.1	0.0	-4.2
13	250	166	5	5	40	40	100	0.	0.	0.0	4.0	0.0	4.1
14	250	249	5	5	40	40	100	0.	0.	-0.1	*	-0.3	*
15	250	249	5	5	40	40	100	10.	0.	-1.0	*	-0.3	*
16	250	249	5	5	40	40	100	20.	0.	-2.0	*	-0.3	*
17	250	249	5	5	40	40	100	0.	20.	-1.8	*	-0.3	*
18	250	249	5	35	40	40	100	0.	20.	1.9	0.5	-0.1	1.9
19	250	249	35	5	40	40	100	0.	20.	1.6	*	-0.4	*
20	250	249	35	5	10	40	100	0.	20.	1.6	*	-0.4	0.0
21	400	1	5	5	40	40	100	0.	0.	-0.1	-8.4	0.2	-8.6
22	400	133	5	5	40	40	100	0.	0.	-0.1	-2.8	-0.1	-2.9
23	400	266	5	5	40	40	100	0.	0.	-0.1	2.8	0.1	2.8
24	400	399	5	5	40	40	100	0.	0.	0.3	8.4	0.0	8.6
25	400	399	5	5	40	40	100	10.	0.	-0.3	8.4	0.0	8.6
26	400	399	5	5	40	40	100	20.	0.	-1.0	8.3	0.0	8.6
27	400	399	5	5	40	40	100	0.	20.	1.6	8.0	0.0	8.6
28	400	399	5	35	40	40	100	0.	20.	1.8	0.4	0.2	1.3
29	400	399	35	5	40	40	100	0.	20.	1.5	8.8	-0.1	9.5
30	400	399	35	5	10	40	100	0.	20.	1.8	0.4	0.2	1.3

Table 5-3 Computed results for 'a'-earth faults on an untransposed double-circuit line using the faulted circuit phasor data only.

Key to Table

S,R=near end source and remote end source, respectively
L=line length, x=actual distance to fault from S
δ_S,δ_R=phase relationship of voltage at busbar-S and busbar-R, respectively. E.g. if $\delta_S=20^o$ and $\delta_R=0^o$ then power transfer is from S to R and vice versa.
Total V&I=total values of postfault voltage and current
Sup. V&I=superimposed values of voltage and current
md-1=mode-1, md-2=mode-2
*=more than 10% error
Error(%)=100x(evaluated distance to fault - actual distance to fault)/total line length

No	L km	x km	Source Data Cap. (GVA) S	R	X/R ratio S	R	R_f (Ω)	Load angle (deg.) δ_S	δ_R	Error (%) Total V&I md-1	md-2	Sup. V&I md-1	md-2
1	100	1	5	5	40	40	100	0.	0.	3.7	1.0	2.9	1.0
2	100	33	5	5	40	40	100	0.	0.	1.3	0.4	1.0	0.4
3	100	66	5	5	40	40	100	0.	0.	-1.2	-0.3	-1.0	-0.3
4	100	99	5	5	40	40	100	0.	0.	-3.7	-1.0	-2.9	-1.0
5	100	99	5	5	40	40	100	10.	0.	-3.5	-6.4	-2.9	-1.0
6	100	99	5	5	40	40	100	20.	0.	-1.6	*	-2.9	-1.0
7	100	99	5	5	40	40	100	0.	20.	0.9	9.2	-2.9	-1.0
8	100	99	5	35	40	40	100	0.	20.	7.7	8.0	-0.6	-0.3
9	100	99	35	5	40	40	100	0.	20.	1.4	6.9	-4.7	-2.3
10	100	99	35	5	10	40	100	0.	20.	1.5	7.0	-4.7	-2.3
11	250	1	5	5	40	40	100	0.	0.	4.2	1.4	2.1	1.4
12	250	83	5	5	40	40	100	0.	0.	1.5	0.5	0.7	0.5
13	250	166	5	5	40	40	100	0.	0.	-1.5	-0.5	-0.7	-0.5
14	250	249	5	5	40	40	100	0.	0.	-4.2	-1.4	-2.1	-1.4
15	250	249	5	5	40	40	100	10.	0.	-3.9	-3.6	-2.1	-1.4
16	250	249	5	5	40	40	100	20.	0.	-3.0	-5.8	-2.1	-1.4
17	250	249	5	5	40	40	100	0.	20.	-2.7	-2.7	-2.1	-1.4
18	250	249	5	35	40	40	100	0.	20.	1.5	2.9	-0.4	-0.3
19	250	249	35	5	40	40	100	0.	20.	-3.1	1.6	-3.2	-2.4
20	250	249	35	5	10	40	100	0.	20.	-3.1	1.6	-3.2	-2.4
21	400	1	5	5	40	40	100	0.	0.	5.0	1.4	1.4	1.4
22	400	133	5	5	40	40	100	0.	0.	1.9	0.5	0.4	0.5
23	400	266	5	5	40	40	100	0.	0.	-1.8	-0.5	-0.4	-0.5
24	400	399	5	5	40	40	100	0.	0.	-4.8	-1.4	-1.2	-1.4
25	400	399	5	5	40	40	100	10.	0.	-4.6	-2.7	-1.2	-1.4
26	400	399	5	5	40	40	100	20.	0.	-4.0	-4.1	-1.2	-1.4
27	400	399	5	5	40	40	100	0.	20.	-3.9	1.2	-1.2	-1.4
28	400	399	5	35	40	40	100	0.	20.	-0.3	1.6	0.0	-0.3
29	400	399	35	5	40	40	100	0.	20.	-4.2	0.4	-2.1	-2.0
30	400	399	35	5	10	40	100	0.	20.	-4.2	0.4	-2.1	-2.0

Table 5-4 Computed results for 'a'-'b' phase faults on an untransposed double-circuit line using the faulted circuit phasor data only.

Key to Table

S,R=near end source and remote end source, respectively
L=line length, x=actual distance to fault from S
δ_S,δ_R=phase relationship of voltage at busbar-S and busbar-R, respectively. E.g. if $\delta_S=20^o$ and $\delta_R=0^o$ then power transfer is from S to R and vice versa.
Total V&I=total values of postfault voltage and current
Sup. V&I=superimposed values of voltage and current
md-1=mode-1, md-2=mode-2
*=more than 10% error
Error(%)=100x(evaluated distance to fault − actual distance to fault)/total line length

No	L km	x km	Source Data Cap. (GVA) S	R	X/R ratio S	R	R_f (Ω)	Load angle (deg.) δ_S	δ_R	Error (%) Total V&I md-1	md-2	Sup. V&I md-1	md-2
1	100	1	5	5	40	40	100	0.	0.	0.5	1.0	0.4	0.7
2	100	33	5	5	40	40	100	0.	0.	0.2	0.3	0.2	0.3
3	100	66	5	5	40	40	100	0.	0.	-0.2	-0.3	-0.1	-0.2
4	100	99	5	5	40	40	100	0.	0.	-0.5	-1.0	-0.4	-0.7
5	100	99	5	5	40	40	100	10.	0.	-2.5	-5.2	-0.4	-0.7
6	100	99	5	5	40	40	100	20.	0.	-4.7	*	-0.4	-0.7
7	100	99	5	5	40	40	100	0.	20.	2.7	3.1	-0.4	-0.7
8	100	99	5	35	40	40	100	0.	20.	2.3	0.5	-0.1	-0.1
9	100	99	35	5	40	40	100	0.	20.	2.4	2.1	-0.6	-1.0
10	100	99	35	5	10	40	100	0.	20.	2.4	2.1	-0.6	-1.0
11	250	1	5	5	40	40	100	0.	0.	0.6	1.1	0.3	0.5
12	250	83	5	5	40	40	100	0.	0.	0.2	0.4	0.1	0.2
13	250	166	5	5	40	40	100	0.	0.	-0.2	-0.4	-0.1	-0.2
14	250	249	5	5	40	40	100	0.	0.	-0.6	-1.1	-0.3	-0.5
15	250	249	5	5	40	40	100	10.	0.	-1.3	-2.9	-0.3	-0.5
16	250	249	5	5	40	40	100	20.	0.	-2.2	-5.1	-0.3	-0.5
17	250	249	5	5	40	40	100	0.	20.	-0.7	-0.8	-0.3	-0.5
18	250	249	5	35	40	40	100	0.	20.	0.6	-0.3	-0.1	-0.1
19	250	249	35	5	40	40	100	0.	20.	0.6	0.6	-0.4	-0.6
20	250	249	35	5	10	40	100	0.	20.	0.6	0.6	-0.4	-0.6
21	400	1	5	5	40	40	100	0.	0.	0.6	1.3	0.2	0.4
22	400	133	5	5	40	40	100	0.	0.	0.2	0.5	0.1	0.1
23	400	266	5	5	40	40	100	0.	0.	-0.2	-0.5	-0.1	-0.1
24	400	399	5	5	40	40	100	0.	0.	-0.6	-1.4	-0.2	-0.4
25	400	399	5	5	40	40	100	10.	0.	-1.1	-2.4	-0.2	-0.4
26	400	399	5	5	40	40	100	20.	0.	-1.6	-3.8	-0.2	-0.4
27	400	399	5	5	40	40	100	0.	20.	0.2	-0.1	-0.2	-0.4
28	400	399	5	35	40	40	100	0.	20.	0.1	-0.7	0.0	-0.1
29	400	399	35	5	40	40	100	0.	20.	-0.1	0.2	-0.3	-0.4
30	400	399	35	5	10	40	100	0.	20.	-0.1	0.2	-0.3	-0.4

Table 5-5 Computed results for 'a'-earth faults on an <u>untransposed</u> single-circuit horizontal line using transposed line parameters.

<u>Key to Table</u>

S,R=near end source and remote end source, respectively
L=line length, x=actual distance to fault from S
δ_S,δ_R=phase relationship of voltage at busbar-S and busbar-R, respectively. E.g. if δ_S=20° and δ_R=0° then power transfer is from S to R and vice versa.
Total V&I=total values of postfault voltage and current
Sup. V&I=superimposed values of voltage and current
md-1=mode-1, md-2=mode-2
*=more than 10% error
Error(%)=100x(evaluated distance to fault − actual distance to fault)/total line length

No	L	x	Source Data Cap. (GVA)		X/R ratio		R_f (Ω)	Load angle (deg.)		Error (%) 'a'-'b'		'b'-'c'	
	km	km	S	R	S	R		δ_S	δ_R	md-2	md-3	md-2	md-3
1	100	1	5	5	40	40	100	0.	0.	-2.8	-2.8	5.8	0.1
2	100	33	5	5	40	40	100	0.	0.	-1.0	-1.0	2.0	0.0
3	100	66	5	5	40	40	100	0.	0.	0.9	0.9	-1.9	0.0
4	100	99	5	5	40	40	100	0.	0.	2.8	2.8	-5.8	-0.1
5	100	99	5	5	40	40	100	10.	0.	2.8	2.8	-5.8	-0.1
6	100	99	5	5	40	40	100	20.	0.	2.8	2.8	-5.8	-0.1
7	100	99	5	5	40	40	100	0.	20.	2.8	2.8	-5.8	-0.1
8	100	99	5	35	40	40	100	0.	20.	0.5	0.5	-1.1	0.0
9	100	99	35	5	40	40	100	0.	20.	3.9	3.9	-8.3	-0.2
10	100	99	35	5	10	40	100	0.	20.	3.9	3.9	-8.3	-0.2
11	250	1	5	5	40	40	100	0.	0.	-1.9	-1.9	4.1	0.1
12	250	83	5	5	40	40	100	0.	0.	-0.7	-0.7	1.4	0.0
13	250	166	5	5	40	40	100	0.	0.	0.6	0.6	-1.4	0.0
14	250	249	5	5	40	40	100	0.	0.	1.9	1.9	-4.1	-0.1
15	250	249	5	5	40	40	100	10.	0.	1.9	1.9	-4.1	-0.1
16	250	249	5	5	40	40	100	20.	0.	1.9	1.9	-4.1	-0.1
17	250	249	5	5	40	40	100	0.	20.	1.9	1.9	-4.1	-0.1
18	250	249	5	35	40	40	100	0.	20.	0.3	0.3	-0.7	0.0
19	250	249	35	5	40	40	100	0.	20.	2.3	2.3	-5.1	-0.2
20	250	249	35	5	10	40	100	0.	20.	2.3	2.3	-5.1	-0.2
21	400	1	5	5	40	40	100	0.	0.	-1.4	-1.4	3.1	0.1
22	400	133	5	5	40	40	100	0.	0.	-0.5	-0.5	1.1	0.0
23	400	266	5	5	40	40	100	0.	0.	0.5	0.5	1.1	0.0
24	400	399	5	5	40	40	100	0.	0.	1.4	1.4	-3.2	-0.1
25	400	399	5	5	40	40	100	10.	0.	1.4	1.4	-3.2	-0.1
26	400	399	5	5	40	40	100	20.	0.	1.4	1.4	-3.2	-0.1
27	400	399	5	5	40	40	100	0.	20.	1.4	1.4	-3.2	-0.1
28	400	399	5	35	40	40	100	0.	20.	0.2	0.2	-0.5	0.0
29	400	399	35	5	40	40	100	0.	20.	1.7	1.7	-3.7	-0.1
30	400	399	35	5	10	40	100	0.	20.	1.7	1.7	-3.7	-0.1

Table 5-6 Computed results for 'a'-'b' and 'b'-'c' faults on an <u>untransposed</u> single-circuit horizontal line using transposed line parameters and the superimposed values of current and voltage.

<u>Key to Table</u>

S,R=near end source and remote end source, respectively

L=line length, x=actual distance to fault from S

δ_S, δ_R=phase relationship of voltage at busbar-S and busbar-R, respectively. E.g. if $\delta_S=20^o$ and $\delta_R=0^o$ then power transfer is from S to R and vice versa.

md-2=mode-2, md-3=mode-3

Error(%)=100x(evaluated distance to fault – actual distance to fault)/total line length

No	L	x	Source Data Cap. (GVA)		X/R ratio		R_f (Ω)	Load angle (deg.)		Error (%) Total V&I		Sup. V&I	
	km	km	S	R	S	R		δ_S	δ_R	md-1	md-2	md-1	md-2
1	100	1	5	5	40	40	100	0.	0.	-0.7	-4.3	-0.5	-4.0
2	100	33	5	5	40	40	100	0.	0.	-0.2	-1.5	-0.2	-1.4
3	100	66	5	5	40	40	100	0.	0.	0.2	1.4	0.2	1.4
4	100	99	5	5	40	40	100	0.	0.	0.7	4.3	0.5	4.2
5	100	99	5	5	40	40	100	10.	0.	4.3	*	0.5	4.2
6	100	99	5	5	40	40	100	20.	0.	8.6	*	0.5	4.2
7	100	99	5	5	40	40	100	0.	20.	-4.0	*	0.5	4.2
8	100	99	5	35	40	40	100	0.	20.	-2.5	*	0.1	0.7
9	100	99	35	5	40	40	100	0.	20.	-3.4	-8.8	0.7	5.5
10	100	99	35	5	10	40	100	0.	20.	-3.4	-8.8	0.7	5.5
11	250	1	5	5	40	40	100	0.	0.	-0.7	-3.0	-0.3	-2.6
12	250	83	5	5	40	40	100	0.	0.	-0.3	-1.0	-0.1	-0.9
13	250	166	5	5	40	40	100	0.	0.	0.3	1.0	0.1	0.8
14	250	249	5	5	40	40	100	0.	0.	0.7	3.0	0.3	2.6
15	250	249	5	5	40	40	100	10.	0.	2.3	6.4	0.3	2.6
16	250	249	5	5	40	40	100	20.	0.	4.1	9.9	0.3	2.6
17	250	249	5	5	40	40	100	0.	20.	-1.4	-3.1	0.3	2.6
18	250	249	5	35	40	40	100	0.	20.	0.9	-4.0	0.1	0.4
19	250	249	35	5	40	40	100	0.	20.	-1.3	-2.5	0.4	3.0
20	250	249	35	5	10	40	100	0.	20.	-1.3	-2.5	0.4	3.0
21	400	1	5	5	40	40	100	0.	0.	-0.8	-2.5	-0.2	-1.9
22	400	133	5	5	40	40	100	0.	0.	-0.4	-0.7	-0.1	-0.6
23	400	266	5	5	40	40	100	0.	0.	0.4	0.7	0.1	0.6
24	400	399	5	5	40	40	100	0.	0.	0.9	2.5	0.2	1.9
25	400	399	5	5	40	40	100	10.	0.	1.9	4.6	0.2	1.9
26	400	399	5	5	40	40	100	20.	0.	3.1	6.7	0.2	1.9
27	400	399	5	5	40	40	100	0.	20.	-0.6	-1.2	0.2	1.9
28	400	399	5	35	40	40	100	0.	20.	-0.3	-1.9	0.1	0.3
29	400	399	35	5	40	40	100	0.	20.	-0.5	-0.9	0.3	2.1
30	400	399	35	5	10	40	100	0.	20.	-0.5	-0.9	0.3	2.1

Table 5-7 Computed results for 'a'-earth faults on an untransposed single-circuit vertical line using transposed line parameters.

Key to Table

S,R=near end source and remote end source, respectively
L=line length, x=actual distance to fault from S
δ_S, δ_R=phase relationship of voltage at busbar-S and busbar-R, respectively. E.g. if $\delta_S=20^o$ and $\delta_R=0^o$ then power transfer is from S to R and vice versa.
Total V&I=total values of postfault voltage and current
Sup. V&I=superimposed values of voltage and current
md-1=mode-1, md-2=mode-2
*=more than 10% error
Error(%)=100x(evaluated distance to fault - actual distance to fault)/total line length

No	L km	x km	Source Data Cap. (GVA) S	R	X/R ratio S	R	R_f (Ω)	Load angle (deg.) δ_S	δ_R	Error (%) 'a'-'b' md-2	md-3	'b'-'c' md-2	md-3
1	100	1	5	5	40	40	100	0.	0.	-1.8	3.7	-4.3	2.9
2	100	33	5	5	40	40	100	0.	0.	-0.6	1.3	-1.5	1.0
3	100	66	5	5	40	40	100	0.	0.	0.6	-1.2	1.4	-0.9
4	100	99	5	5	40	40	100	0.	0.	1.8	-3.7	4.3	-2.9
5	100	99	5	5	40	40	100	10.	0.	1.8	-3.7	4.3	-2.9
6	100	99	5	5	40	40	100	20.	0.	1.8	-3.7	4.3	-2.9
7	100	99	5	5	40	40	100	0.	20.	1.8	-3.7	4.3	-2.9
8	100	99	5	35	40	40	100	0.	20.	0.3	-0.7	0.8	-0.6
9	100	99	35	5	40	40	100	0.	20.	2.5	-5.4	6.0	-4.2
10	100	99	35	5	10	40	100	0.	20.	2.5	-5.4	6.0	-4.2
11	250	1	5	5	40	40	100	0.	0.	-1.2	2.7	-2.9	2.1
12	250	83	5	5	40	40	100	0.	0.	-0.4	0.9	-1.0	0.7
13	250	166	5	5	40	40	100	0.	0.	0.4	-0.9	1.0	-0.7
14	250	249	5	5	40	40	100	0.	0.	1.2	-2.7	2.9	-2.1
15	250	249	5	5	40	40	100	10.	0.	1.2	-2.7	2.9	-2.1
16	250	249	5	5	40	40	100	20.	0.	1.2	-2.7	2.9	-2.1
17	250	249	5	5	40	40	100	0.	20.	1.2	-2.7	2.9	-2.1
18	250	249	5	35	40	40	100	0.	20.	0.2	-0.5	0.5	0.2
19	250	249	35	5	40	40	100	0.	20.	0.7	-1.5	3.6	-2.7
20	250	249	35	5	10	40	100	0.	20.	1.5	-3.3	3.6	-2.7
21	400	1	5	5	40	40	100	0.	0.	-0.9	2.1	-2.2	1.6
22	400	133	5	5	40	40	100	0.	0.	-0.3	0.7	-0.8	0.6
23	400	266	5	5	40	40	100	0.	0.	0.3	-0.7	0.8	0.5
24	400	399	5	5	40	40	100	0.	0.	0.9	-2.1	2.2	-1.6
25	400	399	5	5	40	40	100	10.	0.	0.9	-2.1	2.2	-1.6
26	400	399	5	5	40	40	100	20.	0.	0.9	-2.1	2.2	-1.6
27	400	399	5	5	40	40	100	0.	20.	0.9	-2.1	2.2	-1.6
28	400	399	5	35	40	40	100	0.	20.	0.2	-0.3	0.4	-0.3
29	400	399	35	5	40	40	100	0.	20.	1.0	-2.4	2.6	-1.9
30	400	399	35	5	10	40	100	0.	20.	1.0	-2.4	2.6	-1.9

Table 5-8 Computed results for 'a'-'b' and 'b'-'c' faults on an untransposed single-circuit vertical line using transposed line parameters and the superimposed values of voltage and current.

Key to Table

S,R=near end source and remote end source, respectively

L=line length, x=actual distance to fault from S

δ_S, δ_R=phase relationship of voltage at busbar-S and busbar-R, respectively. E.g. if $\delta_S=20^o$ and $\delta_R=0^o$ then power transfer is from S to R and vice versa.

md-2=mode-2, md-3=mode-3

Error(%)=100x(evaluated distance to fault – actual distance to fault)/total line length

No	L	x	Source Data Cap. (GVA)		X/R ratio		R_f (Ω)	Load angle (deg.)		Error (%) Total V&I		Sup. V&I	
	km	km	S	R	S	R		δ_S	δ_R	md-1	md-2	md-1	md-2
1	100	1	5	5	40	40	100	0.	0.	-0.5	-1.0	-0.3	-0.9
2	100	33	5	5	40	40	100	0.	0.	-0.2	-0.3	-0.1	-0.3
3	100	66	5	5	40	40	100	0.	0.	0.2	0.3	0.1	0.3
4	100	99	5	5	40	40	100	0.	0.	0.5	1.0	0.3	0.9
5	100	99	5	5	40	40	100	10.	0.	4.0	-0.1	0.3	0.9
6	100	99	5	5	40	40	100	20.	0.	7.9	-0.6	0.3	0.9
7	100	99	5	5	40	40	100	0.	20.	-4.5	4.3	0.3	0.9
8	100	99	5	35	40	40	100	0.	20.	-3.4	4.1	0.1	0.1
9	100	99	35	5	40	40	100	0.	20.	-3.9	4.6	0.5	1.0
10	100	99	35	5	10	40	100	0.	20.	-3.9	4.6	0.5	1.0
11	250	1	5	5	40	40	100	0.	0.	-0.7	-0.7	-0.3	-0.4
12	250	83	5	5	40	40	100	0.	0.	-0.3	-0.2	-0.1	-0.1
13	250	166	5	5	40	40	100	0.	0.	0.3	0.2	0.1	0.1
14	250	249	5	5	40	40	100	0.	0.	0.7	0.7	0.3	0.4
15	250	249	5	5	40	40	100	10.	0.	2.2	0.3	0.3	0.4
16	250	249	5	5	40	40	100	20.	0.	3.7	0.1	0.3	0.4
17	250	249	5	5	40	40	100	0.	20.	-1.4	2.0	0.3	0.4
18	250	249	5	35	40	40	100	0.	20.	1.0	1.9	0.1	0.1
19	250	249	35	5	40	40	100	0.	20.	1.2	2.0	0.4	0.3
20	250	249	35	5	10	40	100	0.	20.	1.2	2.0	0.4	0.3
21	400	1	5	5	40	40	100	0.	0.	-1.0	-0.7	-0.2	-0.2
22	400	133	5	5	40	40	100	0.	0.	-0.5	-0.2	-0.2	-0.0
23	400	266	5	5	40	40	100	0.	0.	0.5	0.2	0.2	0.0
24	400	399	5	5	40	40	100	0.	0.	1.2	0.7	0.4	0.2
25	400	399	5	5	40	40	100	10.	0.	2.0	0.5	0.4	0.2
26	400	399	5	5	40	40	100	20.	0.	3.0	0.4	0.4	0.2
27	400	399	5	5	40	40	100	0.	20.	-0.2	1.5	0.4	0.2
28	400	399	5	35	40	40	100	0.	20.	-0.0	1.5	0.2	0.0
29	400	399	35	5	40	40	100	0.	20.	-0.1	1.5	0.5	0.2
30	400	399	35	5	10	40	100	0.	20.	-0.1	1.5	0.5	0.2

Table 5-9 Computed results for 'a'-earths faults on an untransposed double-circuit line using the faulted circuit phasor data and transposed line parameters.

Key to Table

S,R=near end source and remote end source, respectively
L=line length, x=actual distance to fault from S
δ_S, δ_R=phase relationship of voltage at busbar-S and busbar-R, respectively. E.g. if $\delta_S=20^o$ and $\delta_R=0^o$ then power transfer is from S to R and vice versa.
Total V&I=total values of postfault voltage and current
Sup. V&I=superimposed values of voltage and current
md-1=mode-1, md-2=mode-2
Error(%)=100x(evaluated distance to fault − actual distance to fault)/total line length

No	L	x	Source Data Cap. (GVA)		X/R ratio		R_f (Ω)	Load angle (deg.)		Error (%) 'a'-'b'		'b'-'c'	
	km	km	S	R	S	R		δ_S	δ_R	md-2	md-3	md-2	md-3
1	100	1	5	5	40	40	100	0.	0.	1.0	2.0	-0.7	1.6
2	100	33	5	5	40	40	100	0.	0.	0.3	0.7	-0.3	0.6
3	100	66	5	5	40	40	100	0.	0.	-0.3	-0.7	0.2	-0.5
4	100	99	5	5	40	40	100	0.	0.	-1.0	-2.0	0.7	-1.6
5	100	99	5	5	40	40	100	10.	0.	-1.0	-2.0	0.7	-1.6
6	100	99	5	5	40	40	100	20.	0.	-1.0	-2.0	0.7	-1.6
7	100	99	5	5	40	40	100	0.	20.	-1.0	-2.0	0.7	-1.6
8	100	99	5	35	40	40	100	0.	20.	-0.2	-0.4	0.2	-0.3
9	100	99	35	5	40	40	100	0.	20.	-1.5	-3.1	1.1	-2.6
10	100	99	35	5	10	40	100	0.	20.	-1.5	-3.1	1.1	-2.6
11	250	1	5	5	40	40	100	0.	0.	0.8	1.6	-0.6	1.4
12	250	83	5	5	40	40	100	0.	0.	0.3	0.6	-0.2	0.5
13	250	166	5	5	40	40	100	0.	0.	0.3	-0.5	0.2	-0.4
14	250	249	5	5	40	40	100	0.	0.	-0.8	-1.6	0.6	-1.4
15	250	249	5	5	40	40	100	10.	0.	-0.8	-1.6	0.6	-1.4
16	250	249	5	5	40	40	100	20.	0.	-0.8	-1.6	0.6	-1.4
17	250	249	5	5	40	40	100	0.	20.	-0.8	-1.6	0.6	-1.4
18	250	249	5	35	40	40	100	0.	20.	-0.2	-0.3	0.1	-0.3
19	250	249	35	5	40	40	100	0.	20.	-1.1	-2.3	0.8	-1.9
20	250	249	35	5	10	40	100	0.	20.	-1.1	-2.3	0.8	-1.9
21	400	1	5	5	40	40	100	0.	0.	0.7	1.4	-0.6	1.2
22	400	133	5	5	40	40	100	0.	0.	0.2	0.5	-0.2	0.4
23	400	266	5	5	40	40	100	0.	0.	-0.2	-0.5	0.2	-0.4
24	400	399	5	5	40	40	100	0.	0.	-0.7	-1.4	0.6	-1.1
25	400	399	5	5	40	40	100	10.	0.	-0.7	-1.4	0.6	-1.1
26	400	399	5	5	40	40	100	20.	0.	-0.7	-1.4	0.6	-1.1
27	400	399	5	5	40	40	100	0.	20.	-0.7	-1.4	0.6	-1.1
28	400	399	5	35	40	40	100	0.	20.	-0.1	-0.2	0.1	-0.2
29	400	399	35	5	40	40	100	0.	20.	-0.8	-1.8	0.7	-1.5
30	400	399	35	5	10	40	100	0.	20.	-0.8	-1.8	0.7	-1.5

Table 5-10 Computed results for 'a'-'b' and 'b'-'c' faults on an <u>untransposed</u> double-circuit line using transposed line parameters and the superimposed values of voltage and current of the faulted circuit only.

<u>Key to Table</u>

S,R=near end source and remote end source, respectively

L=line length, x=actual distance to fault from S

δ_S, δ_R=phase relationship of voltage at busbar-S and busbar-R, respectively. E.g. if $\delta_S=20^o$ and $\delta_R=0^o$ then power transfer is from S to R and vice versa.

md-2=mode-2, md-3=mode-3

Error(%)=100x(evaluated distance to fault – actual distance to fault)/total line length

CHAPTER 6

COMPARATIVE ANALYSIS OF THE FAULT LOCATORS

6.1 Introduction

As part of the performance evaluation of the new fault location algorithm a number of tests were carried out to establish its accuracy in comparison with competing algorithms. The results reveal the accuracy achieved by the new algorithm.

Many different algorithms have been proposed. However, many of them are not available commercially. The inefficiency of most of the algorithms proposed during the last 10 years has been discussed in Chapter 2. Of those commercially available, the ASEA algorithm used in their RANZA equipment and the Toshiba algorithm used in the Toshiba DLL1M are generally considered to be the best. Under similar fault conditions the test results of the new algorithm are compared with those of the ASEA and Toshiba algorithms. Also the results of the Schweitzer algorithm which modifies the Toshiba algorithm by using the remote source impedance will be given. All these algorithms have been described in Chapter 2.

6.2 Test Methods

Testing of the new and other algorithms was carried out using a digital computer simulation. This simulation consists of the line simulation program described in

Chapter 3 and the separate algorithm simulations. The line simulation program is a fully distributed model and takes full account of the non-transposed nature of the line and its shunt capacitance. It calculates steady-state prefault and postfault voltage and current phasors as well as superimposed ones at both ends of a single- or double-circuit line. These data are then available as input to any fault locator simulation.

The simulations model the algorithms as published. The results presented in this Chapter do not include errors due to hardware.

6.3 Reference Test Conditions

For the majority of the test results presented a horizontal line having the mean geometry illustrated in Fig. 5-1 was modelled. The reference test conditions which were chosen for the line are:

System voltage= 400kV

Line length= 150km

Local source capacity= 5GVA

Local source X/R ratio= 40

Remote source capacity= 5GVA

Remote source X/R ratio= 40

Prefault load= 0 deg. (i.e. no load)

Fault type= phase-'a'-to-earth

Fault resistance= 0Ω

The line conductors and earth wire had the specifications given in Section 5.1.1.

Regarding the reference test conditions, the tests were on what could be described as a very favourable line. No fault resistance was included and there was no prefault power flow. Under such circumstances the algorithms ought to perform very well. In each set of tests one or two parameters of the reference conditions were changed and all the other parameters remained as given above.

6.4 Test Cases

The line simulation program allows a wide number of parameters to be independently adjusted and the algorithm response tested. In order to produce meaningful results, in most cases only one or two parameters were varied from the reference conditions. In general, each of these errors will tend to compound and for some of the more extreme conditions the total error could be somewhat greater than the results quoted here. Although some of these test cases (like fault position close to remote end or high resistance faults) might appear extreme, it should be remembered that it is precisely these cases where fault locators are most likely to be required. It should also be remembered that unlike protection relays, fault locators are required to be accurate along the full line length and not just at the reach points.

Tests were carried out for two major categories; transposed lines and untransposed lines. For both categories, transposed line parameters were set into the fault locator simulations. In other words, the fault

location algorithms were set for transposed line parameters even when the line simulation program had evaluated voltages and currents for an untransposed line.

6.5 Transposed Lines

Although all the other algorithms make a number of assumptions in their solutions, the new algorithm does not make any simplifying assumption. Therefore in this series of tests, i.e. for the transposed lines, the corresponding errors are zero for the new algorithm. This is because the new algorithm is able to fully model the line and, under these conditions, has access to the full line data. As mentioned in Chapter 5, the aerial-modes can be used for any type of fault while the earth-mode is only applicable to earth faults since there is no earth current for phase faults. Also there is the option of using either superimposed values of current and voltage or the total ones. In the following series of tests the effect of each parameter on the fault locators' accuracy for the transposed lines is shown.

6.5.1 Effect of Fault Position

For the reference conditions of Section 6.3, the errors for differing fault positions along the line were measured. The results are shown in Table 6-1. It is important to note that the errors quoted throughout the simulation studies in this thesis are as percentages of the total line length and not the actual distance to fault. The results show that for the other three

algorithms the errors are least for close-up faults and they gradually increase as the fault position moves towards the remote source.

6.5.2 Effect of Line Length

It is seen from Table 6-1 that errors for longer lines, where shunt capacitance has a greater effect, are significant. As the new algorithm considers a distributed model of the line, the error is zero irrespective of line length. The ASEA algorithm gives significant errors since it ignores the effect of shunt capacitance, e.g. in Case 8 for a medium line length (250km) the recorded error is more than 2% though R_f is zero. The Toshiba algorithm gives much better results since to some extent it compensates for the effect of shunt capacitance. Errors on longer lines for the ASEA algorithm are unacceptable, e.g. 5.6% error for a zero resistance fault on a 400km line corresponds to an error of more than 22km in fault location (Case 12). The errors given in Cases 1 to 12 are entirely due to the shunt capacitance effect as all the other parameters, including fault resistance, are set at the reference conditions for the transposed line.

6.5.3 Effect of Fault Resistance

Prior to the current digital techniques the majority of fault locators used the reactance measurement technique described in 2.2 to estimate the fault location. Such measurements are very prone to error when arc resistance is encountered. This error is mainly introduced by

differing phase angles of currents flowing through the fault resistance from either side. In this case the fault resistance, from the relaying point of view, is not pure resistive as assumed by reactance relays. The larger the fault resistance the more error is introduced.

Table 6-1 shows the results of the tests to determine the effect of fault resistance. All conditions other than fault resistance and line length are set at the reference. Three sets of tests for 0Ω (Cases 1 to 12), 10Ω (Cases 13 to 24) and 50Ω (Cases 25 to 36) fault resistances were carried out. For the ASEA algorithm there is little additional error over the zero fault resistance Cases. However, the Toshiba algorithm for some extreme Cases of 50Ω fault resistance gives over 7% additional error (in modulus) even for a short line (compare Cases 4 and 28). Even the modified Toshiba algorithm by Schweitzer gives 4% additional error for these cases. Although extreme, such fault resistances may occur on mid-span vegetation faults for instance, and lines prone to this type of fault are precisely where a fault locator would prove most useful. Apart from the extreme circumstances, the other algorithms could be said to cope quite well with fault resistance. Also, from the results of Table 6-1 it is seen that the Schweitzer modification improves the performance of the Toshiba algorithm in the presence of fault resistance. It is shown in the following test results that the presence of fault resistance can exaggerate errors from other sources.

6.5.4 Effect of Prefault Power Flow

Under normal circumstances there will generally be a power flow on the line prior to a fault. This will result in the equivalent sources at each end of the line being out of phase and consequently will affect the fault current distribution. It can be seen from Table 6-2 that for the competing algorithms, the power transfer has little effect on accuracy when the fault resistance is zero. For the ASEA algorithm, prefault power flow still has no significant effect on the accuracy for a 10Ω fault resistance. However, for the Toshiba algorithm and its modified form by Schweitzer, when the power is exporting from the remote source the errors are higher (compared with no prefault power flow Cases) and vice versa.

6.5.5 Effect of Local and Remote Sources

Ref. 1 which describes the ASEA algorithm states that for the most accurate results this locator should be placed at the end of the line with the strongest source. A number of tests were therefore carried out to investigate the effects of source capacity and X/R ratio mismatch.

Table 6-3 shows the effect of source capacity mismatch on the accuracy of the different fault locators. In Cases 1 to 16 where fault resistance is zero the additional errors for the competing algorithms are negligible in comparison to Cases 1 to 4 of Table 6-2 which are for the reference conditions. Cases 17 to 32 are as Cases 1 to 16 but with 10Ω of fault resistance. In

these Cases for all the competing algorithms the results are indeed worse when the locator is placed at the weaker end of the line compared with those of Cases 13 to 16 of Table 6-2 which are for the reference conditions but 10Ω of fault resistance.

Table 6-4 shows the effect of varying the X/R ratios of the source impedances while the other parameters are set at the reference. Again it can be seen that when fault resistance is zero, the additional error is insignificant. For a 10Ω fault resistance the effect of different X/R ratios is still negligible for the ASEA algorithm. However, differing X/R ratios impairs the accuracy of the Toshiba algorithm because of the assumption that the phase angle of the fault path current is the same as that of the superimposed fault current at the near end. In practice, this is only true when the combined line section and source impedance on either side of the fault point have the same argument. When the sources at the line ends are not identical, this is not the case and extra errors can be seen to be introduced. As the ASEA algorithm uses the remote source impedance data, it gives much better results. Also the improvement in the accuracy of the Toshiba algorithm made by Schweitzer is evident here. Schweitzer uses the remote source impedance and a first estimate of fault position by the Toshiba algorithm to find the combined phase angle on each side of the fault point. It can be seen that in Case 16, an error modulus of more than 3% by the Toshiba algorithm is significantly

reduced to 0.7% by the Schweitzer modification.

6.5.6 Effect of Fault Type

All the test results so far have been for single-phase-to-earth faults. However, for both the ASEA and Toshiba algorithms, the calculation method is dependent on the type of fault. The fault resistance arrangements are as shown in Fig. 5-4 for typical faults. Table 6-5 shows the results for different types of fault. As the line is perfectly transposed, the results for the same type of fault but involving different phase(s) are the same. For example, the results for phase-'c'-to-earth are exactly the same as the results for phase-'a'-to-earth given here.

It can be seen in Table 6-5 that the performance of the ASEA algorithm is not affected by fault type even in the presence of fault resistance. The Toshiba and Schweitzer algorithms give better results for multiphase faults. However, the presence of fault resistance reduces the accuracy of the Toshiba algorithm

6.5.7 Effect of Line Configuration

As in this series of tests the line was considered perfectly transposed, the results are much the same for all the line configurations shown in Figs. 5-1, 5-2 and 5-3.

6.5.8 Typical Fault Conditions

In order to get an idea of the likely cumulative errors on

a typical line, a further group of tests were run with all parameters differing from the reference but still at practicable values. The single-circuit horizontal line was modelled with the following system parameters:

System voltage= 400kV

Line length= 150km

Local source capacity= 5GVA

Local source X/R ratio= 20

Remote source capacity= 10GVA

Remote source X/R ratio= 40

Prefault load=10 degs. (i.e. power flow from S to R)

Fault type= phase-'a'-to-earth

Fault resistance= 10Ω

The line conductors and earth wire had the specifications given in Section 5.1.1.

The results for these tests are plotted in Fig. 6-1. These results represent the sort of accuracy that could reasonably be expected. For the Toshiba algorithm an error of up to 3.4% (equivalent to 5km) is shown while the ASEA algorithm performs somewhat better giving a worst error of 0.8%. The modified Toshiba algorithm by Schweitzer improves the accuracy giving about 1.2% error in the worst case. In practice, additional error due to hardware and software inaccuracies would also occur. As mentioned the new algorithm gives no error in the case of transposed lines.

6.6 Untransposed Lines

In this series of tests the line was untransposed but its assumed transposed parameters were used for fault location. This is the normal practice in real life for the analysis of transmission lines as transposed values of line data are usually available. The majority of the test results presented here are for an untransposed 150km horizontal line configuration shown in Fig. 5-1. This is a realistic circuit because it is very reasonable that no transposition would be made along such a line as it is quite short and has a nearly balanced conductor geometry. The test cases and reference conditions were again those mentioned in Section 6.3. The same set of tests for transposed lines was carried out for untransposed lines. In this way it is possible to see the effect of transposition on the locators' accuracy by comparing the corresponding Tables. It should be noted that the superimposed values of current and voltage are always used for the new algorithm when perfect transposition is assumed for untransposed lines.

6.6.1 Effect of Fault Position

The errors for differing fault position on the 100km, 250km and 400km lines are given in Table 6-6. In this Table the accuracy results for the new algorithm are given for mode-1 (earth-mode) and mode-2 (aerial-mode). It is seen from these results that one can still use an aerial-mode for earth faults with good accuracy. Comparing Case 4 with the same Case in Table 6-1 for the transposed line,

it can be seen that on a short (100km) line there is an extra error of nearly 1% in the results from the other algorithms caused by the non-transposition of the line. The results also show that for the new algorithm, the error is higher at fault positions near both line ends while for the other algorithms the error increases as the fault position moves towards the remote end.

6.6.2 Effect of Line Length

Table 6-6 also shows the effect of line length on the accuracy attainable. Cases 1 to 12 give a very good indication of the effect of line length on the accuracy while the other parameters are set at the reference conditions. For longer lengths, where shunt capacitance has a greater effect, the errors of the ASEA algorithm significantly increase because the algorithm ignores the effect of shunt capacitance. For the Toshiba and Schweitzer algorithms the accuracy slightly improves for longer lines. By a comparison of the results of Cases 1 to 12 with the similar Cases of Table 6-1 for the transposed line, it can be seen that for the Toshiba and Schweitzer algorithms the untransposed line accuracy slightly improves. This is because the error due to line length and non-transposition in Cases 1 to 12 are in different directions, i.e. the error caused by the line length is positive while the error caused by non-transposition is negative, therefore the overall error is smaller for the untransposed line. However, this is not a general rule for these algorithms, as the direction of the error caused by

non-transposition is affected by different parameters like fault type, faulted phase(s), line conductor geometry, etc.

6.6.3 Effect of Fault Resistance

In Table 6-6 Cases 1 to 12 for zero fault resistance are repeated for 10Ω and 50Ω fault resistances. From these results it is evident that the accuracy of the new algorithm is not affected by fault resistance while the accuracy of the other algorithms is reduced as fault resistance increases. In Case 36 for a 50Ω fault resistance there is more than 10% error (which is equivalent to 40km of the line length) in the results from the ASEA and Toshiba algorithms, and the modified Toshiba algorithm by Schweitzer still gives 5.5% error in modulus. It is clear from Table 6-6 that except for the zero fault resistance cases, where the effect of the remote end source infeed through fault is made zero (because R_f=0Ω), the Schweitzer modification on the Toshiba algorithm improves the accuracy but still is not generally good enough for accurate measurement of remote faults.

6.6.4 Effect of Prefault Power Flow

Table 6-7 shows the effect of prefault load on the untransposed line. Cases 1 to 4 are the results for the reference conditions. For the new algorithm power transfer has no effect on accuracy since it uses superimposed values of current and voltage when perfect transposition is assumed for untransposed lines. For the other

algorithms, power flow has a marked effect on accuracy. When the local source is exporting power, the ASEA algorithm improves in accuracy but when it is importing power the algorithm's accuracy is reduced, in the worst case, by nearly 3%. For the Toshiba and Schweitzer algorithms the accuracy is decreased by prefault power flow irrespective of its direction. It should be noted that Cases 13 to 24 are as the Cases 1 to 12 but for a 10Ω fault resistance. Again as explained in Section 6.6.3 the Schweitzer modification is not effective when the fault resistance is zero (Cases 1 to 12).

6.6.5 Effect of Local and Remote Sources

Table 6-8 shows the effect of source capacity on the accuracy of the fault location algorithms. In Cases 1 to 16 where the fault resistance is zero, there is no significant change in the accuracy of any algorithm. Also it can be seen that in Cases 17 to 32 where fault resistance is 10Ω, the accuracy of the new algorithm is unchanged, but for the competing algorithms the accuracy improves when the near end (relaying point) source capacity is stronger than the remote end source capacity. Conversely if the near end source capacity is weaker then the error increases. Errors up to 6.5% (in modulus) for the Toshiba algorithm and more than 4% for the ASEA algorithm are apparent. In the extreme Cases in Table 6-8 the Schweitzer modification gives better results than the Toshiba algorithm.

Results showing the effect of source X/R ratio are given in Table 6-9. Different X/R ratios of the source impedances result in different arguments of the fault currents from the sources through the fault path. Therefore the assumption used by the Toshiba algorithm, that the fault point voltage and superimposed current from the near end source are in phase, is not valid. The amount of discrepancy also depends on line length and source capacity because the combined source and line section impedance on each side of the fault point affects the arguments of the fault currents from the sources. Cases 9 to 16 confirm that for different X/R ratios in the presence of a 10Ω fault resistance, the error of the Toshiba algorithm increases. Since the ASEA and Schweitzer algorithms use the remote source impedance, they compensate for this type of error. As source impedance magnitude is evaluated from source capacity, the same reasoning can be applied to the error due to source capacity.

6.6.6 Effect of Fault Type

Up to now, mainly single-phase-to-earth faults have been considered as they are the most common faults on transmission systems. However, the accuracy of the locators should be tested for other types of fault as they must be able to cope with any fault contingency. For an untransposed line, different phase(s) involved in the same type of fault will give different results. However, as well as 3-phase faults, for the purpose of brevity, the

test results for the reference conditions of Section 6.3 are given only for 'a'-earth, 'a'-'c'-earth and 'b'-'c' faults as examples of different types of fault.

It can be seen from Table 6-10 that the competing algorithms give much higher errors for these types of fault. The measured errors are as high as 9% for the ASEA, 8% for the Toshiba algorithm and 7% for the Schweitzer algorithm for a 3-phase fault (Case 32). Also it can be seen that the Schweitzer modification on the Toshiba algorithm gives very little improvement on the accuracy. For the new algorithm the results for all 3 modes are given. They show that mode selection is required for different types of fault on the untransposed horizontal line, but for all types of fault the selection can be restricted to the aerial-modes (mode-2 or mode-3). However, as discussed in 5.3.1, the new algorithm when using mode-2, gives no error for any type of fault on the untransposed horizontal line, provided that the phase arrangement of the line is taken into account. For example, for the untransposed line with the phase arrangement shown in Fig. 5-1, mode-2 voltage is evaluated from:

$$V_2=V_a-V_b \qquad (6-1)$$

and if in Fig. 5-1 phase-'a' and phase-'c' are the outer phase conductors (as they are in real systems), then:

$$V_2=V_a-V_c \qquad (6-2)$$

6.6.7 Effect of Line Configuration

When the line is untransposed, the accuracy of each algorithm is affected by the degree of conductor asymmetry. For example, the vertical horizontal line configuration shown in Fig. 5-2 has the maximum asymmetry of conductor geometry and is expected to introduce more error in fault location than the other line configurations.

For the reference fault conditions, results are given in Table 6-11 for different line configurations. It is seen from these results that while the competing algorithms give higher errors for vertical single-circuit and double-circuit line configurations, the new algorithm still gives accurate results. As discussed in Chapter 5, for the vertical line configuration it is necessary to use earth-mode for earth faults and an aerial-mode for phase faults, but for single-circuit horizontal lines and double-circuit lines an aerial-mode can be used for any type of fault without impairing the accuracy. The results of the new algorithm for the double-circuit line were obtained by using the faulted circuit phasor data only.

6.6.8 Typical Fault Conditions

The same line parameters and fault conditions of Section 6.5.8 were chosen to measure the accuracy of the locators for likely cumulative errors. However, in this case the line was untransposed but its transposed parameters were used. The results for these tests are plotted in Fig. 6-2.

It is seen by comparing Figs. 6-1 and 6-2 that the accuracy of the Toshiba and Schweitzer algorithms is reduced owing to the non-transposition of the line. Although the Schweitzer modification in this case improves the accuracy of the Toshiba algorithm, there are cases for untransposed lines where it gives higher errors than the original algorithm. This is because in the Schweitzer algorithm the positive sequence line and source impedances are used to estimate the argument of the current contribution from the remote end source to the current through the fault path, while the sequence components can only be used for a perfectly transposed line. Fig. 6.2 shows that the accuracy of the ASEA algorithm slightly improves for the untransposed line. This is because the error caused by non-transposition is in the opposite direction to the total error from other sources. However, similar to the case for the Toshiba and Schweitzer algorithms discussed in Section 6.6.2, this is not general and in most cases the accuracy of the ASEA algorithm is reduced owing to non-transposition.

Considering that for this test the fault conditions, line parameters, line length and line configuration were chosen realistically and the line was not too long to need any transposition along its length, the results give a good indication of the much higher accuracy achieved by the new fault location algorithm.

6.7 Summary

The test results showing the effect of different parameters on the accuracy of the new and competing algorithms have been presented in this Chapter. It has been shown that, for both transposed and untransposed lines, the accuracy of the new algorithm is not affected by fault resistance, line length, source network or prefault power flow, while the competing algorithms, in different degrees, are affected by these parameters. The ASEA algorithm is more affected by line length as it ignores the effect of shunt capacitance which is significant for long lines. Prefault power flow, and different source capacities and X/R ratios at the line ends have more effect on the Toshiba and Schweitzer algorithms. The accuracy of all the competing algorithms is reduced for larger fault resistances. For untransposed lines the new algorithm performs better than the competing algorithms. In most cases the maximum error for the new algorithm is less than 1%.

No	L km	x km	R_f (Ω)	Error (%)			
				New	ASEA	Tosh	Schw
1	100	1	0	0.0	0.0	0.0	0.0
2	100	33	0	0.0	0.0	0.0	0.0
3	100	66	0	0.0	0.1	0.1	0.1
4	100	99	0	0.0	0.3	0.3	0.3
5	250	1	0	0.0	0.0	0.0	0.0
6	250	83	0	0.0	0.1	0.0	0.0
7	250	166	0	0.0	0.6	-0.2	-0.2
8	250	249	0	0.0	2.1	-0.4	-0.4
9	400	1	0	0.0	0.0	0.0	0.0
10	400	133	0	0.0	0.2	-0.1	-0.1
11	400	266	0	0.0	1.5	-0.4	-0.4
12	400	399	0	0.0	5.6	-1.5	-1.5
13	100	1	10	0.0	0.0	0.3	0.1
14	100	33	10	0.0	0.0	0.2	0.1
15	100	66	10	0.0	0.1	-0.2	0.0
16	100	99	10	0.0	0.3	-1.4	-0.5
17	250	1	10	0.0	0.0	0.1	0.0
18	250	83	10	0.0	0.1	0.0	0.0
19	250	166	10	0.0	0.6	-0.3	-0.2
20	250	249	10	0.0	-2.1	-2.0	-1.0
21	400	1	10	0.0	0.0	0.1	0.0
22	400	133	10	0.0	0.2	0.0	0.0
23	400	266	10	0.0	1.5	-0.5	-0.4
24	400	399	10	0.0	6.0	-2.9	-1.7
25	100	1	50	0.0	0.0	1.7	0.7
26	100	33	50	0.0	0.0	0.9	0.4
27	100	66	50	0.0	0.1	-1.2	-0.5
28	100	99	50	0.0	0.3	-8.0	-4.3
29	250	1	50	0.0	0.0	0.5	0.2
30	250	83	50	0.0	0.1	0.3	0.1
31	250	166	50	0.0	0.6	-0.7	-0.3
32	250	249	50	0.0	2.3	-8.1	-3.9
33	400	1	50	0.0	0.0	0.2	0.1
34	400	133	50	0.0	0.2	0.2	0.1
35	400	266	50	0.0	1.5	-0.7	-0.4
36	400	399	50	0.0	9.7	-8.8	-3.4

Table 6-1 Effect of fault position, line length and fault resistance on the fault locators' accuracy for a transposed horizontal line (Fig. 5-1) subjected to 'a'-earth faults. The other parameters are set at the reference conditions of Section 6.3.

Key to Table

S,R=near end source and remote end source, respectively
L=line length(km), x=actual distance to fault from S(km).
Error(%)=100x(estimated distance to fault − actual distance to fault)/total line length

No	L km	x km	R_f (Ω)	Load angle (deg.) δ_S	Load angle (deg.) δ_R	Error (%) New	Error (%) ASEA	Error (%) Tosh	Error (%) Schw
1	150	1	0	0.	0.	0.0	0.0	0.0	0.0
2	150	50	0	0.	0.	0.0	0.0	0.0	0.0
3	150	100	0	0.	0.	0.0	0.2	-0.1	-0.1
4	150	149	0	0.	0.	0.0	0.7	-0.2	-0.2
5	150	1	0	10.	0.	0.0	0.0	0.0	0.0
6	150	50	0	10.	0.	0.0	0.0	0.0	0.0
7	150	100	0	10.	0.	0.0	0.2	-0.1	-0.1
8	150	149	0	10.	0.	0.0	0.7	-0.2	-0.2
9	150	1	0	0.	10.	0.0	0.0	0.0	0.0
10	150	50	0	0.	10.	0.0	0.0	0.0	0.0
11	150	100	0	0.	10.	0.0	0.2	-0.1	-0.1
12	150	149	0	0.	10.	0.0	0.7	-0.2	-0.2
13	150	1	10	0.	0.	0.0	0.0	0.2	0.1
14	150	50	10	0.	0.	0.0	0.0	0.1	0.0
15	150	100	10	0.	0.	0.0	0.2	-0.3	-0.1
16	150	149	10	0.	0.	0.0	0.7	-1.8	-0.9
17	150	1	10	10.	0.	0.0	0.0	0.2	0.1
18	150	50	10	10.	0.	0.0	0.0	0.1	0.0
19	150	100	10	10.	0.	0.0	0.2	-0.1	-0.1
20	150	149	10	10.	0.	0.0	0.7	-1.6	-0.8
21	150	1	10	0.	10.	0.0	0.0	0.2	0.1
22	150	50	10	0.	10.	0.0	0.0	0.1	0.0
23	150	100	10	0.	10.	0.0	0.2	-0.3	-0.2
24	150	149	10	0.	10.	0.0	0.7	-2.1	-1.1

Table 6-2 Effect of prefault load on the fault locators' accuracy for a <u>transposed</u> horizontal line (Fig. 5-1) subjected to 'a'-earth faults. The other parameters are set at the reference conditions of Section 6.3.

Key to Table

S,R=near end source and remote end source, respectively.
L=line length(km), x=actual distance to fault from S(km)
Tosh=Toshiba, Schw=Schweitzer
δ_S, δ_R=phase relationship of voltage at busbar-S and busbar-R, respectively. E.g. if $\delta_S=10^o$ and $\delta_R=0^o$ then power transfer is from S to R and vice versa.
Error(%)=100x(estimated distance to fault − actual distance to fault)/total line length

No	L km	x km	R_f (Ω)	Source caps. (GVA) Q_S	Q_R	Error (%) New	ASEA	Tosh	Schw
1	150	1	0	5	1	0.0	0.0	0.0	0.0
2	150	50	0	5	1	0.0	0.0	0.0	0.0
3	150	100	0	5	1	0.0	0.2	-0.1	-0.1
4	150	149	0	5	1	0.0	0.7	-0.2	-0.2
5	150	1	0	1	5	0.0	0.0	0.0	0.0
6	150	50	0	1	5	0.0	0.0	-0.1	-0.1
7	150	100	0	1	5	0.0	0.0	-0.3	-0.3
8	150	149	0	1	5	0.0	0.3	-0.6	-0.6
9	150	1	0	25	5	0.0	0.0	0.0	0.0
10	150	50	0	25	5	0.0	0.0	0.0	0.0
11	150	100	0	25	5	0.0	0.2	0.0	0.0
12	150	149	0	25	5	0.0	0.8	-0.1	-0.1
13	150	1	0	5	25	0.0	0.0	0.0	0.0
14	150	50	0	5	25	0.0	0.0	0.0	0.0
15	150	100	0	5	25	0.0	0.2	-0.1	-0.1
16	150	149	0	5	25	0.0	0.7	-0.2	-0.2
17	150	1	10	5	1	0.0	0.0	0.0	0.0
18	150	50	10	5	1	0.0	0.0	-0.1	0.0
19	150	100	10	5	1	0.0	0.2	-0.2	-0.2
20	150	149	10	5	1	0.0	0.7	-0.5	-0.4
21	150	1	10	1	5	0.0	0.0	1.1	0.5
22	150	50	10	1	5	0.0	0.0	1.0	0.5
23	150	100	10	1	5	0.0	0.0	0.5	0.1
24	150	149	10	1	5	0.0	0.3	-2.3	-1.5
25	150	1	10	25	5	0.0	0.0	0.0	0.0
26	150	50	10	25	5	0.0	0.0	-0.1	-0.1
27	150	100	10	25	5	0.0	0.2	-0.4	-0.2
28	150	149	10	25	5	0.0	0.8	-1.6	-0.7
29	150	1	10	5	25	0.0	0.0	0.4	0.1
30	150	50	10	5	25	0.0	0.0	0.5	0.1
31	150	100	10	5	25	0.0	0.2	0.4	0.1
32	150	149	10	5	25	0.0	1.5	-7.0	-4.5

Table 6-3 Effect of source capacities on the locators' accuracy for a transposed horizontal line (Fig. 5-1) subjected to 'a'-earth faults. The other parameters are set at the reference conditions of Section 6.3.

Key to Table

S,R=near end source and remote end source, respectively.
L=line length(km), x=actual distance to fault from S(km)
Tosh=Toshiba, Schw=Schweitzer
Q_S,Q_R=Source capacities at near end and remote end, respectively.
Error(%)=100x(estimated distance to fault − actual distance to fault)/total line length

No	L km	x km	R_f (Ω)	Source X/R ratios S	R	Error (%) New	ASEA	Tosh	Schw
1	150	1	0	40	10	0.0	0.0	0.0	0.0
2	150	50	0	40	10	0.0	0.0	0.0	0.0
3	150	100	0	40	10	0.0	0.2	-0.1	-0.1
4	150	149	0	40	10	0.0	0.7	-0.2	-0.2
5	150	1	0	10	40	0.0	0.0	0.0	0.0
6	150	50	0	10	40	0.0	0.0	0.0	0.0
7	150	100	0	10	40	0.0	0.2	-1.0	-0.1
8	150	149	0	10	40	0.0	0.7	-0.2	-0.2
9	150	1	10	40	10	0.0	0.0	0.4	0.0
10	150	50	10	40	10	0.0	0.0	0.5	0.0
11	150	100	10	40	10	0.0	0.2	0.2	-0.2
12	150	149	10	40	10	0.0	0.7	1.7	-0.7
13	150	1	10	10	40	0.0	0.0	-0.2	0.1
14	150	50	10	10	40	0.0	0.0	-0.4	0.1
15	150	100	10	10	40	0.0	0.2	-1.0	0.0
16	150	149	10	10	40	0.0	0.7	-3.1	-0.7

Table 6-4 Effect of source X/R ratios on the fault locators' accuracy for a transposed horizontal line subjected to 'a'-earth faults. The other parameters are set at the reference conditions of Section 6.3.

Key to Table

S,R=near end source and remote end source, respectively.
L=line length(km), x=actual distance to fault from S(km)
Tosh=Toshiba, Schw=Schweitzer
Error(%)=100x(estimated distance to fault - actual distance to fault)/total line length

No	L km	x km	R_f (Ω)	Fault type	Error (%)			
					New	ASEA	Tosh	Schw
1	150	1	0	a-e	0.0	0.0	0.0	0.0
2	150	50	0	a-e	0.0	0.0	0.0	0.0
3	150	100	0	a-e	0.0	0.2	-0.1	-0.1
4	150	149	0	a-e	0.0	0.7	-0.2	-0.2
5	150	1	0	a-c-e	0.0	0.0	0.0	0.0
6	150	50	0	a-c-e	0.0	0.0	0.0	0.0
7	150	100	0	a-c-e	0.0	0.3	0.0	0.0
8	150	149	0	a-c-e	0.0	0.8	0.0	0.0
9	150	1	0	b-c	0.0	0.0	0.0	0.0
10	150	50	0	b-c	0.0	0.0	0.0	0.0
11	150	100	0	b-c	0.0	0.3	0.0	0.0
12	150	149	0	b-c	0.0	0.8	0.0	0.0
13	150	1	0	a-b-c	0.0	0.0	0.0	0.0
14	150	50	0	a-b-c	0.0	0.0	0.0	0.0
15	150	100	0	a-b-c	0.0	0.3	0.0	0.0
16	150	149	0	a-b-c	0.0	0.8	0.0	0.0
17	150	1	10	a-e	0.0	0.0	0.2	0.1
18	150	50	10	a-e	0.0	0.0	0.1	0.0
19	150	100	10	a-e	0.0	0.2	-0.3	-0.1
20	150	149	10	a-e	0.0	0.7	-1.8	-0.9
21	150	1	10	a-b-e	0.0	0.0	0.2	0.0
22	150	50	10	a-b-e	0.0	0.0	0.1	0.0
23	150	100	10	a-b-e	0.0	0.3	-0.2	0.0
24	150	149	10	a-b-e	0.0	0.9	-1.1	0.0
25	150	1	10	b-c	0.0	0.0	0.1	0.0
26	150	50	10	b-c	0.0	0.0	0.1	0.0
27	150	100	10	b-c	0.0	0.3	-0.1	-0.1
28	150	149	10	b-c	0.0	0.9	-0.5	0.0
29	150	1	10	a-b-c	0.0	0.0	0.2	0.0
30	150	50	10	a-b-c	0.0	0.0	0.1	0.0
31	150	100	10	a-b-c	0.0	0.3	-0.2	0.0
32	150	149	10	a-b-c	0.0	0.9	-1.1	0.0

Table 6-5 Effect of fault type on the fault locators' accuracy for a transposed horizontal line subjected to 'a'-earth faults. Other parameters are set at the reference conditions of Section 6.3.

Key to Table

S,R=near end source and remote end source, respectively.
L=line length(km), x=actual distance to fault from S(km)
a-e=phase-'a'-to-earth fault
a-c-e=phase-'a'-to-phase-'c'-to-earth fault
b-c=phase-'b'-to-phase-'c' fault
a-b-c=3-phase fault
Tosh=Toshiba, Schw=Schweitzer
Error(%)=100x(estimated distance to fault - actual distance to fault)/total line length

No	L km	x km	R_f (Ω)	Error (%)				
				New		ASEA	Tosh	Schw
				md-1	md-2			
1	100	1	0	0.4	0.7	0.0	0.0	0.0
2	100	33	0	0.2	0.3	0.3	0.3	0.3
3	100	66	0	-0.1	-0.2	0.6	0.6	0.6
4	100	99	0	-0.4	1.2	1.2	1.2	1.2
5	250	1	0	0.3	0.5	0.0	0.0	0.0
6	250	83	0	0.1	0.2	0.3	0.2	0.2
7	250	166	0	-0.1	-0.2	1.1	0.3	0.3
8	250	249	0	-0.3	-0.5	3.0	0.4	0.4
9	400	1	0	0.2	0.4	0.0	0.0	0.0
10	400	133	0	0.1	0.1	0.4	0.2	0.2
11	400	266	0	-0.1	-0.1	1.9	0.0	0.0
12	400	399	0	-0.2	-0.4	6.5	-0.9	-0.8
13	100	1	10	0.4	0.7	0.0	0.3	0.2
14	100	33	10	0.2	0.3	0.3	0.4	0.3
15	100	66	10	-0.1	-0.2	0.6	0.3	0.5
16	100	99	10	-0.4	-0.7	1.2	-0.5	-0.3
17	250	1	10	0.3	0.5	0.0	0.1	0.0
18	250	83	10	0.1	0.2	0.3	0.3	0.2
19	250	166	10	-0.1	-0.2	1.1	0.2	0.3
20	250	249	10	-0.3	-0.5	3.0	-1.4	-0.4
21	400	1	10	0.2	0.4	0.0	0.1	0.0
22	400	133	10	0.1	0.1	0.4	0.2	0.2
23	400	266	10	-0.1	-0.1	1.9	-0.2	-0.1
24	400	399	10	-0.2	-0.4	6.6	-2.7	-1.4
25	100	1	50	0.4	0.7	0.1	1.7	0.7
26	100	33	50	0.2	0.3	0.4	1.1	0.7
27	100	66	50	-0.1	-0.2	0.8	-0.8	-0.1
28	100	99	50	-0.4	-0.7	1.5	-7.5	-3.6
29	250	1	50	0.3	0.5	0.1	0.5	0.2
30	250	83	50	0.1	0.2	0.4	0.5	0.3
31	250	166	50	-0.1	-0.2	1.1	-0.5	-0.1
32	250	249	50	-0.3	-0.5	3.4	-8.3	-4.2
33	400	1	50	0.2	0.4	0.1	0.2	0.1
34	400	133	50	0.1	0.1	0.2	0.2	0.1
35	400	266	50	-0.1	-0.1	1.9	-0.5	-0.5
36	400	399	50	-0.2	-0.4	*	*	-5.5

Table 6-6 Effect of fault position, line length and fault resistance on the fault locators' accuracy for an untransposed horizontal line represented by the transposed line data, subjected to 'a'-earth faults. The other parameters are set at the reference conditions of Section 6.3.

Key to Table

S,R=near end source and remote end source, respectively
L=line length(km), x=actual distance to fault from S(km)
Tosh=Toshiba, Schw=Schweitzer, * more than 10% error
Error(%)=100x(estimated distance to fault − actual distance to fault)/total line length

No	L km	x km	R_f (Ω)	Load angle (deg.) δ_S	δ_R	Error (%) New md-1	md-2	ASEA	Tosh	Schw
1	150	1	0	0.	0.	0.4	0.6	0.0	0.0	0.0
2	150	50	0	0.	0.	0.1	0.2	0.3	0.3	0.3
3	150	100	0	0.	0.	-0.1	-0.2	0.7	0.5	0.5
4	150	149	0	0.	0.	-0.4	-0.6	1.6	0.7	0.8
5	150	1	0	10.	0.	0.4	0.6	0.0	0.0	0.0
6	150	50	0	10.	0.	0.1	0.2	-0.2	-0.2	-0.2
7	150	100	0	10.	0.	-0.1	-0.2	-0.6	-0.9	-0.9
8	150	149	0	10.	0.	-0.4	-0.6	-1.0	-1.8	-1.8
9	150	1	0	0.	10.	0.4	0.6	0.0	0.0	0.0
10	150	50	0	0.	10.	0.1	0.2	0.8	0.8	0.8
11	150	100	0	0.	10.	-0.1	-0.2	2.2	1.9	1.9
12	150	149	0	0.	10.	-0.4	-0.6	4.4	3.5	3.5
13	150	1	10	0.	0.	0.4	0.6	0.0	0.2	0.1
14	150	50	10	0.	0.	0.1	0.2	0.3	0.4	0.3
15	150	100	10	0.	0.	-0.1	-0.2	0.7	0.2	0.4
16	150	149	10	0.	0.	-0.4	-0.6	1.6	-1.0	-0.1
17	150	1	10	10.	0.	0.4	0.6	0.0	0.2	0.1
18	150	50	10	10.	0.	0.1	0.2	-0.1	-0.1	-0.2
19	150	100	10	10.	0.	-0.1	-0.2	-0.4	-1.0	-0.9
20	150	149	10	10.	0.	-0.4	-0.6	-0.7	-3.1	-2.3
21	150	1	10	0.	10.	0.4	0.6	0.0	0.2	0.1
22	150	50	10	0.	10.	0.1	0.2	0.9	0.9	0.8
23	150	100	10	0.	10.	-0.1	-0.2	2.2	1.7	1.8
24	150	149	10	0.	10.	-0.4	-0.6	4.6	1.5	2.7

Table 6-7 Effect of pre-fault load on the fault locators' accuracy for an <u>untransposed</u> horizontal line (Fig. 5-1) represented by the transposed line data and subjected to 'a'-earth faults. The other parameters are set at the reference conditions of Section 6.3.

<u>Key to Table</u>

S,R=near end source and remote end source, respectively.
L=line length(km), x=actual distance to fault from S(km)
Tosh=Toshiba, Schw=Schweitzer
md-1=mode-1, md-2=mode-2
δ_S, δ_R=phase relationship of voltage at busbar-S and busbar-R, respectively. E.g. if $\delta_S=10^o$ and $\delta_R=0^o$ then power transfer is from S to R and vice versa.
Error(%)=100x(estimated distance to fault – actual distance to fault)/total line length

No	L km	x km	R_f (Ω)	Source caps. (GVA) Q_S	Q_R	Error (%) New md-1	md-2	ASEA	Tosh	Schw
1	150	1	0	5	1	0.2	0.3	0.0	0.0	0.0
2	150	50	0	5	1	0.2	-0.3	0.3	0.3	0.3
3	150	100	0	5	1	-0.5	-0.9	0.8	0.5	0.5
4	150	149	0	5	1	-0.8	-1.6	-1.5	0.7	0.7
5	150	1	0	1	5	0.8	1.6	0.0	0.0	0.0
6	150	50	0	1	5	0.5	0.9	0.2	0.1	0.1
7	150	100	0	1	5	0.2	0.3	0.4	0.2	0.2
8	150	149	0	1	5	-0.2	-0.3	1.1	0.2	0.2
9	150	1	0	25	5	0.1	0.2	0.0	0.0	0.0
10	150	50	0	25	5	-0.1	-0.2	0.3	0.3	0.3
11	150	100	0	25	5	-0.3	-0.5	0.8	0.5	0.5
12	150	149	0	25	5	-0.5	-0.8	1.7	0.8	0.9
13	150	1	0	5	25	0.5	0.8	0.0	0.0	0.0
14	150	50	0	5	25	0.3	0.5	0.3	0.2	0.2
15	150	100	0	5	25	0.1	0.2	0.7	0.4	0.4
16	150	149	0	5	25	-0.1	-0.2	1.6	0.8	0.8
17	150	1	10	5	1	0.2	0.3	0.0	0.1	0.0
18	150	50	10	5	1	-0.2	-0.3	0.2	0.2	0.2
19	150	100	10	5	1	-0.5	-0.9	0.8	0.3	0.4
20	150	149	10	5	1	-0.8	-1.6	1.5	0.3	0.5
21	150	1	10	1	5	0.8	1.6	0.1	1.1	0.5
22	150	50	10	1	5	0.5	0.9	0.3	1.2	0.7
23	150	100	10	1	5	0.2	0.3	0.6	0.8	0.5
24	150	149	10	1	5	-0.2	-0.3	1.3	-1.7	-0.9
25	150	1	10	25	5	0.1	0.2	0.0	0.0	0.0
26	150	50	10	25	5	-0.1	-0.2	0.3	0.2	0.3
27	150	100	10	25	5	-0.3	-0.5	0.8	0.2	0.4
28	150	149	10	25	5	-0.5	-0.8	1.7	-0.8	0.2
29	150	1	10	5	25	0.5	0.8	0.0	0.4	0.1
30	150	50	10	5	25	0.3	0.5	0.3	0.7	0.7
31	150	100	10	5	25	0.1	0.2	0.7	0.9	0.9
32	150	149	10	5	25	-0.1	-0.2	4.2	-6.5	-3.7

Table 6-8 Effect of source capacities on the fault locators' accuracy for an untransposed horizontal line (Fig. 5-1) represented by the transposed line data, subjected to 'a'-earth faults. The other parameters are set at the reference conditions of Section 6.3.

Key to Table

S,R=near end source and remote end source, respectively.
L=line length(km), x=actual distance to fault from S(km)
md-1=mode-1, md-2=mode-2
Tosh=Toshiba, Schw=Schweitzer
Q_S,Q_R=Source capacities at near end and remote end, respectively.
Error(%)=100x(estimated distance to fault − actual distance to fault)/total line length

No	L km	x km	R_f (Ω)	Source X/R ratios S	R	Error (%) New md-1	md-2	ASEA	Tosh	Schw
1	150	1	0	40	10	0.4	0.6	0.0	0.0	0.0
2	150	50	0	40	10	0.1	0.2	0.3	0.2	0.2
3	150	100	0	40	10	-0.1	-0.2	0.7	0.5	0.5
4	150	149	0	40	10	-0.4	-0.6	1.6	0.7	0.7
5	150	1	0	10	40	0.4	0.6	0.0	0.0	0.0
6	150	50	0	10	40	0.1	0.2	0.3	0.2	0.2
7	150	100	0	10	40	-0.1	-0.2	0.7	0.5	0.5
8	150	149	0	10	40	-0.4	-0.6	1.6	0.7	0.7
9	150	1	10	40	10	0.4	0.6	0.0	0.4	0.0
10	150	50	10	40	10	0.1	0.2	0.3	0.8	0.2
11	150	100	10	40	10	-0.1	-0.2	0.7	1.3	0.3
12	150	149	10	40	10	-0.4	-0.6	1.5	2.5	0.0
13	150	1	10	10	40	0.4	0.6	0.0	-0.2	0.1
14	150	50	10	10	40	0.1	0.2	0.3	-0.2	0.4
15	150	100	10	10	40	-0.1	-0.2	0.8	-0.5	0.5
16	150	149	10	10	40	-0.4	-0.6	1.7	-2.3	0.1

Table 6-9 Effect of source X/R ratios on the fault locators' accuracy for the untransposed horizontal line (Fig. 5-1) represented by the transposed line data, subjected to 'a'-earth faults. The other parameters are set at the reference conditions of Section 6.3.

Key to Table

S,R=near end source and remote end source, respectively.
L=line length(km), x=actual distance to fault from S(km)
md-1=mode-1, md-2=mode-2
Tosh=Toshiba, Schw=Schweitzer
Error(%)=100x(estimated distance to fault - actual distance to fault)/total line length

No	L km	x km	R_f (Ω)	Fault type	Error (%)					
					New			ASEA	Tosh	Schw
					md-1	md-2	md-3			
1	150	1	0	a-e	0.4	0.6	-5.4	0.0	0.2	0.0
2	150	50	0	a-e	0.1	0.2	-1.8	0.3	0.3	0.3
3	150	100	0	a-e	-0.1	-0.2	1.8	0.7	0.5	0.5
4	150	149	0	a-e	-0.4	-0.6	5.4	1.6	0.7	0.8
5	150	1	0	a-c-e	-0.1	1.3	-1.9	0.0	0.2	0.0
6	150	50	0	a-c-e	0.0	0.5	-0.6	-1.4	-1.4	-1.4
7	150	100	0	a-c-e	0.0	-0.5	0.6	-2.6	-2.9	-2.9
8	150	149	0	a-c-e	0.1	-1.3	1.9	-3.6	-4.4	-4.4
9	150	1	0	b-c	*	5.1	0.1	0.0	0.0	0.0
10	150	50	0	b-c	*	1.7	0.0	-1.4	-1.4	-1.4
11	150	100	0	b-c	*	-1.7	0.0	-2.6	-2.9	-2.8
12	150	149	0	b-c	*	-5.1	-0.1	-3.7	-4.4	-4.4
13	150	1	0	a-b-c	*	1.5	-1.2	0.1	0.0	0.0
14	150	50	0	a-b-c	*	0.5	-0.4	2.9	-1.6	-1.6
15	150	100	0	a-b-c	*	0.4	-0.5	6.0	-3.3	-3.3
16	150	149	0	a-b-c	*	-1.5	1.2	9.4	-5.0	-4.9
17	150	1	10	a-e	0.4	0.6	-5.4	0.0	0.2	0.1
18	150	50	10	a-e	0.1	0.2	-1.8	0.3	0.4	0.3
19	150	100	10	a-e	-0.1	-0.2	1.8	0.7	0.2	0.4
20	150	149	10	a-e	-0.4	-0.6	5.4	1.6	-1.0	-0.1
21	150	1	10	a-c-e	0.0	1.3	-2.2	-0.1	0.1	-0.1
22	150	50	10	a-c-e	0.0	0.5	-0.8	-1.4	-1.3	-1.4
23	150	100	10	a-c-e	0.0	-0.5	0.8	-2.6	-3.0	-2.8
24	150	149	10	a-c-e	0.0	-1.3	2.2	-3.4	-5.0	-4.2
25	150	1	10	b-c	*	5.1	0.1	0.0	0.1	0.0
26	150	50	10	b-c	*	1.7	0.0	-1.4	-1.3	-1.4
27	150	100	10	b-c	*	-1.7	0.0	-2.6	-2.9	-2.8
28	150	149	10	b-c	*	-5.1	-0.1	-3.7	-4.9	-4.5
29	150	1	10	a-b-c	*	1.5	-1.2	0.1	0.6	0.4
30	150	50	10	a-b-c	*	0.5	-0.4	2.9	-1.3	-1.4
31	150	100	10	a-b-c	*	-0.5	0.4	6.0	-3.8	-3.8
32	150	149	10	a-b-c	*	-1.5	1.2	9.8	-8.1	-7.3

Table 6-10 Effect of fault type on the fault locators' accuracy for an untransposed horizontal line (Fig. 5-1) represented by the transposed line parameters, subjected to 'a'-earth faults. The other parameters are set at the reference conditions of Section 6.3.

Key to Table

L=line length(km), x=actual distance to fault from S(km)
a-e=phase-'a'-to-earth fault
a-c-e=phase-'a'-to-phase-'c'-to-earth fault
b-c=phase-'b'-to-phase-'c' fault, a-b-c=3-phase fault
md-1=mode-1, md-2=mode-2, md-3=mode-3
* more than 10% error, Tosh=Toshiba, Schw=Schweitzer
Error(%)=100x(estimated distance to fault - actual distance to fault)/total line length

No	L km	x km	R_f (Ω)	Line configuration	Error (%)				
					New md-1	New md-2	ASEA	Tosh	Schw
1	150	1	0	H	0.4	0.6	0.0	0.0	0.0
2	150	50	0	H	0.1	0.2	0.3	0.3	0.3
3	150	100	0	H	-0.1	-0.2	0.7	0.5	0.5
4	150	149	0	H	-0.4	-0.6	1.6	0.7	0.8
5	150	1	0	V	-0.4	-3.5	0.0	0.0	0.0
6	150	50	0	V	-0.1	-1.2	1.1	1.1	1.1
7	150	100	0	V	0.1	1.2	2.4	2.2	2.2
8	150	149	0	V	0.4	3.4	4.1	3.1	3.1
9	150	1	0	D	-0.3	-0.6	0.0	0.0	0.0
10	150	50	0	D	-0.1	-0.2	1.3	1.3	1.3
11	150	100	0	D	0.1	0.2	1.9	1.6	1.6
12	150	149	0	D	0.3	0.6	-1.0	-1.8	-1.8
13	150	1	10	H	0.4	0.6	0.0	0.2	0.1
14	150	50	10	H	0.1	0.2	0.3	0.4	0.3
15	150	100	10	H	-0.1	-0.2	0.7	0.2	0.4
16	150	149	10	H	-0.4	-0.6	1.6	-1.0	-0.1
17	150	1	10	V	0.0	0.0	0.0	0.2	0.1
18	150	50	10	V	-0.4	-3.4	0.0	0.2	0.0
19	150	100	10	V	-0.1	-1.2	1.2	1.2	1.2
20	150	149	10	V	0.1	1.2	2.5	2.0	2.2
21	150	1	10	D	-0.3	-0.6	0.0	0.1	0.0
22	150	50	10	D	-0.1	-0.2	1.3	1.3	1.3
23	150	100	10	D	0.1	0.2	2.0	1.6	1.7
24	150	149	10	D	0.3	0.6	-0.9	-3.2	-2.1

Table 6-11 Effect of line configurations on the fault locators' accuracy for an untransposed line represented by the transposed line data, subjected to 'a'-earth faults. The other parameters are set at the reference conditions of Section 6.3.

Key to Table

S,R=near end source and remote end source, respectively.
L=line length(km), x=actual distance to fault from S(km)
H=horizontal single-circuit line (Fig. 5-1)
V=vertical single-circuit line (Fig. 5-2)
D=double-circuit line (Fig. 5-3)
Tosh=Toshiba, Schw=Schweitzer
md-1=mode-1, md-2=mode-2
Error(%)=100x(estimated distance to fault − actual distance to fault)/total line length

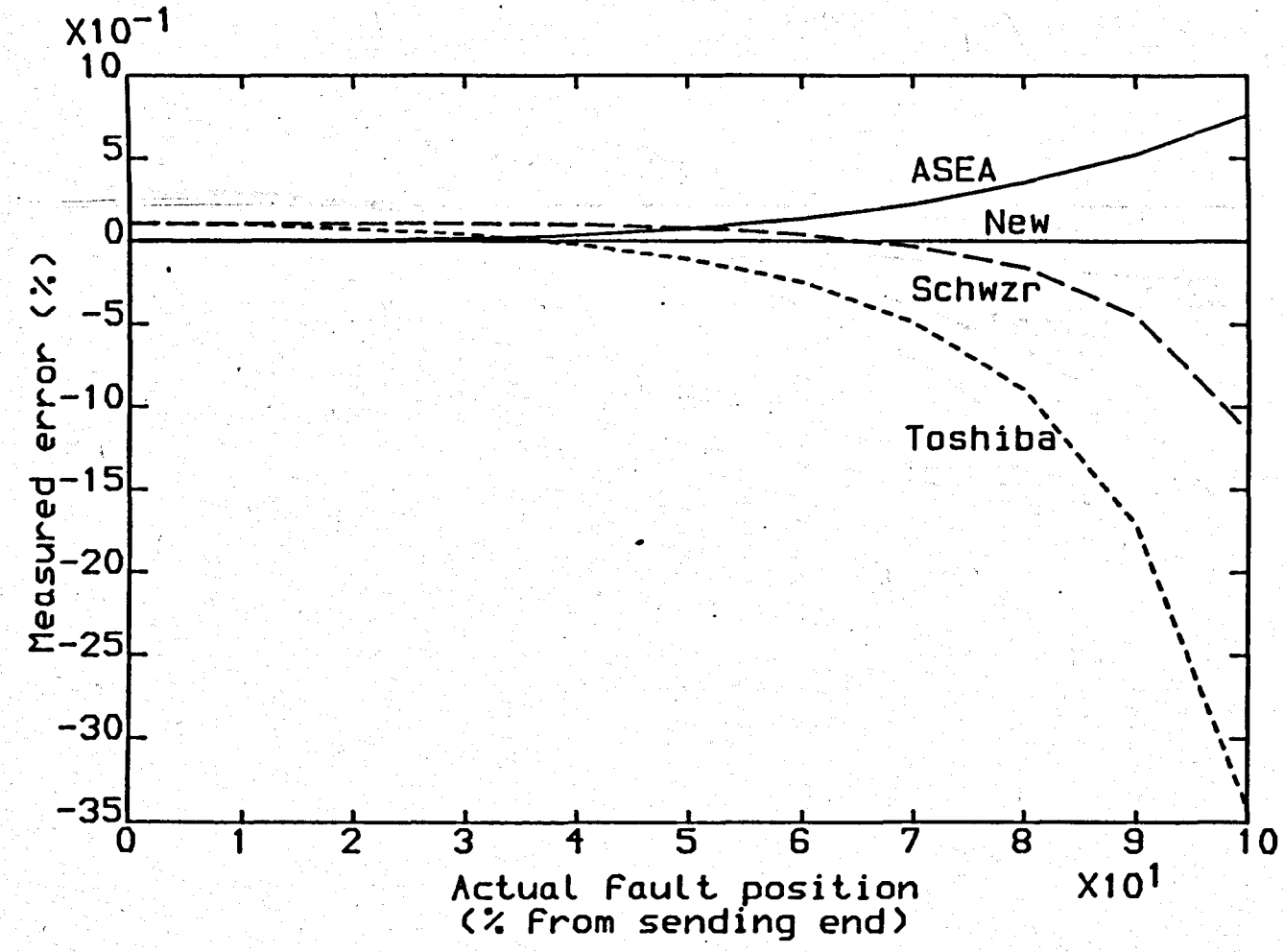

Fig. 6-1 Measured accuracy for the typical fault conditions on a transposed line

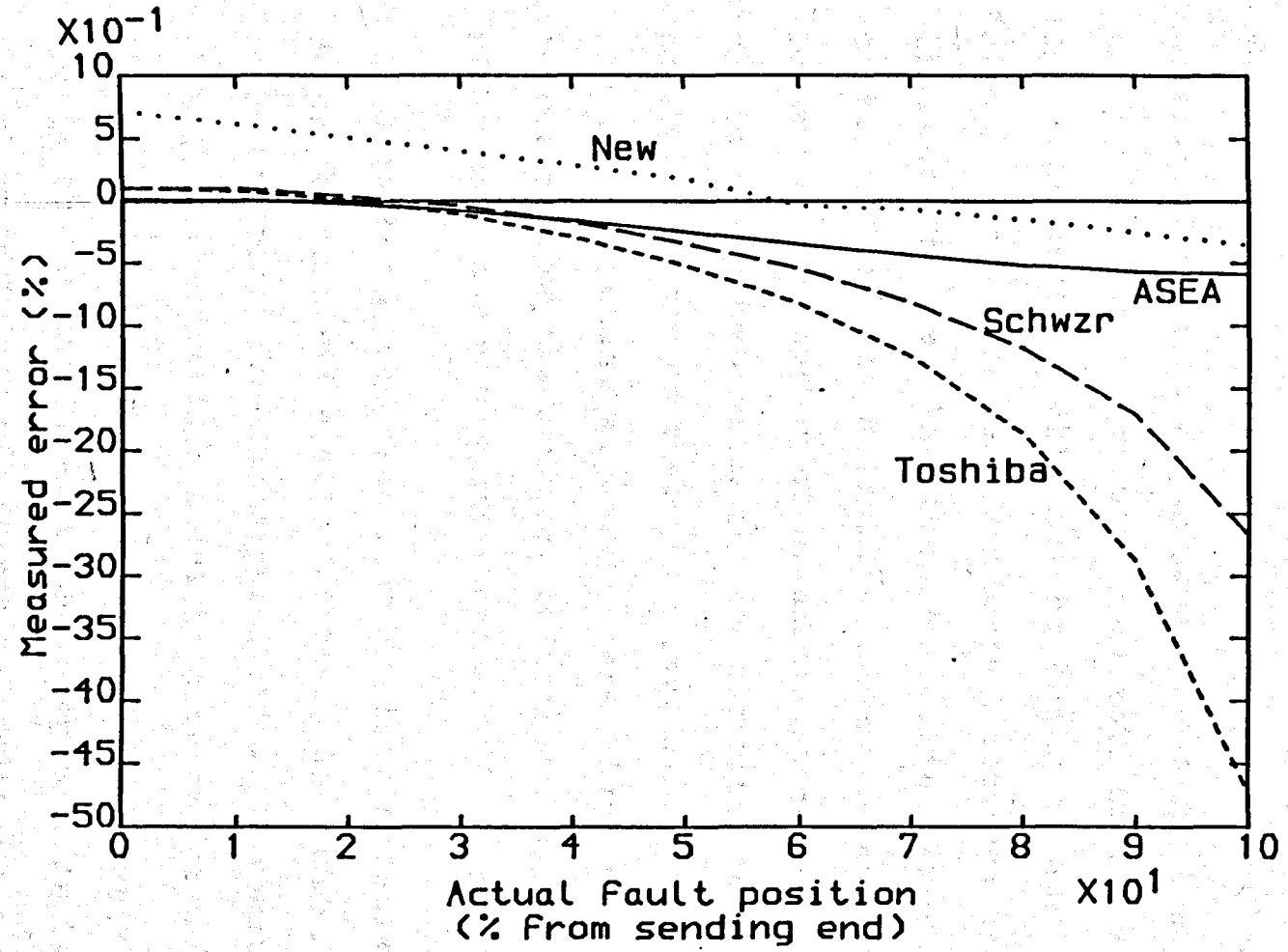

Fig. 6-2 Measured accuracy for the typical fault conditions on an untransposed line

CHAPTER 7

EFFECT OF SETTING AND HARDWARE INACCURACIES

7.1 Introduction

In the simulated performance tests described in the previous Chapter it was assumed that perfect setting data and perfect input data were available to the algorithms. In practice this will not be the case and some non-algorithmic errors due to incorrect settings and hardware limitations are inevitable. These errors must be considered in any overall accuracy assessment of the locators and a number of simulation tests were therefore run to determine whether the new algorithm is particularly sensitive to any of these factors. Again the test results for the competing algorithms are given to see if any improvement on the accuracy is achieved by the new algorithm under the same circumstances.

Once again the transmission line modelled is that described in Section 6.3. The tests were carried out for both transposed and untransposed lines. It should be noted that like the previous simulation tests for untransposed lines, ideally transposed line parameters were used even though the actual line was untransposed. As before, the superimposed values of current and voltage should be used in the new algorithm when perfect transposition is assumed for untransposed lines, but in other cases either the

superimposed or total values can be used. In the following Sections, setting and hardware inaccuracies on the locators' performance are investigated.

7.2 Effect of Remote Source Settings

Both the ASEA and the Schweitzer algorithms require a setting for the remote source impedance. In practice, this value may well change as different combinations of plant are connected or disconnected with changing load conditions. It is thus of interest to know how much effect errors on this setting will have on the fault location accuracy for the different locators.

The test conditions of Section 6.3 were used for a 10Ω fault resistance thereby having the remote source capacity and X/R ratio set in the line simulation program to 5GVA and 40, respectively. For the algorithms, however, the remote source capacity setting was varied from 1 to 25 GVA and for two settings of the X/R ratio at 20 and 40. The results of the tests are shown in Table 7-1 for the transposed line and in Table 7-2 for the untransposed line. Cases 1 to 4 in these Tables give the results when the correct remote source data were set into the locators and should be considered as the reference Cases to measure the extra errors introduced by incorrect remote source settings. Cases 5 to 16 show the effect of changing source capacity on the accuracy while the X/R ratio remains at the correct setting. Cases 17 to 32 are as Cases 1 to 16

but with X/R ratio set at 20.

As expected, the new and the Toshiba algorithms are unaffected by the remote source impedance setting since they make no use of it. Also the ASEA algorithm is not affected significantly by the remote source settings and a maximum 0.5% extra error was recorded (Case 16 of Table 7-2). Therefore, it can be said that the ASEA algorithm is quite immune against inaccurate remote source settings. But the results of the Schweitzer algorithm are more affected by incorrect settings, particularly by any inaccuracy in the X/R ratio setting. It is seen that for both the transposed and untransposed lines more than 1% extra error was recorded in Case 20 when the X/R ratio is set at 20. These results show that the Schweitzer modification to the Toshiba algorithm does not improve the accuracy achieved and in most cases when there are errors in the remote source settings the results are worse than those of the original algorithm.

7.3 Effect of [Z] Matrix Errors

All input parameters are derived from line geometry and electrical parameters which are in turn converted into [Z] and [Y] matrices. To investigate the effect of inaccurate input parameters, the [Z] matrix was adjusted for the fault location algorithms only, the values used by the line simulation remaining as described in Section 5.1.1. The [Y] matrix, which mainly represents the effect of

shunt capacitance, has much smaller effect and most algorithms ignore its effect. The results of [Z] matrix errors are shown in Table 7-3 for the transposed line and in Table 7-4 for the untransposed line. The test conditions were as described in Section 6.3.

Cases 1 to 4 give the results of the reference conditions with no errors in the [Z] matrix. Cases 5 to 12 are the results for ±5% errors in the magnitude and Cases 13 to 20 are for ±5% errors in the argument of the [Z] matrix elements. As line [Z] matrix elements are predominantly inductive, 5% error in the argument is equivalent to about 4 degrees error. The combined effect of magnitude and argument errors on the accuracy are shown in Cases 21 to 28. It is evident from these results that any error in magnitude has a larger effect on the accuracy; but it is important to note that in all cases the new fault location algorithm maintains its high accuracy and is less affected by the errors in the [Z] matrix setting. For example, in Case 12, for a -5% error in the [Z] matrix magnitude, the errors for the other algorithms are at least twice that for the new algorithm for the transposed line, while for the untransposed line the errors are at least four times higher than the new algorithm. Also the Schweitzer algorithm gives no improvement over the Toshiba algorithm and even in some cases reduces the accuracy.

The results for -5% error in magnitude and in argument

of the [Z] matrix are plotted in Figs. 7-3 and 7-4 for the transposed and untransposed lines respectively. Fault conditions are as described in Section 6.3 for a 10Ω fault resistance. The results for the new algorithm, are those obtained using mode-2 which gives higher errors than mode-1 in this fault study. In order to see how much extra error is introduced, these graphs can be compared with the graphs of Figs. 7-1 and 7-2 which are for the reference test conditions of transposed and untransposed lines for a 10Ω fault resistance. It is clear from Figs. 7-3 and 7-4 that the errors of the competing algorithms increase as the fault position moves towards the remote end. Also it can be seen that the Schweitzer modification reduces the accuracy of the Toshiba algorithm.

To summarize, all the algorithms are affected by inaccuracy of the [Z] matrix setting. For the competing algorithms the results are nearly the same; at the remote end of the line a 5% error in the magnitude giving roughly a further 5% of error and a 5% error in the argument giving at least 2% additional error. At the near end the additional errors are less but still significant. By contrast the new algorithm performs very well; a 5% error in the [Z] matrix magnitude and/or argument resulting in only a maximum 1% additional error using earth-mode (mode-1) and 1.6% using aerial-mode (mode-2).

7.4 Line Length Setting Errors

A further source of setting errors relates to the line length. For the reference test conditions with 10Ω fault resistance the results are plotted in Figs. 7-5 and 7-6 for the transposed and untransposed lines respectively. It is seen from these graphs that the new algorithm is significantly affected by the line length setting errors. A -5% error in the line length keyed into the locator will introduce up to -3.5% error in the fault location estimate for the transposed line. Since when the correct value of line length is set into the new algorithm there is no error for transposed lines, then the errors shown in Fig. 7-5 for the new algorithm are entirely due to the line length setting error. By comparing these graphs with graphs 7-1 and 7-2 for the reference fault conditions, it is seen that the competing algorithms are not affected very much by these line length setting errors.

Note, however, that the reason for the higher accuracy of the competing algorithms is that they calculate, directly or indirectly, distance to fault as a percentage of line length. Also, the new algorithm gives no error if the fault position is displayed as a percentage of line length. In other words, if the fault is actually, say, 10% down the line, the distance to fault is still calculated at 10% by the new algorithm. Therefore if the fault location is displayed in terms of number of towers from the relaying point, then there will be no error. For example,

if the actual length of a line is 150km and it is set into the locator 160km, then for a fault at 80% of the line the new algorithm evaluates 128km by using the 160km setting, instead of actual fault position at 120km, thereby giving 8km error in fault location. Now if, instead, the fault location is converted into 80% of the number of towers along the line the exact position of the tower can be found and the accuracy of the new locator is not affected by the line length setting errors. In general it was found that the maximum error introduced is less than the setting error if the fault position to be displayed in actual length (e.g. km).

7.5 Simulated Hardware Errors

Such errors arise due to the combined effect of transducer errors, hardware errors in the calculation of the voltage and current phasors which are used in the fault location algorithms. A good indication of the likely effect of hardware errors on the accuracy of fault locators can be obtained by introducing various combinations of errors in the magnitude and phase angle of the voltage and current phasors entered into the fault location algorithms.

Table 7-5 shows four cases involving a ±2% error in the magnitude of the near and remote end voltage and current phasors which were obtained from the fault conditions of Section 6.3 for a transposed line. Since distance to fault is evaluated from the voltage to current

ratio, the fault location error is zero when all voltage and current phasors are simultaneously subjected to the same proportion of magnitude and/or argument errors. Therefore, in Cases 5 to 12 there is no extra error for the competing algorithms (in comparison to the reference Cases 1 to 4) as they use the single-end phasor data and the proportional errors in voltage and current phasors of the relaying end are the same. However, in Cases 13 to 20 the extra errors of the competing algorithms are significant. Overall, the competing algorithms all have maximum errors of at least twice the maximum of the new algorithm.

Table 7-6 shows some corresponding cases involving $\pm 10^{o}$ error in the argument of the voltages and currents entered into the locators. The maximum modulus of the errors over all Cases using the new algorithm is 1.9% for mode-2. But in Cases 13 to 20 the accuracy of the other algorithms is severely impaired by the argument errors; in most of these Cases the additional error is more than 10% while there is at least 7% additional error in the other Cases. As these algorithms are very sensitive to the argument error they require more accurate hardware equipment and software data processing. By contrast, because of good performance of the new algorithm against these errors, it requires less delicate equipment and data processing. As discussed in Section 4.8, the need for a very accurate synchronisation of phasor data at the line

ends is therefore obviated.

7.6 Summary

The sensitivity of the different algorithms has been shown against various non-algorithmic errors. Except for the line length setting, the accuracy of the new algorithm is much less affected by setting errors than the competing algorithms. Also the errors due to the signal recording and processing, which appear in the phase values, have less effects on the accuracy of the new algorithm. It should be noted that for the purpose of brevity, the results presented in this Chapter have been selected from the simulation tests carried out for different lines and fault conditions and they well represent the general performance of the algorithms when subjected to non-algorithmic errors.

No	L km	x km	R_f (Ω)	Remote-source setting Q_R	X/R	Error (%) New	ASEA	Tosh	Schw
1	150	1	10	5	40	0.0	0.0	0.2	0.1
2	150	50	10	5	40	0.0	0.0	0.1	0.0
3	150	100	10	5	40	0.0	0.2	-0.3	-0.1
4	150	149	10	5	40	0.0	0.7	-1.8	-0.9
5	150	1	10	1	40	0.0	0.1	0.2	0.2
6	150	50	10	1	40	0.0	0.1	0.1	0.1
7	150	100	10	1	40	0.0	0.2	-0.3	-0.1
8	150	149	10	1	40	0.0	0.2	-1.8	-1.4
9	150	1	10	10	40	0.0	-0.1	0.2	0.0
10	150	50	10	10	40	0.0	-0.1	0.1	-0.1
11	150	100	10	10	40	0.0	0.1	-0.3	-0.3
12	150	149	10	10	40	0.0	0.9	-1.8	-0.8
13	150	1	10	25	40	0.0	0.1	0.2	-0.1
14	150	50	10	25	40	0.0	-0.2	0.1	-0.2
15	150	100	10	25	40	0.0	0.2	-0.3	-0.5
16	150	149	10	25	40	0.0	1.0	-1.8	-0.7
17	150	1	10	5	20	0.0	-0.1	0.2	0.0
18	150	50	10	5	20	0.0	-0.1	0.1	-0.1
19	150	100	10	5	20	0.0	-0.2	-0.3	-0.5
20	150	149	10	5	20	0.0	-0.5	-1.8	-2.0
21	150	1	10	1	20	0.0	0.1	0.2	0.1
22	150	50	10	1	20	0.0	0.0	0.1	0.0
23	150	100	10	1	20	0.0	0.0	-0.3	-0.4
24	150	149	10	1	20	0.0	-0.4	-1.8	-1.9
25	150	1	10	10	20	0.0	-0.1	0.2	0.0
26	150	50	10	10	20	0.0	-0.2	0.1	-0.2
27	150	100	10	10	20	0.0	-0.3	-0.3	-0.6
28	150	149	10	10	20	0.0	-0.6	-1.8	-2.1
29	150	1	10	25	20	0.0	-0.2	0.2	-0.1
30	150	50	10	25	20	0.0	-0.3	0.1	-0.2
31	150	100	10	25	20	0.0	-0.4	-0.3	-0.7
32	150	149	10	25	20	0.0	-0.5	-1.8	-2.0

Table 7-1 Effect of the remote source settings on the locators' accuracy for a transposed horizontal line (Fig. 5-1) subjected to 'a'-earth faults. The actual values of source capacity and X/R ratio at both ends are 5GVA and 40 respectively. The other parameters are set at the reference conditions of Section 6.3.

Key to Table

L=line length, x=actual distance to fault from near end

Tosh=Toshiba, Schw=Schweitzer

Q_R,X/R=Source capacity and X/R ratio settings at the remote end.

Error(%)=100x(estimated distance to fault − actual distance to fault)/total line length

No	L km	x km	R_f (Ω)	Remote-source setting Q_R	X/R	Error (%) New md-1	md-2	ASEA	Tosh	Schw
1	150	1	10	5	40	0.4	0.6	0.0	0.2	0.1
2	150	50	10	5	40	0.1	0.2	0.3	0.4	0.3
3	150	100	10	5	40	-0.1	-0.2	0.7	0.2	0.4
4	150	149	10	5	40	-0.4	-0.6	1.6	-1.0	-0.1
5	150	1	10	1	40	0.4	0.6	0.1	0.2	0.2
6	150	50	10	1	40	0.1	0.2	0.4	0.4	0.4
7	150	100	10	1	40	-0.1	-0.2	0.8	0.2	0.4
8	150	149	10	1	40	-0.4	-0.6	1.1	-1.0	-0.6
9	150	1	10	10	40	0.4	0.6	-0.1	0.2	0.0
10	150	50	10	10	40	0.1	0.2	0.2	0.4	0.2
11	150	100	10	10	40	-0.1	-0.2	0.6	0.2	0.3
12	150	149	10	10	40	-0.4	-0.6	1.8	-1.0	0.1
13	150	1	10	25	40	0.4	0.6	-0.1	0.2	-0.1
14	150	50	10	25	40	0.1	0.2	0.1	0.4	0.1
15	150	100	10	25	40	-0.1	-0.2	0.4	0.2	0.0
16	150	149	10	25	40	-0.4	-0.6	2.1	-1.0	0.3
17	150	1	10	5	20	0.4	0.6	-0.1	0.2	0.0
18	150	50	10	5	20	0.1	0.2	0.1	0.4	0.1
19	150	100	10	5	20	-0.1	-0.2	0.4	0.2	0.0
20	150	149	10	5	20	-0.4	-0.6	0.4	-1.0	-1.2
21	150	1	10	1	20	0.4	0.6	0.1	0.2	0.1
22	150	50	10	1	20	0.1	0.2	0.3	0.4	0.3
23	150	100	10	1	20	-0.1	-0.2	0.5	0.2	0.1
24	150	149	10	1	20	-0.4	-0.6	0.6	-1.0	-1.1
25	150	1	10	10	20	0.4	0.6	-0.1	0.2	0.0
26	150	50	10	10	20	0.1	0.2	0.1	0.4	0.4
27	150	100	10	10	20	-0.1	-0.2	0.3	0.2	-0.1
28	150	149	10	10	20	-0.4	-0.6	0.4	-1.0	-1.3
29	150	1	10	25	20	0.4	0.6	-0.1	0.2	-0.1
30	150	50	10	25	20	0.1	0.2	0.0	0.4	0.0
31	150	100	10	25	20	-0.1	-0.2	0.2	0.2	-0.2
32	150	149	10	25	20	-0.4	-0.6	0.3	-1.0	-1.3

Table 7-2 Effect of the remote source settings on the locators' accuracy for an untransposed horizontal line (Fig. 5-1) represented by the transposed line data, subjected to 'a'-earth faults. The actual values of source capacity and X/R ratio at both ends are 5GVA and 40 respectively. The other parameters are set at the reference conditions of Section 6.3.

Key to Table

L=line length, x=actual distance to fault from near end

Tosh=Toshiba, Schw=Schweitzer

Q_R, X/R=Source capacity and X/R ratio settings at the remote end

Error(%)=100x(estimated distance to fault − actual distance to fault)/total line length

No	L km	x km	R_f (Ω)	% error in [Z]-matrix mag	% error in [Z]-matrix arg	Error (%) New md-1	Error (%) New md-2	Error (%) ASEA	Error (%) Tosh	Error (%) Schw
1	150	1	10	0	0	0.0	0.0	0.0	0.2	0.1
2	150	50	10	0	0	0.0	0.0	0.0	0.1	0.0
3	150	100	10	0	0	0.0	0.0	0.2	-0.3	-0.1
4	150	149	10	0	0	0.0	0.0	0.7	-1.8	-0.9
5	150	1	10	+5	0	1.0	1.4	0.0	0.2	0.0
6	150	50	10	+5	0	0.3	0.5	-1.6	-1.5	-1.6
7	150	100	10	+5	0	-0.3	-0.5	-3.0	-3.4	-3.3
8	150	149	10	+5	0	-1.0	-1.4	-4.2	-6.3	-5.6
9	150	1	10	-5	0	-1.1	-1.6	0.0	0.2	0.1
10	150	50	10	-5	0	-0.4	-0.5	1.8	1.9	1.8
11	150	100	10	-5	0	0.4	0.5	3.7	3.2	3.4
12	150	149	10	-5	0	1.1	1.6	6.1	3.3	4.4
13	150	1	10	0	+5	0.0	0.1	0.3	0.2	0.4
14	150	50	10	0	+5	0.0	0.0	0.1	0.0	0.1
15	150	100	10	0	+5	0.0	0.0	-0.3	-0.7	-0.5
16	150	149	10	0	+5	0.0	-0.1	-1.6	-3.1	-2.0
17	150	1	10	0	-5	0.1	0.1	-0.3	0.2	-0.2
18	150	50	10	0	-5	0.1	0.0	0.2	0.4	0.2
19	150	100	10	0	-5	-0.1	0.0	1.0	0.3	0.7
20	150	149	10	0	-5	-0.1	-0.1	3.4	-1.0	1.8
21	150	1	10	+5	+5	0.9	1.5	0.2	0.2	0.3
22	150	50	10	+5	+5	0.3	0.5	-1.5	-1.6	-1.5
23	150	100	10	+5	+5	-0.3	-0.5	-3.5	-3.6	-3.8
24	150	149	10	+5	+5	-0.9	-1.5	-6.1	-6.6	-7.5
25	150	1	10	+5	-5	1.1	1.5	0.3	0.2	-0.2
26	150	50	10	+5	-5	0.4	0.5	-1.4	-1.2	-1.4
27	150	100	10	+5	-5	-0.4	-0.5	-2.3	-2.8	-2.6
28	150	149	10	+5	-5	-1.1	-1.5	-1.9	-5.6	-3.3

Table 7-3 Effect of the [Z] matrix errors on the locators' accuracy for a transposed horizontal line (Fig. 5-1) subjected to 'a'-earth faults. The other parameters are set at the reference conditions of Section 6.3.

Key to Table

L=line length, x=actual distance to fault from near end
mag=magnitude, arg=argument
Tosh=Toshiba, Schw=Schweitzer
Error(%)=100x(estimated distance to fault – actual distance to fault)/total line length

No	L km	x km	R_f (Ω)	% error in [Z]-matrix mag	arg	Error (%) New md-1	md-2	ASEA	Tosh	Schw
1	150	1	10	0	0	0.4	0.6	0.0	0.2	0.1
2	150	50	10	0	0	0.1	0.2	0.3	0.4	0.3
3	150	100	10	0	0	-0.1	-0.2	0.7	0.2	0.4
4	150	149	10	0	0	-0.4	-0.6	1.6	-1.0	-0.1
5	150	1	10	+5	0	1.3	2.0	0.0	0.2	0.0
6	150	50	10	+5	0	0.5	0.7	-1.3	-1.3	-1.3
7	150	100	10	+5	0	-0.5	-0.7	-2.5	-2.9	-2.8
8	150	149	10	+5	0	-1.3	-2.0	-3.3	-5.6	-4.8
9	150	1	10	-5	0	-0.7	-0.9	0.1	0.3	0.1
10	150	50	10	-5	0	-0.2	-0.3	2.1	2.1	2.1
11	150	100	10	-5	0	0.2	0.3	4.3	3.7	3.9
12	150	149	10	-5	0	0.7	0.9	7.1	4.1	5.2
13	150	1	10	0	+5	0.3	0.7	0.3	0.2	0.4
14	150	50	10	0	+5	0.1	0.2	0.3	0.2	0.3
15	150	100	10	0	+5	-0.1	-0.2	0.2	0.0	-0.2
16	150	149	10	0	+5	-0.3	-0.7	-0.7	-1.2	-2.3
17	150	1	10	0	-5	0.5	0.7	-0.3	0.2	-0.2
18	150	50	10	0	-5	0.2	0.3	0.5	0.7	0.5
19	150	100	10	0	-5	-0.2	-0.3	1.6	0.8	1.2
20	150	149	10	0	-5	-0.5	-0.7	4.4	-0.2	2.7
21	150	1	10	+5	+5	1.3	2.1	0.2	0.2	0.3
22	150	50	10	+5	+5	0.4	0.7	-1.3	-1.4	-1.3
23	150	100	10	+5	+5	-0.4	-0.7	-2.9	-3.1	-3.3
24	150	149	10	+5	+5	-1.3	-2.0	-5.2	-5.8	-6.8
25	150	1	10	+5	-5	1.5	2.1	-0.3	0.2	-0.2
26	150	50	10	+5	-5	0.5	0.7	-1.2	-1.0	-1.2
27	150	100	10	+5	-5	-0.5	-0.7	-1.7	-2.4	-2.1
28	150	149	10	+5	-5	-1.4	-2.1	-1.0	-4.9	-2.5

Table 7-4 Effect of the [Z] matrix errors on the locators' accuracy for an <u>untransposed</u> horizontal line (Fig. 5-1) represented by the transposed line data, subjected to 'a'-earth faults. The other parameters are set at the reference conditions of Section 6.3.

<u>Key to Table</u>

L=line length, x=actual distance to fault from near end
mag=magnitude, arg=argument
Tosh=Toshiba, Schw=Schweitzer
Error(%)=100x(estimated distance to fault − actual distance to fault)/total line length

No	L	x	Magnitude errors in the phasors (%)				Error (%)				
							New		ASEA	Tosh	Schw
	km	km	$\overline{V}_S$	$\overline{I}_S$	$\overline{V}_R$	$\overline{I}_R$	md-1	md-2			
1	150	1	0	0	0	0	0.0	0.0	0.0	0.2	0.1
2	150	50	0	0	0	0	0.0	0.0	0.0	0.1	0.0
3	150	100	0	0	0	0	0.0	0.0	0.2	-0.3	-0.1
4	150	149	0	0	0	0	0.0	0.0	0.7	-1.8	-0.9
5	150	1	+2	+2	-2	-2	1.1	2.0	0.0	0.2	0.1
6	150	50	+2	+2	-2	-2	1.6	2.4	0.0	0.1	0.0
7	150	100	+2	+2	-2	-2	1.6	2.4	0.2	-0.3	-0.1
8	150	149	+2	+2	-2	-2	1.1	2.1	0.7	-1.8	-0.9
9	150	1	-2	-2	+2	+2	-1.1	-2.0	0.0	0.2	0.1
10	150	50	-2	-2	+2	+2	-1.6	-2.4	0.0	0.1	0.0
11	150	100	-2	-2	+2	+2	-1.6	-2.4	0.2	-0.3	-0.1
12	150	149	-2	-2	+2	+2	-1.1	-2.1	0.7	-1.8	-0.9
13	150	1	+2	-2	+2	-2	-0.8	-1.2	0.0	0.2	0.1
14	150	50	+2	-2	+2	-2	-0.3	-0.4	1.4	1.5	1.4
15	150	100	+2	-2	+2	-2	0.3	0.4	2.4	2.4	2.6
16	150	149	+2	-2	+2	-2	0.8	1.2	4.9	2.1	3.2
17	150	1	-2	+2	-2	+2	0.8	1.2	0.0	0.2	0.0
18	150	50	-2	+2	-2	+2	0.3	0.4	-1.3	-1.2	-1.3
19	150	100	-2	+2	-2	+2	-0.3	-0.4	-2.5	-2.9	-2.8
20	150	149	-2	+2	-2	+2	-0.8	-1.2	-3.4	-5.6	-4.8

Table 7-5 Effect of the phasor magnitude errors on the locators' accuracy for a transposed horizontal line (Fig. 5-1) subjected to 'a'-earth faults. The other parameters are set at the reference conditions of Section 6.3 for a 10Ω fault resistance.

Key to Table

L=line length, x=actual distance to fault from near end
S,R=subscripts for sending and receiving end, respectively
Tosh=Toshiba, Schw=Schweitzer
Error(%)=100x(estimated distance to fault - actual distance to fault)/total line length

No	L	x	Argument errors in the phasors (degrees)				Error (%)				
							New		ASEA	Tosh	Schw
	km	km	$\bar{V}_S$	$\bar{I}_S$	$\bar{V}_R$	$\bar{I}_R$	md-1	md-2			
1	150	1	0	0	0	0	0.0	0.0	0.0	0.2	0.1
2	150	50	0	0	0	0	0.0	0.0	0.0	0.1	0.0
3	150	100	0	0	0	0	0.0	0.0	0.2	-0.3	-0.1
4	150	149	0	0	0	0	0.0	0.0	0.7	-1.8	-0.9
5	150	1	$+10^o$	$+10^o$	-10^o	-10^o	-1.8	-1.8	0.0	0.2	0.1
6	150	50	$+10^o$	$+10^o$	-10^o	-10^o	-1.1	-0.9	0.0	0.1	0.0
7	150	100	$+10^o$	$+10^o$	-10^o	-10^o	-0.1	0.1	0.2	-0.3	-0.1
8	150	149	$+10^o$	$+10^o$	-10^o	-10^o	0.2	0.8	0.7	-1.8	-0.9
9	150	1	-10^o	-10^o	$+10^o$	$+10^o$	-0.2	-0.8	0.0	0.2	0.1
10	150	50	-10^o	-10^o	$+10^o$	$+10^o$	0.1	-0.1	0.0	0.1	0.0
11	150	100	-10^o	-10^o	$+10^o$	$+10^o$	1.1	0.9	0.2	-0.3	-0.1
12	150	149	-10^o	-10^o	$+10^o$	$+10^o$	1.8	1.8	0.7	-1.8	-0.9
13	150	1	$+10^o$	-10^o	$+10^o$	-10^o	1.6	1.9	7.4	7.6	7.5
14	150	50	$+10^o$	-10^o	$+10^o$	-10^o	0.5	0.6	8.6	8.6	8.6
15	150	100	$+10^o$	-10^o	$+10^o$	-10^o	-0.5	-0.6	*	*	*
16	150	149	$+10^o$	-10^o	$+10^o$	-10^o	-1.6	-1.9	*	*	*
17	150	1	-10^o	$+10^o$	-10^o	$+10^o$	0.8	1.6	-7.3	7.3	-7.4
18	150	50	-10^o	$+10^o$	-10^o	$+10^o$	0.3	0.6	*	*	*
19	150	100	-10^o	$+10^o$	-10^o	$+10^o$	-0.3	-0.6	*	*	*
20	150	149	-10^o	$+10^o$	-10^o	$+10^o$	-0.8	-1.6	*	*	*

Table 7-6 Effect of the phasor argument errors on the locators' accuracy for a transposed horizontal line (Fig. 5-1) subjected to 'a'-earth faults. The other parameters are set at the reference conditions of Section 6.3 for a 10Ω fault resistance.

Key to Table

L=line length, x=actual distance to fault from near end
S,R=subscripts for sending and receiving end, respectively
Tosh=Toshiba, Schw=Schweitzer
* more than 10% error
Error(%)=100x(estimated distance to fault − actual distance to fault)/total line length

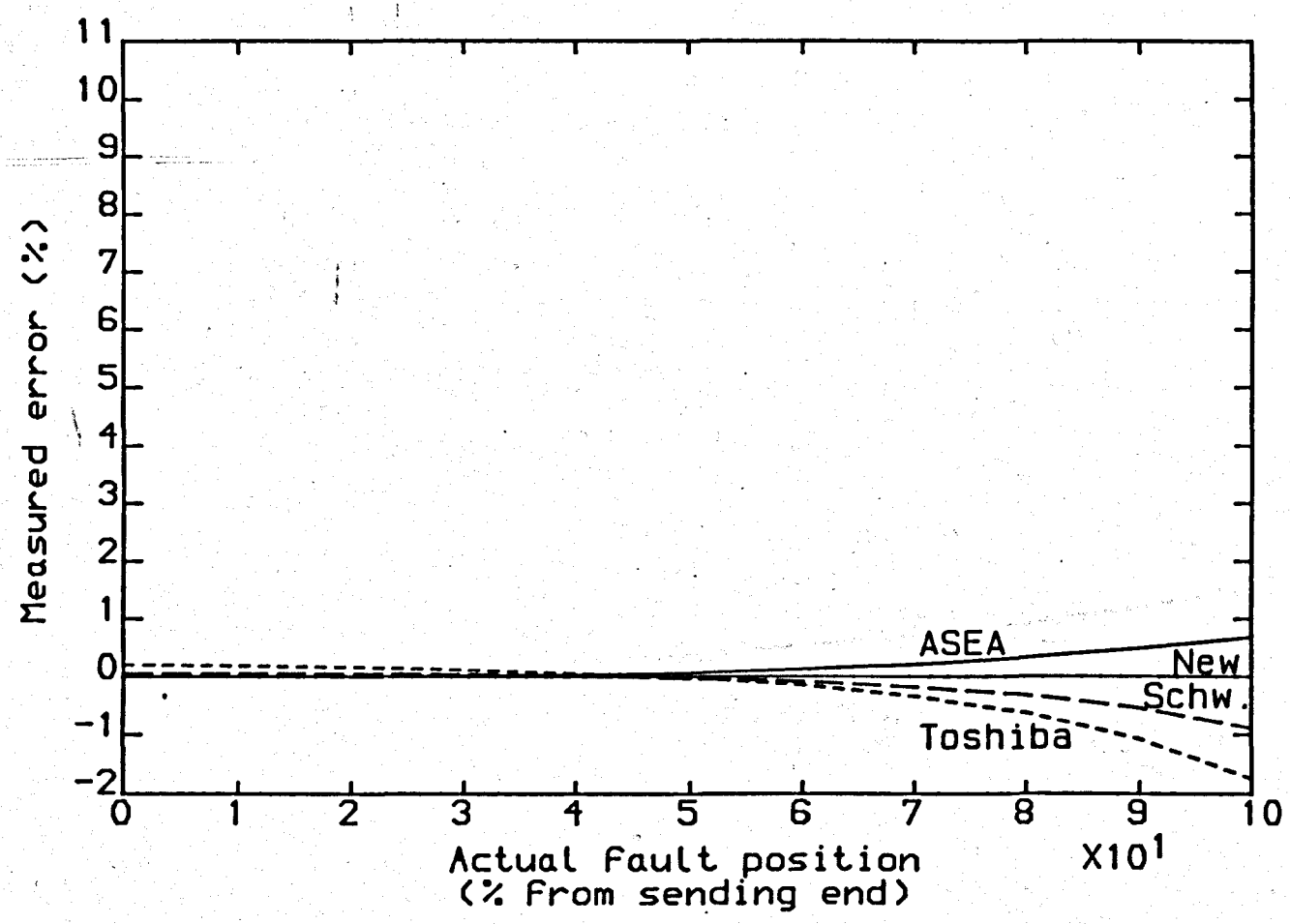

Fig. 7-1 Measured errors of the reference fault conditions for a transposed line

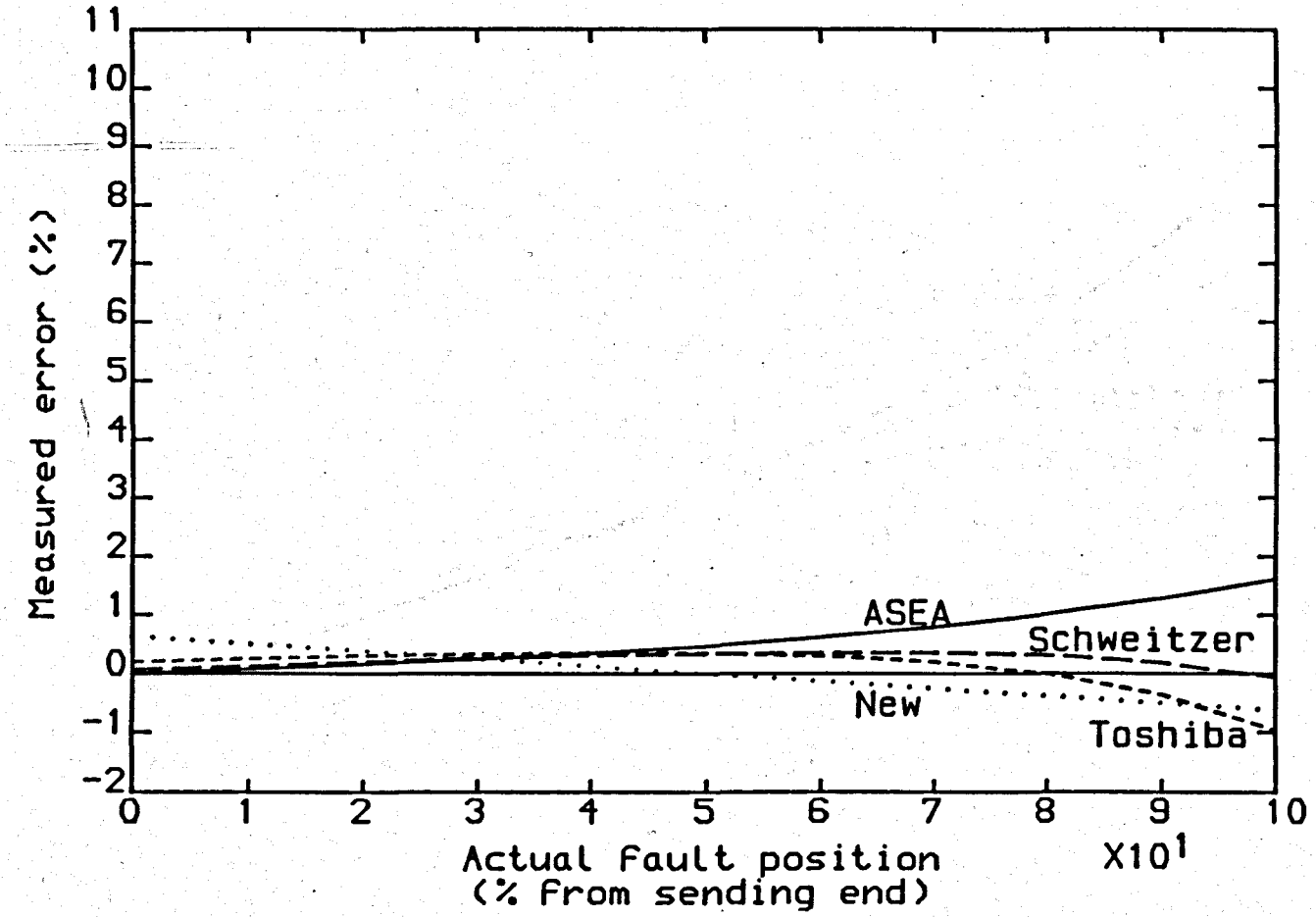

Fig. 7-2 Measured errors of the reference fault conditions for an untransposed line

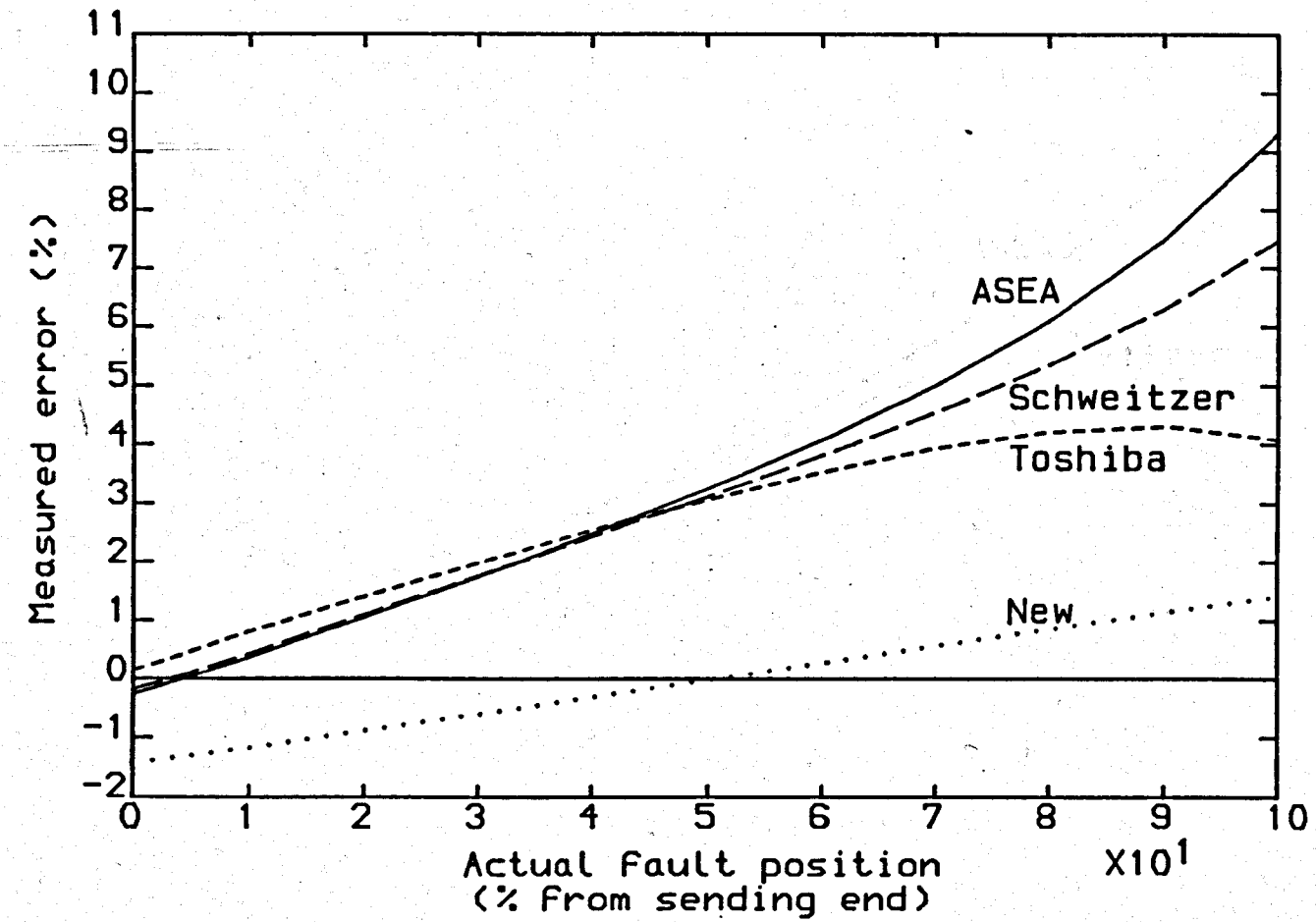

Fig. 7-3 Effect of [Z] matrix errors on the locators' accuracy for a transposed line

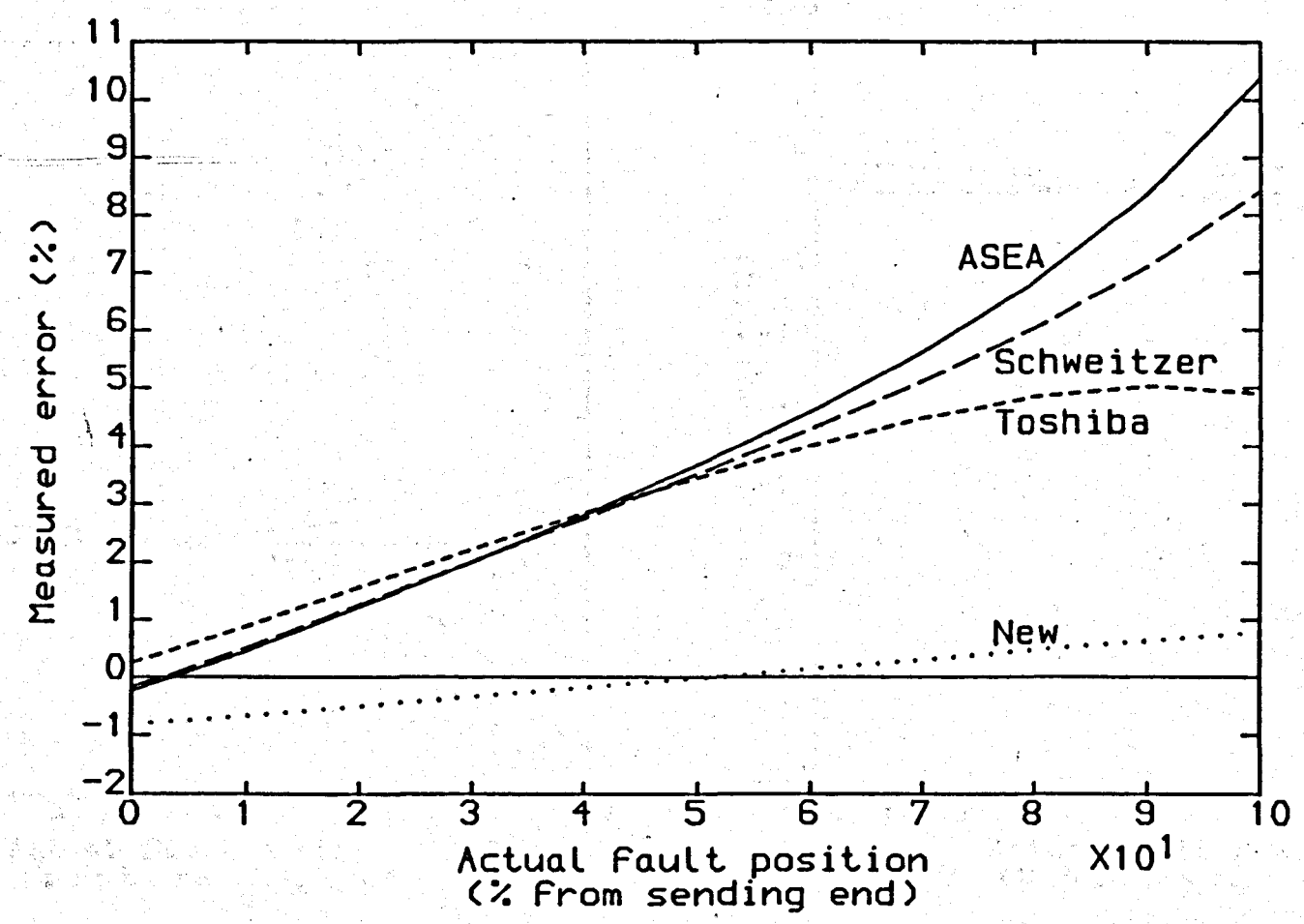

Fig. 7-4 Effect of [Z] matrix errors on the locators' accuracy for an utransposed line

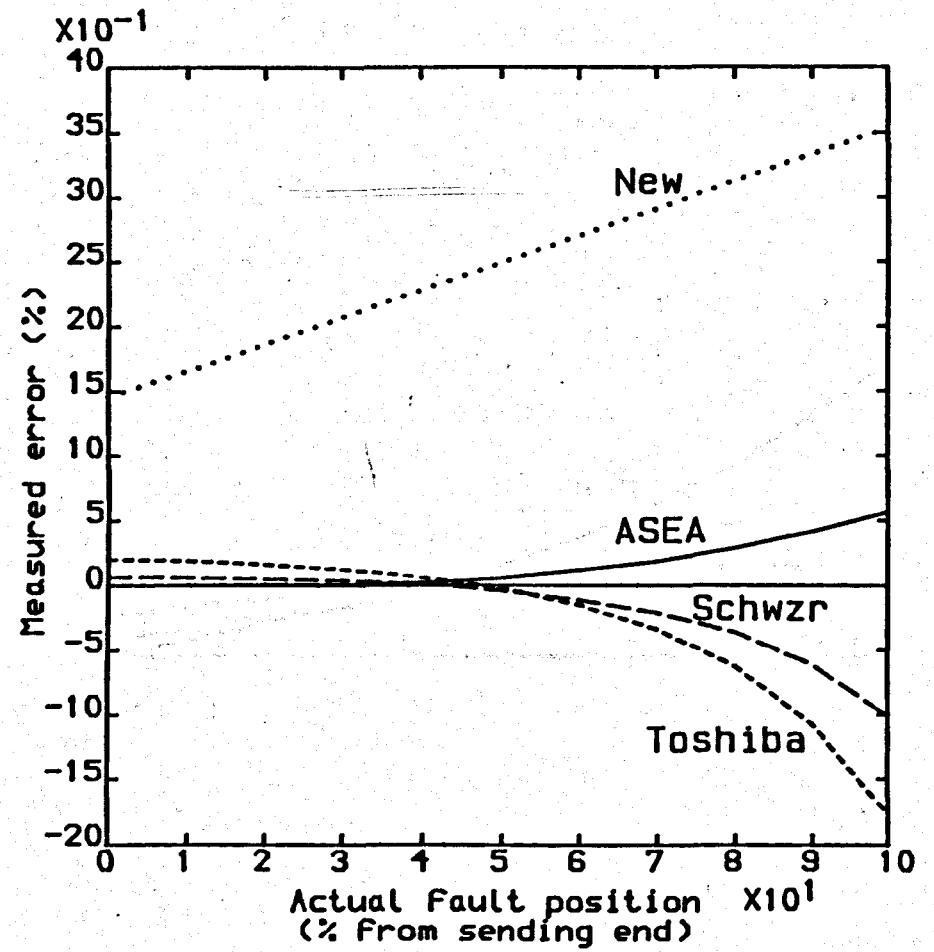

(a) +5% setting error

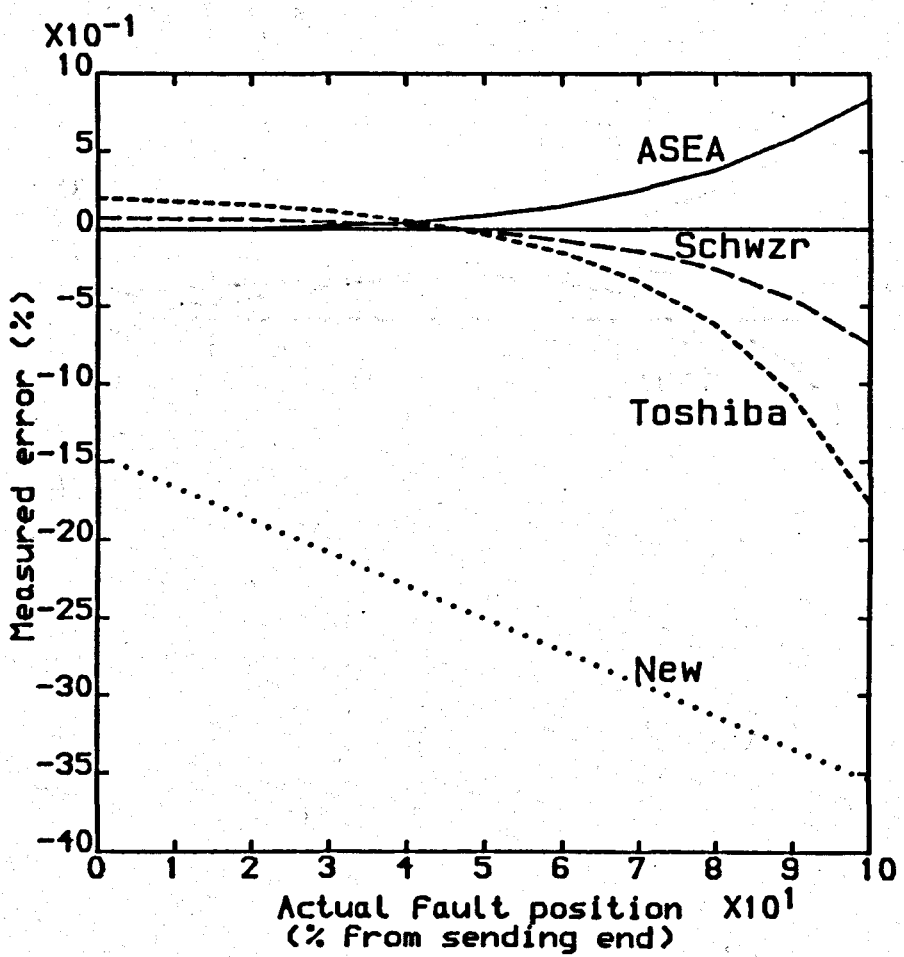

(b) -5% setting error

Fig. 7-5 Effect of line length setting errors on the locators' accuracy for a transposed line

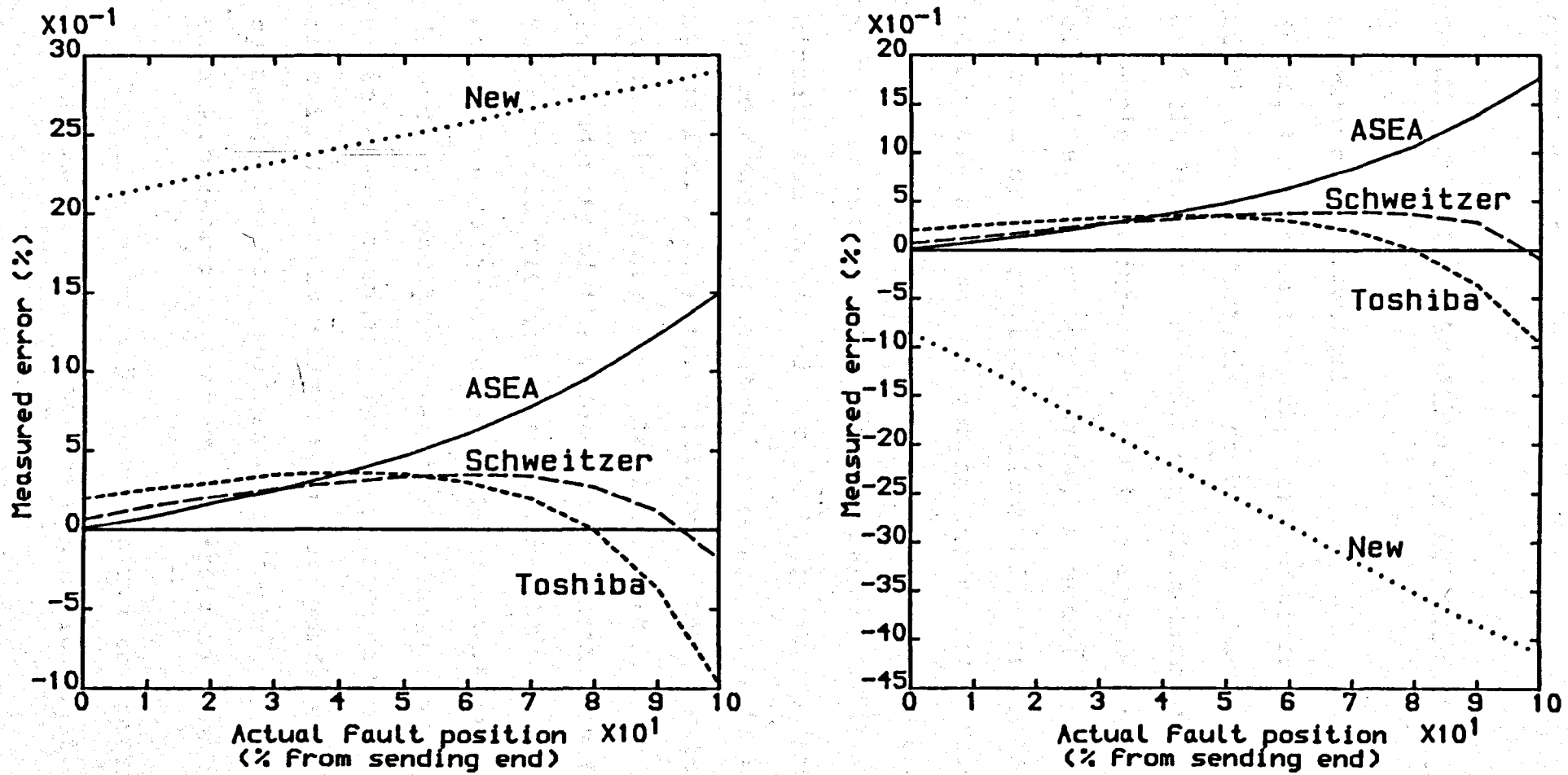

Fig. 7-6 Effect of line length setting errors on the locators' accuracy for an untransposed line

CHAPTER 8

CONCLUSIONS AND SUGGESTIONS FOR FUTURE WORK

8.1 General Conclusions

It has been shown that the new technique can successfully utilise modal quantities to render an accurate estimation of fault location. A modal transformation has been used to decouple a multiphase system into a number of single-phase circuits. In other words, a modal transformation eliminates mutual coupling effects inherent in a multiphase system. The particular transformations adopted for 3-phase systems define wave propagation in three modes; an earth-mode and two aerial-modes. Each modal circuit can be solved for fault location, provided that the corresponding modal voltages and currents are produced by the fault. However, utilising an aerial circuit is more desirable since the fault location is evaluated independently of the indeterminate earth path resistivity. For example, it has been shown that for a perfectly transposed line an aerial-mode (mode-2) network is only dependent upon the positive sequence network. Also, aerial-mode coupling between each circuit of double-circuit lines is eliminated for perfectly transposed systems, i.e. the fault location technique can be applied to a double-circuit line on a circuit-by-circuit basis.

The line eigenvalues and eigenvector matrix required for the modal transformation are evaluated from the line

geometry and line parameters. For perfectly transposed lines an eigenvector matrix with real elements can be defined and the eigenvalues are simply evaluated from the sequence networks. However, for each untransposed line application, a set of eigenvalues and an eigenvector matrix are required to be evaluated which involves some mathematical operations. The line simulation program described in Chapter 3 can evaluate eigenvalues and eigenvectors for any line application. Once the line eigenvalues and eigenvector matrix are evaluated they are then set into the locators.

Given the exact line eigenvalues and eigenvector matrix, the new algorithm gives no error in fault location irrespective of line transposition status, line length, fault position, fault resistance, source configuration, etc. An aerial-mode can be used for any type of fault and no fault type identification is required. Previous fault location algorithms use different routines for different types of fault. Either superimposed or total postfault voltages and currents can be used.

Because of difficulties associated with the evaluation of eigenvalues and the eigenvector matrix for untransposed lines, the performance of the new algorithm was tested using assumed transposed line eigenvalues and eigenvectors. For extreme fault conditions which rarely occur in practice, acceptable accuracy has been observed from the simulation test results. Moreover, for

untransposed double-circuit lines even by assuming perfect transposition as well as using only the data from the faulted circuit, very accurate results have been obtained. Also it has been shown that for any type of fault on single-circuit horizontal lines and double-circuit lines an aerial-mode can be used thereby avoiding the use of indeterminate earth path resistivity as required for earth-mode surge impedance and eigenvalue calculations.

In summary, when perfect transposition is assumed for untransposed lines the following points must be considered:

(a) For any type of fault and line configuration the superimposed values of current and voltage should be used.

(b) For the vertical single-circuit line configuration (Fig. 5-2), mode selection is required as the earth-mode must be used for earth faults and an aerial-mode for phase faults.

(c) For the horizontal line configuration with the phase arrangement of Fig. 5-1, an aerial-mode can be used for any type of fault. In practice, mode-2 can be used for any type of fault giving almost no error.

(d) For the double-circuit line configuration using the data from the faulted circuit only, mode-2 can be used for any type of fault.

Knowing that the single-circuit horizontal line configuration with 'a'-'b'-'c' phase arrangement and the

double-circuit line configuration are commonly used in practice, it is concluded that for most untransposed lines, assumed transposed eigenvalues and associated eigenvector matrix can be used. It has been shown that for these lines the accuracy of fault location is better than 1% in nearly all cases, even by using an aerial-mode for all types of fault.

In a comparative analysis of different techniques it has been shown that the new algorithm has achieved much higher accuracy than the other algorithms used in the best commercially available fault locators for which published information is available. For transposed lines while the new algorithm gives no error irrespective of fault position, line length, fault resistance, prefault power flow, source configuration or fault type, the competing algorithms are affected (in different scales) by these parameters.

For untransposed lines, some errors are inevitable if the transposed line parameters are used. However, the new algorithm gives more accurate results than the alternatives. The accuracy of the new algorithm is not affected by fault resistance, prefault power flow or source impedances. The maximum error recorded for the new algorithm was less than 1% in nearly all test cases. For the competing algorithms it has been shown that non-transposition of lines exaggerates the errors from other sources, and very large errors have been observed in some

cases.

The effect of non-algorithmic errors has also been considered in the performance evaluation of the algorithms. These errors are caused by incorrect settings and inaccuracy in signal recording and processing.

Those algorithms which require a remote source impedance setting are prone to errors if the set value is different from the actual one. This usually occurs as the remote source configuration changes under different load conditions. The new algorithm does not require a remote source setting and therefore it is immune to this source of error.

Any fault location algorithm requires a setting either for the [Z] matrix or the sequence impedances per unit length. The [Y] matrix, which mainly represents the effect of shunt capacitance, has much smaller effect and most algorithms ignore its effect. It has been shown that for typical test cases the competing algorithms give 5% extra error for a 5% error in the magnitudes of the [Z] matrix elements and 2% extra error for a 5% error in the arguments. By contrast the new algorithm performs very well; a 5% error in the magnitudes and/or the arguments resulting in only a maximum 1.6% extra error.

A further source of setting errors relates to the line length. The competing algorithms are not affected very much by line length setting errors since they calculate

distance to fault, directly or indirectly, as a percentage of the line length. The new algorithm also gives no error if the fault location is displayed as a percentage of the line length.

A good indication of the likely effect of hardware errors on the accuracy has been obtained by introducing various combinations of errors in the magnitudes and arguments of the voltage and current phasors entered into the fault location algorithms. It has been shown that for magnitude errors the maximum error of the competing algorithms is at least twice the maximum error of the new algorithm. For the typical fault cases involving $\pm 10^{o}$ error in the arguments there is at least 7% additional error for the competing algorithms, while the maximum error for the new algorithm is 1.9%. The high sensitivity of the competing algorithms necessitates more accurate hardware equipment and software signal processing to minimise the errors in the phasor data input. On the other hand the insensitivity of the new algorithms is advantageous in some cases. For example, the synchronisation of the phasor data at the line ends can be obtained by assuming the prefault current at both ends is equal, even for long lines, therefore the zero crossing of these currents can be used as common reference for phasor measurements at the line ends, in spite of some phase shift caused by the capacitance currents.

8.2 Suggestions for Future Work

Pursuit of the work in some major areas is discussed in this Section.

8.2.1 Further Simulation Tests

Many simulation tests were carried out for different line configurations and fault types for both transposed and untransposed lines. Further tests can be performed by using the line simulation program and the algorithm simulations, but it is most probable that the tests performed up to now are conclusive for the research part of the work. In the simulation studies, however, for untransposed lines it was assumed that no discrete transpositions were made along the line. A series of tests, similar to those for transposed and untransposed lines, can be carried out for untransposed lines with some discrete transpositions along the lines. The line simulation program can be used section by section and voltages and currents at any point on the line can be evaluated. It is expected that all the algorithms will give more accurate results for this case than the similar case for untransposed lines without any discrete transposition.

8.2.2 Site Tests

The accuracy of the new algorithm should be tested by input data captured from real systems. These data could also be used to measure the accuracy of the competing algorithms. As fault location estimation is an off-line

process, the fault location techniques can be programmed on a small computer at any site. For the new algorithm, the line simulation program may also be used to evaluate the required eigenvalues and eigenvectors. Another method of implementing the new technique is to develop a prototype unit type fault locator for site trials. In the future commercial application the new locator could, if necessary, be an integral part of a microprocessor-based protection unit.

8.2.3 Single-End Measurement Fault Location

The new technique requires phasor data from both ends of a transmission line. However, there is no need for a continuous data link between the line ends and data can be transferred by voice over a telephone link, for example. In return, the new technique renders a more accurate estimation of fault location when compared with other fault location techniques. Also, as discussed previously, its insensitivity to most sources of error, either algorithmic or non-algorithmic, is a considerable achievement. Nevertheless, a considerable effort has been made in applying the modal principles when the phasor data from the near end and a representative value of source impedance from the remote end are available. The idea was to obtain the fault path current for two different modes in terms of the sending end data and the equivalent circuit beyond the fault point. Then from the eigenvector matrix the relationship between these currents are obtained. For example, if for a particular fault mode-1

and mode-2 fault path currents are equal, equating the equations eliminates the need for defining the fault path currents and distance to fault is evaluated. The idea, however, could only be applied to a perfectly transposed line with a balanced source network; because the mode-2 and mode-3 eigenvalues are identical in a perfectly transposed line, one of the two modes considered should be mode-1.

For untransposed lines, the source and line eigenvector matrices are generally different and therefore the equivalent circuit beyond the fault point cannot be defined in modal networks. In other words, for untransposed lines, the source voltage-current relationship is not decoupled in modal networks by using the same eigenvalues and eigenvectors of the line. It will be very difficult to find similar eigenvalues and eigenvectors for the source and line. A solution to this problem is to transfer modal source impedances from the remote source, obtained by dividing modal voltages to corresponding modal currents, following a fault. Obviously, this may be considered as a two-end measurement technique. Perhaps the only merit of this technique is that the synchronisation can be obviated as only the modal impedances are transferred; this requires extensive investigations for a practical system.

The simulation test results show that the above technique gives no error for transposed systems if all the

input data are set accurately, otherwise substantial errors can occur, i.e. the technique is very sensitive to non-algorithmic errors. Some further work in this area can be carried out when the remote source modal impedances are available, otherwise the single-end measurement algorithms used by Toshiba and ASEA studied in this thesis generally have better performances.

8.2.4 Teed Transmission Line Fault Location

It appears from the literature survey that no research work in power frequency based fault location has been published for Teed transmission lines. The growing number of such lines necessitates research in this area. Extending the new fault location idea to Teed lines could be the subject of another PhD study. This thesis gives an outline for conducting such work. It should be noted that the protection scheme of Teed lines provides the data link between the terminals as will be required for fault location purposes. A line simulation program, on the same basis developed in this thesis for two-ended lines, is required.

APPENDIX 3A

3A.1 Calculation Method of Shunt Admittance Matrix [Y]

The admittance matrix is a function only of the physical geometry of the conductors relative to the earth plane, because the conductor and earth surface may each be regarded as equipotential surfaces [19]. The [Y] matrix has no real part because the conductance of the earth path is negligible. The physical location of the conductors is defined with respect to a coordinate system, with the earth plane as horizontal reference axis and the axis of symmetry of the tower as vertical reference. From the coordinates of the conductors and the conductor radii, elements of a matrix [T] are calculated with i,jth element defined as:

$$T_{ij}=\log_e(D_{ij}/d_{ij}) \qquad (3A\text{-}1)$$

where D_{ij}=distance between ith conductor and the image of the jth conductor

d_{ij}=distance between ith conductor and jth conductor for $i\neq j$

d_{ij}=radius of ith conductor for $i=j$

The matrix [T] has order 3p+q where p is the number of circuits and q is the number of earth wires. If the charge vector is represented by $\bar{\Phi}$ and the voltage vector by $\bar{V}$, then:

$$\bar{V}=(1/2\pi\epsilon)([T]\bar{\Phi}) \qquad (3A\text{-}2)$$

it follows that:

$$\bar{\Phi}=2\pi\epsilon[T]^{-1}\bar{V} \qquad (3A-3)$$

but $\bar{V}$ is a column matrix whose last q elements are zero (the voltage of the earth wires), so that the last q columns of $[T]^{-1}$ can be discarded. The last q rows of $[T]^{-1}$ give the earth wire charges, and as these are not generally required, these q rows are also discarded. The matrix obtained by discarding the last q rows and columns of $[T]^{-1}$ is $[T_A]^{-1}$ and has order 3p.

The shunt admittance matrix is defined by the equation $\bar{I}=[Y]\bar{V}$ and since:

$$\bar{I}=d\bar{\Phi}/dt=jw\bar{\Phi}=j2\pi w\epsilon[T_A]^{-1}\bar{V} \qquad (3A-4)$$

therefore;

$$[Y]=j2\pi w\epsilon[T_A]^{-1} \qquad (3A-5)$$

where [Y] includes for the effect of earth wires.

3A.2 Calculation Method of Series Impedance Matrix [Z]

The series impedance matrix consists of five components as is given by:

$$[Z]=[R_c+R_e+j(X_c+X_g+X_e)] \qquad (3A-6)$$

where R and X are series resistance and inductance matrices per unit length with the suffices standing for:

c=contribution of the conductor

e=contribution of the earth path

g=contribution of the reactance due to physical geometry of the conductors

Reactance due to physical geometry, X_g, is calculated directly from:

$$X_g = w\mu[T]/2\pi \qquad (3A-7)$$

where [T] was derived for the [Y] matrix and is of order 3p+q.

The contribution of resistance and reactance R_e and X_e, due to the earth return path, is calculated by using infinite series developed by Carson [20].

The calculation of R_c and x_c is complicated by the irregular surface profile of the conductor due to stranding. At power frequency it is assumed that R_c is equal to the d.c. resistance per unit length of the conductor. However, if skin effect is significant, the manufacturer's power frequency value is used. The internal inductance and hence X_c is calculated in the standard way by the concept of geometric mean radius [19].

In general the [Z] matrix calculated in the above manner will have order 3p+q, where p is the number of circuits and q is the number of earth wires. As in the case of [Y] matrix, the last q rows and columns are discarded, and the modified matrix of order 3p is reinverted to give the corrected [Z] matrix which allows for the effect of the earth wires.

3A.3 Bundled Conductors

Transmission lines are usually constructed with more than one conductor per phase separated at regular intervals along the span length by metal spaces. The purpose of these bundled conductors is to reduce potential gradients at the surface of the conductors and hence minimise losses due to corona which must also be considered from the point of view of noise generation.

One method of dealing with the bundled conductors in analysis is to replace them by means of an equivalent phase conductor whose diameter Di is given by:

$$Di=\{ndG^{(n-1)}\}^{1/n}$$

where: d=diameter of the bundled conductor

n=number of bundled conductors

G=the diameter of the circle through the centres of the bundled conductors

The internal impedance of the equivalent conductor is obtained by taking the impedance of one of the bundled conductors and dividing by the number of conductors in the bundle.

APPENDIX 3B

Calculation Methods for Eigenvalues and Eigenvectors

Putting $[Z][Y]=[P]$ then $[P]=[Q][\Gamma^2][Q]^{-1}$ or $[P][Q]=[Q][\Gamma^2]$, so that the kth eigenvalue Γ_k^2 of $[Z][Y]$ is given by:

$$[P][Q_k]=[Q_k]\Gamma_k^2 \text{ or } ([P]-\Gamma_k^2[U])[Q_k]=0 \qquad (3B\text{-}1)$$

The trivial solution is $Q_k=0$ applies unless the determinant of the coefficient is zero, i.e. unless:

$$\det([P]-\Gamma_k^2[U])=0 \text{ for } k=1,2,..,n \qquad (3B\text{-}2)$$

This leads to n equations with n roots $\Gamma_1^2,\Gamma_2^2,..,\Gamma_n^2$ which are the eigenvalues of [P].

The root squaring method of finding eigenvalues and eigenvectors has been found particularly useful in processing the [Z][Y] matrix. It must be pointed out, however, that in the case of near equal roots direct application of the method can lead to an excessive number of squaring in order to separate them out and so reach convergence. Methods are available for improving the rate of convergence and of taking advantage of symmetry in the system and are discussed in Refs. 15 and 16.

The foregoing method cannot be used to evaluate eigenvalues and eigenvectors when the line is perfectly transposed as the matrix product of [Z][Y] gives two equal eigenvalues and the routine does not converge. Instead a

matrix of eigenvectors can be defined for transposed lines. It should be noted that this matrix is not unique and as an example the sequence component transformation matrix given in Eq. (3B-3) is well-known in the analysis of power systems.

$$[Q]=\begin{bmatrix}1 & 1 & 1\\ 1 & a^2 & a\\ 1 & a & a^2\end{bmatrix} \quad \text{where } a=\exp(j120^{o}) \tag{3B-3}$$

But the eigenvector matrix and its inverse given in Eq. (3B-4) has the advantage of having real elements only and it is more suitable for the purpose of the work presented in this thesis. Also, for this special case, the modal propagation constants (which are the square root of the eigenvalues) and the surge impedances take a simplified form as given in Eq. (3B-5). Having the general form of the [Z] and [Y] matrices shown in Eq. (3B-6) the assumed self and mutual parameters (Z_S, Z_m, Y_S, Y_m) in this case are as given in Eq. (3B-7).

$$[Q]=\begin{bmatrix}1 & 1 & 1\\ 1 & 0 & -2\\ 1 & -1 & 1\end{bmatrix},\quad [Q]^{-1}=\frac{1}{6}\begin{bmatrix}2 & 2 & 2\\ 3 & 0 & -3\\ 1 & -2 & 1\end{bmatrix} \tag{3B-4}$$

$$\left.\begin{aligned}&\Gamma_1=[(Z_S+2Z_m)(Y_S-2Y_m)]^{\frac{1}{2}}=(Z_0Y_0)^{\frac{1}{2}}\\ &\Gamma_2=\Gamma_3=[(Z_S-Z_m)(Y_S+Y_m)]^{\frac{1}{2}}=(Z_PY_P)^{\frac{1}{2}}\\ &Z_{01}=(Z_0/Y_0)^{\frac{1}{2}},\quad Z_{02}=Z_{03}=(Z_P/Y_P)^{\frac{1}{2}}\end{aligned}\right\} \tag{3B-5}$$

$$[Z]=\begin{bmatrix} Z_{aa} & Z_{ab} & Z_{ac} \\ Z_{ba} & Z_{bb} & Z_{bc} \\ Z_{ca} & Z_{cb} & Z_{cc} \end{bmatrix} \qquad [Y]=\begin{bmatrix} Y_{aa} & -Y_{ab} & -Y_{ac} \\ -Y_{ba} & Y_{bb} & -Y_{bc} \\ -Y_{ca} & -Y_{cb} & Y_{cc} \end{bmatrix} \tag{3B-6}$$

$$\left.\begin{aligned} Z_S&=(Z_{aa}+Z_{bb}+Z_{cc})/3 \ , \ Y_S=(Y_{aa}+Y_{bb}+Y_{cc})/3 \\ Z_m&=(Z_{ab}+Z_{ac}+Z_{bc})/3 \ , \ Y_m=(Y_{ab}+Y_{ac}+Y_{bc})/3 \end{aligned}\right\} \tag{3B-7}$$

If perfect transposition of a double-circuit line is assumed, where the conductors are ordered a,b,c,A,B,C, say, the eigenvector matrix take the form of Eq. (3B-8). The modal parameters are likewise obtained in the simplified form of Eq. (3B-9) where the self and mutual terms are obtained from series impedance and shunt admittance matrices as shown in Eq. (3B-12).

$$[Q]=\begin{bmatrix} [Q_A] & -[Q_A] \\ [Q_A] & [Q_A] \end{bmatrix} \text{ where } [Q_A]=\begin{bmatrix} 1 & 1 & 1 \\ 1 & 0 & -2 \\ 1 & -1 & 1 \end{bmatrix} \tag{3B-8}$$

$$\left.\begin{aligned} \Gamma_1&=[(Z_S+2Z_m+3Z_M)(Y_S-2Y_m-3Y_M)]^{\frac{1}{2}} \\ \Gamma_2&=\Gamma_3=\Gamma_5=\Gamma_6=[(Z_S-Z_m)(Y_S+Y_m)]^{\frac{1}{2}} \\ \Gamma_4&=[(Z_S+2Z_m-3Z_M)(Y_S-2Y_m+3Y_M)]^{\frac{1}{2}} \\ Z_{01}&=[(Z_S+2Z_m+3Z_M)/(Y_S-2Y_m-3Y_M)]^{\frac{1}{2}} \\ Z_{02}&=Z_{03}=Z_{05}=Z_{06}=[(Z_S-Z_m)/(Y_S+Y_m)]^{\frac{1}{2}} \\ Z_{04}&=[(Z_S+2Z_m-3Z_M)/(Y_S-2Y_m+3Y_M)]^{\frac{1}{2}} \end{aligned}\right\} \tag{3B-9}$$

$$[Z]=\begin{bmatrix} Z_{aa} & Z_{ab} & Z_{ac} & Z_{aA} & Z_{aB} & Z_{aC} \\ Z_{ba} & Z_{bb} & Z_{bc} & Z_{bA} & Z_{bB} & Z_{bC} \\ Z_{ca} & Z_{cb} & Z_{cc} & Z_{cA} & Z_{cB} & Z_{cC} \\ Z_{Aa} & Z_{Ab} & Z_{Ac} & Z_{AA} & Z_{AB} & Z_{AC} \\ Z_{Ba} & Z_{Bb} & Z_{Bc} & Z_{BA} & Z_{BB} & Z_{BC} \\ Z_{Ca} & Z_{Cb} & Z_{Cc} & Z_{CA} & Z_{CB} & Z_{CC} \end{bmatrix} \qquad (3B\text{-}10)$$

$$[Y]=\begin{bmatrix} Y_{aa} & -Y_{ab} & -Y_{ac} & -Y_{aA} & -Y_{aB} & -Y_{aC} \\ -Y_{ba} & Y_{bb} & -Y_{bc} & -Y_{bA} & -Y_{bB} & -Y_{bC} \\ -Y_{ca} & -Y_{cb} & Y_{cc} & -Y_{cA} & -Y_{cB} & -Y_{cC} \\ -Y_{Aa} & -Y_{Ab} & -Y_{Ac} & Y_{AA} & -Y_{AB} & -Y_{AC} \\ -Y_{Ba} & -Y_{Bb} & -Y_{Bc} & -Y_{BA} & Y_{BB} & -Y_{BC} \\ -Y_{Ca} & -Y_{Cb} & -Y_{Cc} & -Y_{CA} & -Y_{CB} & Y_{CC} \end{bmatrix} \qquad (3B\text{-}11)$$

$$\left.\begin{aligned} Z_S&=(Z_{aa}+Z_{bb}+Z_{cc})/3=(Z_{AA}+Z_{BB}+Z_{CC})/3 \\ Z_m&=(Z_{ab}+Z_{ac}+Z_{bc})/3=(Z_{AB}+Z_{AC}+Z_{BC})/3 \\ Z_M&=(Z_{aA}+Z_{aB}+Z_{aC}+Z_{bA}+Z_{bB}+Z_{bC}+Z_{cA}+Z_{cB}+Z_{cC})/9 \end{aligned}\right\} \qquad (3B\text{-}12)$$

Similarly, Y_S, Y_m and Y_M are obtained from the [Y] matrix elements.

APPENDIX 3C

Evaluation of Superimposed Voltage-Current Relationship at Fault Point for Single-Circuit Lines

With reference to Fig. 3-4, if homogeneous line sections are assumed, two principal relationships emerge:

$$\begin{bmatrix} \overline{E}_{Ff} \\ -\overline{I}_{FSf} \end{bmatrix} = \begin{bmatrix} A_1 & B_1 \\ C_1 & D_1 \end{bmatrix} \begin{bmatrix} \overline{V}_{Sf} \\ -\overline{I}_{Sf} \end{bmatrix} \tag{3C-1}$$

$$\begin{bmatrix} \overline{E}_{Ff} \\ \overline{I}_{FRf} \end{bmatrix} = \begin{bmatrix} A_2 & B_2 \\ C_2 & D_2 \end{bmatrix} \begin{bmatrix} \overline{V}_{Rf} \\ \overline{I}_{Rf} \end{bmatrix} \tag{3C-2}$$

The voltages and currents at each end are related to the source impedance matrix by:

$$\overline{V}_{Sf} = -[Z_{SS}]\overline{I}_{Sf} \tag{3C-3}$$

$$\overline{V}_{Rf} = [Z_{SR}]\overline{I}_{Rf} \tag{3C-4}$$

Substituting Eq. (3C-4) into Eq. (3C-2) gives:

$$\left.\begin{aligned} \overline{E}_{Ff} &= (A_2 + B_2[Z_{SR}]^{-1})\overline{V}_{Rf} \\ \overline{I}_{FRf} &= (C_2 + D_2[Z_{SR}]^{-1})\overline{V}_{Rf} \end{aligned}\right\} \tag{3C-5}$$

from which:

$$\overline{E}_{Ff} = (A_2 + B_2[Z_{SR}]^{-1})(C_2 + D_2[Z_{SR}]^{-1})^{-1}\overline{I}_{FRf} \tag{3C-6}$$

Likewise using Eqs. (3C-1) and (3C-3):

$$\bar{E}_{Ff}=-(A_1+B_1[Z_{SS}]^{-1})(C_1+D_1[Z_{SS}]^{-1})^{-1}\bar{I}_{FSf} \qquad (3C-7)$$

Now considering any general earth fault:

$$\bar{E}_{Ff}=\bar{V}_{Ff}+[R_f](\bar{I}_{FSf}-\bar{I}_{FRf}) \qquad (3C-8)$$

where $[R_f]$ is a diagonal matrix of the required values of fault resistance in each phase. Using Eqs. (3C-6) and (3C-7) we have:

$$(\bar{I}_{FSf}-\bar{I}_{FRf})=-\{(C_1+D_1[Z_{SS}]^{-1})(A_1+B_1[Z_{SS}]^{-1})^{-1}+ (C_2+D_2[Z_{SR}]^{-1})(A_2+B_2[Z_{SR}]^{-1})^{-1}\}\bar{E}_{Ff} \qquad (3C-9)$$

Finally substituting Eq. (3C-9) in Eq. (3C-8):

$$\bar{V}_{Ff}=-\{[(C_1+D_1[Z_{SS}]^{-1})(A_1+B_1[Z_{SS}]^{-1})^{-1}+(C_2+D_2[Z_{SR}]^{-1}) (A_2+B_2[Z_{SR}]^{-1})^{-1}]^{-1}+[R_f]\}(\bar{I}_{FSf}-\bar{I}_{FRf}) \qquad (3C-10)$$

APPENDIX 3D

Evaluation of Superimposed Voltage-Current Relationship at Fault Point for Double-Circuit Lines

Because both circuits in a double-circuit line are connected to the same busbar at each end, Eq. (3-46) is not valid for double-circuit line because of the singularity of the source impedance matrix. To solve this problem a matrix partitioning technique is used.

For simplicity Eq. (3C-1) and (3C-2) are rewritten, noting that $A_1,\ldots,D_2$ are 6x6 matrices and $\bar{V}_{Sf},\ldots,\bar{I}_{Rf}$ are 6x1 vectors for double-circuit lines:

$$\begin{bmatrix} \bar{E}_{Ff} \\ -\bar{I}_{FSf} \end{bmatrix} = \begin{bmatrix} A_1 & B_1 \\ C_1 & D_1 \end{bmatrix} \begin{bmatrix} \bar{V}_{Sf} \\ -\bar{I}_{Sf} \end{bmatrix} \tag{3D-1}$$

$$\begin{bmatrix} \bar{E}_{Ff} \\ \bar{I}_{FRf} \end{bmatrix} = \begin{bmatrix} A_2 & B_2 \\ C_2 & D_2 \end{bmatrix} \begin{bmatrix} \bar{V}_{Rf} \\ \bar{I}_{Rf} \end{bmatrix} \tag{3D-2}$$

At double-circuit busbars, source voltage-current relationships, say, for sending end have the following form:

$$\begin{bmatrix} V_{Sa}=V_{SA} \\ V_{Sb}=V_{SB} \\ V_{Sc}=V_{SC} \end{bmatrix} = \begin{bmatrix} Z_{ss} & Z_{sm} & Z_{sm} \\ Z_{sm} & Z_{ss} & Z_{sm} \\ Z_{sm} & Z_{sm} & Z_{ss} \end{bmatrix} \begin{bmatrix} I_{Sa}+I_{SA} \\ I_{Sb}+I_{SB} \\ I_{Sc}+I_{SC} \end{bmatrix} \tag{3D-3}$$

Partitioning Eq. (3D-1) yields:

$$\begin{bmatrix} \bar{E}_{Ff1} \\ \bar{E}_{Ff2} \\ -\bar{I}_{FSf1} \\ -\bar{I}_{FSf2} \end{bmatrix} = \begin{bmatrix} A_{11} & A_{12} & B_{11} & B_{12} \\ A_{21} & A_{22} & B_{21} & B_{22} \\ C_{11} & C_{12} & D_{11} & D_{12} \\ C_{21} & C_{22} & D_{21} & D_{22} \end{bmatrix} \begin{bmatrix} \bar{V}_{Sf1} \\ \bar{V}_{Sf2} \\ -\bar{I}_{Sf1} \\ -\bar{I}_{Sf1} \end{bmatrix} \qquad (3D\text{-}4)$$

In the above equation $A_{11},\ldots,D_{22}$ are 3x3 matrices. Knowing that $\bar{V}_{Sf1}=\bar{V}_{Sf2}=\bar{V}'_{Sf}$ then:

$$\bar{V}'_{Sf}=-[Z_{SS}](\bar{I}_{Sf1}+\bar{I}_{Sf2}) \qquad (3D\text{-}5)$$

$$\bar{I}_{Sf2}=-[Z_{SS}]^{-1}\bar{V}'_{Sf}-\bar{I}_{Sf1} \qquad (3D\text{-}6)$$

Similarly at receiving end using $\bar{V}_{Rf1}=\bar{V}_{Rf2}=\bar{V}'_{Rf}$:

$$\bar{I}_{Rf2}=[Z_{SR}]^{-1}\bar{V}'_{Rf}-\bar{I}_{Rf1} \qquad (3D\text{-}7)$$

It is obvious $[Z_{SS}]$ and $[Z_{SR}]$ are 3x3 matrices. Now using Eq. (3D-4) and substituting for $\bar{I}_{Sf2}$, $\bar{V}_{Sf1}$ and $\bar{V}_{Sf2}$:

$$\begin{aligned} \bar{E}_{Ff1} &= (A_{11}+A_{12})\bar{V}'_{Sf}-B_{11}\bar{I}_{Sf1}-B_{12}\bar{I}_{Sf2} \\ &= (A_{11}+A_{12})\bar{V}'_{Sf}-B_{11}\bar{I}_{Sf1}-B_{12}(-[Z_{SS}]^{-1}\bar{V}'_{Sf}-\bar{I}_{Sf1}) \\ &= (A_{11}+A_{12}+B_{12}[Z_{SS}]^{-1})\bar{V}'_{Sf}-(B_{11}-B_{12})\bar{I}_{Sf1} \end{aligned} \qquad (3D\text{-}8)$$

$$\begin{aligned} \bar{E}_{Ff2} &= (A_{21}+A_{22})\bar{V}'_{Sf}-B_{21}\bar{I}_{Sf1}-B_{22}\bar{I}_{Sf2} \\ &= (A_{21}+A_{22})\bar{V}'_{Sf}-B_{21}\bar{I}_{Sf1}-B_{22}(-[Z_{SS}]^{-1}\bar{V}'_{Sf}-\bar{I}_{Sf1}) \\ &= (A_{21}+A_{22}+B_{22}[Z_{SS}]^{-1})\bar{V}'_{Sf}-(B_{21}-B_{22})\bar{I}_{Sf1} \end{aligned} \qquad (3D\text{-}9)$$

$$-\bar{I}_{FSf1}=(C_{11}+C_{12})\bar{V}'_{Sf}-D_{11}\bar{I}_{Sf1}-D_{12}\bar{I}_{Sf2}$$

$$=(C_{11}+C_{12})\bar{V}'_{Sf}-D_{11}\bar{I}_{Sf1}-D_{12}(-[Z_{SS}]^{-1}\bar{V}'_{Sf}-\bar{I}_{Sf1})$$

$$=(C_{11}+C_{12}+D_{12}[Z_{SS}]^{-1})\bar{V}'_{Sf}-(D_{11}-D_{12})\bar{I}_{Sf1} \qquad (3D\text{-}10)$$

$$-\bar{I}_{FSf2}=(C_{21}+C_{22})\bar{V}'_{Sf}-D_{21}\bar{I}_{Sf1}-D_{22}\bar{I}_{Sf2}$$

$$=(C_{21}+C_{22})\bar{V}'_{Sf}-D_{21}\bar{I}_{Sf1}-D_{22}(-[Z_{SS}]^{-1}\bar{V}'_{Sf}-\bar{I}_{Sf1})$$

$$=(C_{21}+C_{22}+D_{22}[Z_{SS}]^{-1})\bar{V}'_{Sf}-(D_{21}-D_{22})\bar{I}_{Sf1} \qquad (3D\text{-}11)$$

Writing the above equations in matrix form:

$$\begin{bmatrix}\bar{E}_{Ff1}\\ \bar{E}_{Ff2}\end{bmatrix}=\begin{bmatrix}A_{11}+A_{12}+B_{12}[Z_{SS}]^{-1} & -B_{11}+B_{12}\\ A_{21}+A_{22}+B_{22}[Z_{SS}]^{-1} & -B_{21}+B_{22}\end{bmatrix}\begin{bmatrix}\bar{V}'_{Sf}\\ \bar{I}_{Sf1}\end{bmatrix} \qquad (3D\text{-}12)$$

$$-\begin{bmatrix}\bar{I}_{FSf1}\\ \bar{I}_{FSf2}\end{bmatrix}=\begin{bmatrix}C_{11}+C_{12}+D_{12}[Z_{SS}]^{-1} & -D_{11}+D_{12}\\ C_{21}+C_{22}+D_{22}[Z_{SS}]^{-1} & -D_{21}+D_{22}\end{bmatrix}\begin{bmatrix}\bar{V}'_{Sf}\\ \bar{I}_{Sf1}\end{bmatrix} \qquad (3D\text{-}13)$$

Similarly for the receiving end busbar:

$$\begin{bmatrix}\bar{E}_{Ff1}\\ \bar{E}_{Ff2}\end{bmatrix}=\begin{bmatrix}A'_{11}+A'_{12}+B'_{12}[Z_{SR}]^{-1} & B'_{11}-B'_{12}\\ A'_{21}+A'_{22}+B'_{22}[Z_{SR}]^{-1} & B'_{21}-B'_{22}\end{bmatrix}\begin{bmatrix}\bar{V}'_{Rf}\\ \bar{I}_{Rf1}\end{bmatrix} \qquad (3D\text{-}14)$$

$$\begin{bmatrix}\bar{I}_{FRf1}\\ \bar{I}_{FRf2}\end{bmatrix}=\begin{bmatrix}C'_{11}+C'_{12}+D'_{12}[Z_{SR}]^{-1} & D'_{11}-D'_{12}\\ C'_{21}+C'_{22}+D'_{22}[Z_{SR}]^{-1} & D'_{21}-D'_{22}\end{bmatrix}\begin{bmatrix}\bar{V}'_{Rf}\\ \bar{I}_{Rf1}\end{bmatrix} \qquad (3D\text{-}15)$$

where $A'_{11},\ldots,D'_{22}$ are obtained by the partitioning of A_2,B_2,C_2,D_2 matrices. For brevity, the following abbreviations are used for the above transfer matrices:

$$\begin{bmatrix} A_{11}+A_{12}+B_{12}[Z_{SS}]^{-1} & -B_{11}+B_{12} \\ A_{21}+A_{22}+B_{22}[Z_{SS}]^{-1} & -B_{21}+B_{22} \end{bmatrix} = [J] \qquad (3D\text{-}16)$$

$$\begin{bmatrix} C_{11}+C_{12}+D_{12}[Z_{SS}]^{-1} & -D_{11}+D_{12} \\ C_{21}+C_{22}+D_{22}[Z_{SS}]^{-1} & -D_{21}+D_{22} \end{bmatrix} = [K] \qquad (3D\text{-}17)$$

$$\begin{bmatrix} A'_{11}+A'_{12}+B'_{12}[Z_{SR}]^{-1} & B'_{11}-B'_{12} \\ A'_{21}+A'_{22}+B'_{22}[Z_{SR}]^{-1} & B'_{21}-B'_{22} \end{bmatrix} = [M] \qquad (3D\text{-}18)$$

$$\begin{bmatrix} C'_{11}+C'_{12}+D'_{12}[Z_{SR}]^{-1} & D'_{11}-D'_{12} \\ C'_{21}+C'_{22}+D'_{22}[Z_{SR}]^{-1} & D'_{21}-D'_{22} \end{bmatrix} = [N] \qquad (3D\text{-}19)$$

$$\begin{bmatrix} \bar{E}_{Ff1} \\ \bar{E}_{Ff2} \end{bmatrix} = \bar{E}_{Ff} \qquad (3D\text{-}20)$$

From the above equations we can write:

$$-\bar{I}_{FSf} = [K][J]^{-1}\bar{E}_{Ff} \qquad (3D\text{-}21)$$

$$\bar{I}_{FRf} = [N][M]^{-1}\bar{E}_{Ff} \qquad (3D\text{-}22)$$

$$\bar{E}_{Ff} = ([K][J]^{-1}+[N][M]^{-1})^{-1}(-\bar{I}_{FSf}+\bar{I}_{FRf}) \qquad (3D\text{-}23)$$

Now considering any general earth fault:

$$\bar{V}_{Ff} = \bar{E}_{Ff} - [R_f](\bar{I}_{FSf}-\bar{I}_{FRf}) \qquad (3D\text{-}24)$$

$$\bar{V}_{Ff} = -\{([K][J]^{-1}+[N][M]^{-1})^{-1}+[R_f]\}(\bar{I}_{FSf}-\bar{I}_{FRf}) \qquad (3D\text{-}25)$$

Postfault superimposed voltages and currents at sending end busbars are evaluated from Eq. (3D-12), i.e.:

$$\begin{bmatrix} \bar{V}'_{Sf} \\ \bar{I}_{Sf1} \end{bmatrix} = [J]^{-1} \begin{bmatrix} \bar{E}_{Ff1} \\ \bar{E}_{Ff2} \end{bmatrix} = [J]^{-1} \bar{E}_{Ff} \qquad (3D\text{-}26)$$

Substituting $\bar{V}'_{Sf}$ and $\bar{I}_{Sf1}$ in Eq. (3D-6) $\bar{I}_{Sf2}$ is obtained. Likewise using Eq. (3D-14) for the receiving end busbar:

$$\begin{bmatrix} \bar{V}'_{Rf} \\ \bar{I}_{Rf1} \end{bmatrix} = [M]^{-1} \begin{bmatrix} \bar{E}_{Ff1} \\ \bar{E}_{Ff2} \end{bmatrix} = [M]^{-1} \bar{E}_{Ff} \qquad (3D\text{-}27)$$

$$\bar{I}_{Rf2} = [Z_{SR}]^{-1} \bar{V}'_{Rf} - \bar{I}_{Rf1} \qquad (3D\text{-}28)$$

APPENDIX 3E

Solving Sound Phase Voltage Problem for Different Fault Types

Similar to the method shown in 3.4.4 for single-phase-to-earth faults, using Eq. (3-46) for single-circuit lines and Eq. (3D-25) from Appendix 3D for double-circuit lines, solution can be found for other types of fault.

For a double-phase-to-earth fault on a single-circuit line involving , say, the 'a' and 'c' phases the currents are calculated from the knowledge of faulted phases superimposed voltages, that is:

$$\begin{bmatrix} I_{FSfa}-I_{FRfa} \\ I_{FSfc}-I_{FRfc} \end{bmatrix} = \begin{bmatrix} Z_{11} & Z_{13} \\ Z_{31} & Z_{33} \end{bmatrix}^{-1} \begin{bmatrix} V_{Ffa} \\ V_{Ffc} \end{bmatrix} \qquad (3E\text{-}1)$$

From Eq. (3E-1) the superimposed voltage vector is evaluated:

$$\begin{bmatrix} V_{Ffa} \\ V_{Ffb} \\ V_{Ffc} \end{bmatrix} = \begin{bmatrix} Z_{11} & Z_{13} \\ Z_{21} & Z_{23} \\ Z_{31} & Z_{33} \end{bmatrix} \begin{bmatrix} I_{FSfa}-I_{FRfa} \\ I_{FSfc}-I_{FRfc} \end{bmatrix} \qquad (3E\text{-}2)$$

Obviously there is no sound phase voltage problem for 3-phase faults on single-circuit lines as all phase voltages in the voltage vector $\bar{V}_{Ff}$ are known and there is no sound phases.

For double-circuit lines, by analogy, the superimposed current for the mentioned earth fault is evaluated. For example, for 'a'-'c'-earth faults using Eq. (3D-25) from Appendix 3D we have:

$$\begin{bmatrix} V_{Ffa} \\ V_{Ffb} \\ V_{Ffc} \\ V_{FfA} \\ V_{FfB} \\ V_{FfC} \end{bmatrix} = \begin{bmatrix} Z_{11} & Z_{13} \\ Z_{21} & Z_{23} \\ Z_{31} & Z_{33} \\ Z_{41} & Z_{43} \\ Z_{51} & Z_{53} \\ Z_{61} & Z_{63} \end{bmatrix} \begin{bmatrix} I_{FSfa}-I_{FRfa} \\ I_{FSfc}-I_{FRfc} \end{bmatrix} \qquad (3E\text{-}3)$$

For phase-to-phase faults the following matrices are firstly constructed (for faults on circuit-'abc'):

$$\begin{bmatrix} V'_1 \\ V'_2 \\ V'_3 \end{bmatrix} = \begin{bmatrix} V_{Ffa}-V_{Ffb} \\ V_{Ffb}-V_{Ffc} \\ V_{Ffc}-V_{Ffa} \end{bmatrix} \qquad (3E\text{-}4)$$

$$\begin{bmatrix} Z'_{11} & Z'_{12} & Z'_{13} \\ Z'_{21} & Z'_{22} & Z'_{23} \\ Z'_{31} & Z'_{32} & Z'_{33} \end{bmatrix} = \begin{bmatrix} Z_{11}-Z_{21} & Z_{12}-Z_{22} & Z_{13}-Z_{23} \\ Z_{21}-Z_{31} & Z_{22}-Z_{32} & Z_{23}-Z_{33} \\ Z_{31}-Z_{11} & Z_{32}-Z_{12} & Z_{33}-Z_{13} \end{bmatrix} \qquad (3E\text{-}5)$$

Now, for the phase faults involving, say, phases 'a' and 'c' the currents are evaluated from:

$$\left.\begin{aligned}(I_{FSfa}-I_{FRfa})&=V'_3/(Z'_{33}-Z'_{31}+R_f)\\(I_{FSfb}-I_{FRfb})&=0\\(I_{FSfc}-I_{FRfc})&=-(I_{FSfa}-I_{FRfa})\end{aligned}\right\} \qquad (3E\text{-}6)$$

Then using Eq. (3-46) for single-circuit lines or Eq. (3D-25) for double-circuit lines the superimposed voltage vector is evaluated.

Simultaneous earth faults on both circuits (at the same location on the line) are dealt with as shown in Eq. (3E-7) for 'a'-earth and 'B'-earth simultaneous faults:

$$\begin{bmatrix}I_{FSfa}-I_{FRfa}\\I_{FSfB}-I_{FRfB}\end{bmatrix}=\begin{bmatrix}Z_{11} & Z_{15}\\Z_{51} & Z_{55}\end{bmatrix}^{-1}\begin{bmatrix}V_{Ffa}\\V_{FfB}\end{bmatrix} \qquad (3E\text{-}7)$$

Then a similar equation to Eq. (3E-3) gives the superimposed voltage vector.

For inter-circuit faults the routine will be as shown below for the faults, say, involving phases 'b' and 'A':

$$Z_E=Z_{22}-Z_{42}-Z_{24}+Z_{44} \qquad (3E\text{-}8)$$

$$(I_{FSfb}-I_{FRfb})=(V_{Ffb}-V_{FfA})/Z_E \qquad (3E\text{-}9)$$

$$(I_{FSfA}-I_{FRfA})=-(I_{FSfb}-I_{FRfb}) \qquad (3E\text{-}10)$$

APPENDIX 3F

Program User Manual

The program written in standard 'FORTRAN' can print out prefault and postfault voltage and current phasors as well as the superimposed ones. If other lines are connected to the busbars of a line, their effect can be considered in the source impedance matrices. Examples of fault resistance arrangements used by the program are shown in Fig. 5-4. A brief description of the parameters in each line of the input data is given here:

#1 NB,NC,KE,JC,EPR

NB=No. of conductors per bundle

NC=No. of conductors (including earth wires)

KE=No. of earth wires

JC=No. of terms in Carson formulas

EPR=Earth plane resistivity (Ω-meter)

#2 CR,EWR

CR=Conductor radius (equivalent bundle radius,inches)

EWR=Earth wire radius (inches)

#3 XX(I),(I=1,NC)

XX is the distance between conductors from the centre line of the tower in meter. E.g. in the double-circuit line configuration shown in Fig. 3-1 the distances are given in the following order:

$X_a, X_b, X_c, X_A, X_B, X_C, X_{EW}$

#4 H(I),(I=1,NC)

H is the height of a conductor from the earth plane in meter. For the double-circuit line shown in Fig. 3-1 the heights are given in the order of:

$H_a, H_b, H_c, H_A, H_B, H_C, H_{EW}$

It should be noted that the above order of the physical geometry (XX(I),H(I)) must be examined in the input data, as the order of output phase values is specified by the input line geometry.

#5 RC,REW,XC,XEW

These are the natural resistance and inductance of each conductor and earth wire at power frequency, respectively (Ω/mile).

#6 KTRAN, KSHUNT

These are logical statements used as below:

KTRAN=1 Untransposed line

KTRAN=2 Perfectly transposed line

KSHUNT=1 Line with shunt capacitance

KSHUNT=2 Line without shunt capacitance

#7 VLL=System voltage (volts)

#8 VSPM,VSQM

VSPM=Voltage magnitude relationship in p.u. at S-end

VSQM=Voltage magnitude relationship in p.u. at R-end

#9 PSP,PSQ

PSP=Phase angle relationship at S-end (degrees)

PSQ=Phase angle relationship at R-end (degrees)

For example, if PSP=20° and PSQ=0° then the power transfer is from S to R and vice versa. If PSP=0° and

PSP=0^{o} then there is no power transfer.

#10 LPF=Distance to fault from S-end (km)

#11 LPQ=Line length(km)

#12 FPOS,FTYPE,FF1,FF2

FPOS=Fault position

FPOS=1 Fault on circuit 1

FPOS=2 Fault on circuit 2

FTYPE=Fault type

FTYPE=1 Phase-to-earth

FTYPE=2 Double-phase-to-earth

FTYPE=3 Phase-to-phase

FTYPE=4 3-phase-to-earth

FTYPE=5 Simultaneous fault on circuits 1 & 2

FTYPE=6 Inter-circuit phase-to-phase

FF1=Faulted phase

FF2=Faulted phase (for a double-phase fault)

#13 RF=Fault resistance

#14 VAP,VAQ

VAP=Lumped source capacity at S-end

VAQ=Lumped source capacity at R-end

#15 QP,QQ

QP=X/R ratio of the S-end source

QQ=X/R ratio of the R-end source

#16 LNP,LNQ

LNP=Z_{S0}/Z_{SP} ratio at the S-end source

LNQ=Z_{S0}/Z_{SP} ratio at the R-end source

REFERENCES

1. Eriksson, L., Saha, M.M. and Rockefeller, G.D., "An accurate fault locator with compensation for apparent reactance in the fault resistance resulting from remote end infeed", IEEE Trans., PAS-104, Feb. 1985, pp 424-435.

2. Takagi, T., Yamakoshi, Y., Yamaura, M., Kondow, R. and Matsushima, T., "Development of a new type fault locator using the one-terminal voltage and current data". IEEE Trans., PAS-101, Aug. 1982, pp 2892-2898.

3. Kondow, R., Sugiyama, Y. and Yamada, M., "Microprocessor-based fault locator" IEE conference publication No. 249, 1985, pp 188-192.

4. Schweitzer, E.O., III, "Evaluation and development of transmission line fault locating techniques which use sinusoidal steady-state information", Computers & Elec. Engng USA, 10, (4), 1983, pp 269-278.

5. Cook, V., "Fundamental aspects of fault location algorithms used in distance protection", Proc. IEE, 133, Pt. C, (6), Nov. 1986, pp 354-368.

6. Yang, Q.S. and Morrison, I.F., "Microprocessor-based algorithm for high resistance earth fault distance protection", Proc. IEE, 130, Pt. C, (6), Nov. 1983, pp

306-310.

7. Cornick, K.J., Ko, Y.M. and Pek, B., "Power system transient caused by arcing faults", Proc. IEE, 128, Pt. C, (1), Jan. 1981, pp 18-27.

8. Sachdev, M.S. and Agarwal, R., "A technique for estimating transmission line fault location from digital relay measurements", IEEE Trans., PWRD-3, (1), Jan. 1988, PP 121-129.

9. Sachdev, M.S. and Agarwal, R., "Accurate fault location methods from digital impedance relay measurements", IEE Conference Publication No. 249, 1985, PP 180-184.

10. Wiszniewsky, A., " Accurate fault impedance locating algorithm", Proc. IEE, 130, Pt. C, (6), Nov. 1983, pp 311-314.

11. Jeyasurya, B. and Rahman, M.A., "Accurate fault location of transmission line using microprocessors", IEE conference publication No. 302, 1989, pp 13-17.

12. Sant, M.T. and Paithankar, Y.G., "On-line digital fault locator for overhead transmission line", Proc. IEE, 126, (11), Nov. 1979, pp 1181-1185.

13. Richards, G.G. and Tan, O.T., "An accurate fault location estimation for transmission lines", IEEE Trans., PAS-101, Apr. 1982, pp 945-950.

14. Lawrence, D.J. and Waser, D.L., "Transmission line fault location using digital fault recorder", IEEE Trans., PWRD-3, (2), Apr. 1988, pp 496-502.

15. Wedepohl, L.M., "Application of matrix methods to the solution of travelling-wave phenomena in poly-phase systems", Proc. IEE, 110, (12), 1963, pp 2200-2212.

16. Wedepohl, L.M., Galloway, R. M. and Shorrocks, W.B., "Calculation of electrical parameters for short and long lines", Proc. IEE, 111, (12), 1964, pp 2051-2059.

17. Johns, A.T. and Aggarwal, R.K., "Digital simulation of faulted ehv transmission lines with particular reference to very-high-speed protection", Proc. IEE, 123, (4), Apr. 1976, pp 353-359.

18. Johns, A.T. and Walker, E.P., "Cooperative research into the engineering and design of a new digital directional comparison scheme", Proc. IEE, 135, Pt. C, (4), July 1988, pp 334-368.

19. Butterworth, S., "Electrical characteristic of overhead lines", ERA, 1954, p. 13.

20. Carson, J.R., "Wave propagation in overhead lines with ground return", Bell Syst. Tech. J., 5, 1926, p. 539.

21. Bickford, J.P., "Analysis of multiconductor lines", MSc studying course notes, UMIST, 1984.

22. Ibe, A.O. and Cory, B.J., "Fault location algorithm for multiphase power lines", Proc. IEE, 134, Pt. C, (1), Jan. 1987, pp 43-50.

PUBLISHED WORK

The following papers are based on the work described in this thesis. Copies of Papers 1 and 2 are enclosed, but Paper 3 was not available in its published form before the submission of the thesis.

1. Johns, A.T., Jamali, S., Haden, S.M., "New accurate transmission line fault location equipment", the IEE Fourth International Conference on Developments in Power System Protection at the University of Edinburgh, 11-13 April 1989, IEE Conference Publication No. 302, pp. 1-5.

2. Jamali, S. and Johns, A.T., "A very accurate fault location for transmission lines", 24th Universities Power Engineering Conference at Queen's University of Belfast, 19-21 September 1989.

3. Johns, A.T. and Jamali, S., "Accurate fault location technique for power transmission lines", Proc. IEE, Part C, (In print).

The following paper was presented to the IEE fourth International Conference on Development in Power System Protection at the University of Edinburgh, 11-13 April 1989.

NEW ACCURATE TRANSMISSION LINE FAULT LOCATION EQUIPMENT

A.T. Johns and S. Jamali

The City University, London, UK

S.M. Haden

GEC Measurements Ltd., Stafford, UK

INTRODUCTION

The use of longer distance transmission lines coupled with demands for reduced circuit outage times is stimulating a requirement for reliable and accurate fault location methods. The need for very high accuracy is generally becoming more important since, in ehv systems, there is often little visual evidence of a fault, and post-fault clearance tests performed at reduced system voltage can be inconclusive. In general, the degree of accuracy required is increasing and is much higher than can be obtained using simple conventional impedance to fault measuring techniques; even a small measurement error may require detailed local examination over several kilometres of a typical line.

The foregoing considerations account for the activity in the development of improved fault location techniques which has occurred in recent years; particular contributions being recorded in references 1 - 4. This paper will first outline the basis of an accurate fault location technique that has been designed to achieve an extremely high location accuracy and which, in particular, has been developed to overcome long standing problems caused by loss of accuracy due to:-

(a) Non-transposition of conductors and neglect of circuit shunt capacitance.

(b) Fault path impedance non-linearity and the effect of remote source infeeds.

(c) Changes in the power system source operating configuration from those assumed in setting fault location equipment.

(d) The need to utilise voltage signals derived from conventional capacitor voltage transformers.

An extensive survey of the literature shows that, at the present time, there is no single fault location technique which considers all the above causes of error. Most previous proposals for example assume perfect line transposition and/or neglect line shunt capcitance, require some means of determining the phase(s) involved in a particular fault and involve making assumptions regarding both the form and linearity of the fault point impedances. In the case of wide band type measurements e.g., so called travelling-wave methods, difficulties are often encountered in the use of capacitor voltage transformers, which are generally incapable of passing the necessary higher frequency phenomena.

In this paper, the results of simulation studies to determine the basic accuracy of the new methods will be given. The paper concludes with a description of the hardware implementation of the new fault location equipment that is currently under development.

BASIC PRINCIPLES

The method involves monitoring and filtering the voltages and currents measured at each end of a line so as to produce a measure of the steady-state power frequency voltage and current phasors. The latter are obtained as data described by means of post-fault processing applied to data captured during the fault clearance process.

Single-Phase Relationship

For ease of explanation, it is first convenient to consider the relationship applicable to an assumed single-phase line application. With reference to Fig. 1, the post-fault steady-state voltage V_F for a fault at a distance x from say end S is readily expressed in terms of the voltages and currents measured at the ends:-

$$V_F = \cosh(\gamma x)V_S - Z_0\sinh(\gamma x)I_S \quad 1$$

$$V_F = \cosh(\gamma(L - x))V_R - Z_0\sinh(\gamma(L - x))I_R \quad 2$$

In equations 1 and 2, the surge (or characteristic) impedance Z_0 and line propagation constant γ are given by $Z_0 = (Z/Y)^{\frac{1}{2}}$ and $\gamma = (ZY)^{\frac{1}{2}}$ respectively, where Z is the line series impedance and Y is the shunt admittance per unit length. Equating equations 1 and 2 eliminates any necessity for defining the fault point network; resort to this artifice is useful practically due to uncertainties as to the nature of the fault path. Rearrangement of equations 1 and 2 provides an exact evaluation of the distance to the fault x as given in equation 3.

$$x = [\tanh^{-1}(-B/A)]/\gamma \quad 3$$

where $A = Z_0\cosh(\gamma L)I_R - \sinh(\gamma L)V_R + Z_0I_S$

and $B = \cosh(\gamma L)V_R - Z_0\sinh(\gamma L)I_R - V_S$

Equation 3 is seen to require only known line data (ZY) and known phasor voltages derived from measurands at the line ends. As such, any fault location estimate thereby derived is independent of both fault impedance and source impedance values, a fact which is of practical importance due to their somewhat indeterminate and variable nature. It is also of interest to note that the equation is valid for both total and superimposed values of voltage and current. Thus for example, the method could readily utilise superimposed measurands of the type used in high speed directional comparison protection equipment (Johns et al (5)). Furthermore, the fault location algorithm relates to a true distributed line i.e., the practical situation, and inherently includes for the effect of shunt capacitance.

Application to 3-Phase Power Lines

The foregoing techniques cannot be applied directly to a multi-phase power line since a number of voltages and currents are involved and mutual inductive and capacitive coupling exists between phases. For simplicity, consider a single-circuit 3-phase transmission line in which the phases are identified by a,b,c as indicated in the single-line equivalent of Fig. 2. In this case, the vector of voltages and currents ($[V_{Fa,b,c}]$, $[I_{Sa,b,c}]$ etc) at the various points of interest are related using the 2-port matrices $[A_S]$, $[B_S]$, $[A_R]$, $[B_R]$ which in turn are 3 x 3 matrices defined using the line series impedance matrix [Z] and the line shunt admittance matrix [Y]. With reference to Fig. 2, the multi-conductor equivalent of equations 1 and 2 is thus:-

$$[V_{Fa,b,c}] = [A_S][V_{Sa,b,c}] - [B_S][I_{Sa,b,c}] \quad 4$$

$$[V_{Fa,b,c}] = [A_R][V_{Ra,b,c}] - [B_R][I_{Ra,b,c}] \quad 5$$

where $[V_{Fa,b,c}]$, $[V_{Sa,b,c}]$, $[I_{Ra,b,c}]$ etc are vectors defining voltages and currents associated with each phase e.g., $[V_{Ra,b,c}] = [V_{Ra}\ V_{Rb}\ V_{Rc}]^T$, $[\ ]^T$ denoting a matrix transpose.

It is important to note that the 2-port matrices $[A_S]$, $[B_S]$ etc. can, if necessary, be formed to include any discrete line transpositions, which in turn is conducive to maintaining very high levels of measurement accuracy in long-line applications. In most cases however it is sufficient to treat each line section as homogeneous.

The key to extending the fault location algorithm for use in actual multi-phase transmission lines lies in de-coupling equations 4 and 5 into uncoupled or independent equations which in effect describe equivalent single-phase networks of the type shown in Fig. 1. This is done using the theory of natural modes and matrix function theory (Wedephol (6)) as commonly used in the digital simulation of faulted ehv transmission systems (Johns and Aggarwal (7)). The theory underlying such techniques, though well known to power system analysts, is much too long and involved to explain in a paper of this type; the reader is therefore referred to the latter references for further details. Briefly, the method involves finding the matrix of Eigenvectors of the [Z][Y] product ([Q] say) and the [Y][Z] product ([S] say). In this way, the voltages and currents derived from each phase a,b,c at say the sending end would be transformed to coresponding modal voltage quantities 1,2,3 by means of the corresponding [Q] and [S] Eigenvector matrices (7):-

$$\left.\begin{aligned}[V_{Sn}] &= \begin{bmatrix}V_{S1}\\V_{S2}\\V_{S3}\end{bmatrix} = [V_{S1}\ V_{S2}\ V_{S3}]^T = [Q]^{-1}[V_{Sa}\ V_{Sb}\ V_{Sc}]^T\\ [I_{Sn}] &= \begin{bmatrix}I_{S1}\\I_{S2}\\I_{S3}\end{bmatrix} = [I_{S1}\ I_{S2}\ I_{S3}]^T = [S]^{-1}[I_{Sa}\ I_{Sb}\ I_{Sc}]^T\end{aligned}\right\} 6$$

The significance of applying the transformation to modal quantities is that even a multi-conductor line is decomposed into a number of single-phase uncoupled models of the type shown in Fig. 1. For each modal component, there is an equation pair of the form of equations 1 and 2. Thus for a single circuit line, there are three pairs of such equations corresponding to the modes 1,2,3 so that, for mode 2 for example the equation pair used that would form the basis of the fault location in an actual 3-phase line would take the form of equations 7 and 8.

$$V_{F2} = A_{S2}V_{S2} - B_{S2}I_{S2} \quad 7$$

$$V_{F2} = A_{R2}V_{R2} - B_{R2}I_{R2} \quad 8$$

The method is general in that, for a double-circuit line for example, six modes are involved which in turn results in six pairs of equations all of the basic form of equations 7 and 8. Any one or more mode pair equations can be used to effect a fault location x by equating such equations to obtain for example a mode-2 based evaluation given by equation 9.

$$x = [\tanh^{-1}(-B_2/A_2)]/\gamma_2 \quad 9$$

where $A_2 = Z_{02}\cosh(\gamma_2 L)I_{R2} - \sinh(\gamma_2 L)V_{R2} + Z_{02}I_{S2}$

$$B_2 = \cosh(\gamma_2 L)V_{R2} - Z_{02}\sinh(\gamma_2 L)I_{R2} - V_{S2}$$

Equation 9 and its companion equations formed using the other modes is the exact equivalent of equation 3 which was derived for the single phase model in section 2.1. The appropriate modal surge impedances required are readily determined from the matrix product $[Z_{0n}] = [\gamma]^{-1}[Q]^{-1}[Z][S]$ in which $[\gamma]$ is a diagonal matrix of so called modal propagation constants comprising the square root of the Eigenvalues of the matrix product [Z][Y] (6,7). Matrix $[Z_{0n}]$ thus takes the form of $[Z_{01}\ Z_{02}\ Z_{03}]$ diag for a 3-phase line, the individual values being modal surge impedances.

Practical Considerations

The modal surge impedances and propagation constants are pre-computed as indicated in the previous section from the line impedance and shunt admittance matrices ([Z], [Y]). The latter are in turn computed from a knowledge of the line conductor geometry, earth plane resistivity and the conductor parameters. In essence they represent basic parameters set into the algorithm according to the line application involved. However, the algorithm has been found to be so accurate that, even if perfect line transposition is assumed, the resulting accuracy is more than acceptable for most applications. If perfect line transposition is assumed, the calculation of the modal surge impedances and propagation constants is simplified since it is readily shown that, for example, the mode-2 surge impedance for a single circuit line can be expressed directly in terms of the well known positive phase sequence line impedance (Z_1) and shunt admittance (Y_1) per unit length of line as $Z_{02} = (Z_1/Y_1)^{\frac{1}{2}}$. Similarly $\gamma_2 = (Z_1Y_1)^{\frac{1}{2}}$. Furthermore, the assumption of perfect transposition leads to Eigenvector matrices which are equal ([S] = [Q]) and which are independent of line geometry. The need to calculate the voltage and current Eigenvector matrices is thereby obviated and in this case they take the special form given in equation 10.

$$[S] = [Q] = \begin{bmatrix}1 & 1 & 1\\ 1 & 0 & -2\\ 1 & -1 & 1\end{bmatrix} \quad 10$$

PERFORMANCE EVALUATION

The fundamental characteristics of the new fault location algorithm have been determined by testing using a steady-state line simulation programme. This means of testing reveals the inaccuracies in the algorithm itself and does not include any errors introduced by the hardware and/or transducers i.e., it reveals the best that can be expected by way of fault location accuracy. The programme uses distributed line parameters in deriving phase variable relationships and thereby gives a more detailed and realistic line representation under operating and fault conditions. The values of voltage and current at the terminating busbars are produced for any fault type and source conditions.

The results presented in this paper relate to one circuit of a typical 400 kV vertical constructed line of the type commonly used on the UK supergrid system and to a typical single-circuit 500 kV horizontally constructed line as commonly used in longer distance transmission applications in the USA. Details of the line configuration involved are given in Figs. 3a and b. A wide range of line lengths and source conditions have been considered but, for reasons of brevity, the results presented are necessarily limited, though they give a clear indication of the accuracy obtained under typical operating earth fault conditions. Relevant parameters used are:-

(a) Earth resistivity, assumed homogeneous = 100 Ωm.

(b) Terminating source short circuit levels = 5 GVA and X/R ratio = 40.

(c) Fault resistance = 100 Ω.

(d) Line lengths = 100 km and 250 km.

(e) Prefault line loading is zero.

The lines considered are deliberately untransposed so as to adequately reveal the effect on accuracy of assuming perfect transposition when setting the parameters into the new locator. The results relate to typical earth faults, fault location estimates being those obtained using mode-1 (earth-mode) quantities.

It will be appreciated from the foregoing that, if the new locator is set using the exact parameters derived from the actual Eigenvectors/Eigenvalues for an

untransposed line, the only errors that occur are those due to hardware i.e., the algorithmic error is zero. The results presented are for a locator having approximate settings derived on the assumption of ideal line transposition. Table 1 shows the percentage error in fault location that occurs for an "a"-earth fault on a 100 km horizontal configured line. The error is expressed as a percentage of the total line length i.e.:-

$$\% \text{ error} = \frac{[(\text{estimated location})-(\text{actual location})]\times 100}{\text{total line length}}$$

It can be seen from Table 1 that despite the assumption of perfect line transposition, the new locator gives an extremely accurate evaluation of fault position that is largely independent of the actual fault point. Table 2 shows the corresponding performance for a long line application (250 km). It will be evident that the accuracy attainable is largely unaffected by the line length, a factor that is a consequence of the fact that the algorithm inherently takes account of shunt capacitance. In particular, the latter results enable the extent of the improvement in accuracy made possible using the new algorithm to be put in perspective.

FAULT POSITION km FROM END -S	% ERROR
0	0.4
5	0.4
25	0.2
50	0.0
75	-0.2
95	-0.4
100	-0.4

TABLE 1: Measurement errors for "a"-earth faults on 100 km, horizontal line configuration.

FAULT POSITION km FROM END -S	% ERROR
0	0.3
10	0.3
50	0.2
100	0.1
150	-0.1
200	-0.2
245	-0.3
250	-0.3

TABLE 2: Measurement errors for "a"-earth faults on 250 km, horizontal line configuration.

Figs. 4a and b show a comparison of the performance obtained for short 100 km lines of vertical (Fig. 4a) and horizontal (Fig. 4b) lines. The consistency of the new algorithm and its relative independence of line configuration is apparent, the magnitude of the error always being less than 0.5% for all fault positions.

Tables 3 and 4 show the response for a double-phase-to-earth fault on a vertical line construction involving a 100 Ω fault resistance to earth in each faulted phase. In this case, the error for the new algorithm is less than approximately 1.1% for all fault positions. The consistency of operation as between long and short line applications is again apparent. It is of interest to note that the new algorithm is independent of fault type and, unlike many of its predecessors, does not require any fault-type identification routine. This is a desirable feature in that potential problems due to incorrect fault-type determination, which can in turn result in an incorrect fault location algorithm being applied, are avoided.

FAULT POSITION km FROM END -S	% ERROR
0	-1.1
5	-1.0
25	-0.5
50	0.0
75	0.6
95	1.0
100	1.1

TABLE 3: Measurement errors for "a"-"b"-earth fault on 100 km, vertical line configuration.

FAULT POSITION km FROM END -S	% ERROR
0	-0.7
10	-0.7
50	-0.5
100	-0.2
150	0.2
200	0.5
245	0.7
250	0.7

TABLE 4: Measurement errors for "a"-"b"-earth fault on 250 km, vertical line configuration.

The foregoing results are typical of very many studies performed over a range of fault type (including fault resistance), fault location, source capacity, prefault line loading and line configuration conditions; in all cases, the algorithmic error was less than approximately 1.5% when the algorithm was set assuming perfect line transposition. Algorithmic measurement errors observed under conditions when untransposed parameters are set into the locator are generally negligible.

HARDWARE DESCRIPTION

Voltage and current waveforms are sampled in real time at both line ends. When a start signal is received this process continues until the post fault data has also been captured. All further processing can be done off-line. The data is band pass filtered and the power frequency phasor information extracted. The modal transformation is then applied to these phasors using the previously calculated Eigenvectors. The modal voltage and current phasors are then exchanged with those from the equipment at the remote line end. Note that it is only the phasor values that need to be transferred and not the entire data set. This can be done either automatically or by voice over a telephone link, for example. Once the values are exchanged, the A and B coefficients e.g. A_2 and B_2 of equation 9, are formed using the input line parameters and the distance to the fault is then determined.

Fig. 5 shows in block diagram form the main hardware elements required for the distance to fault locator equipment. The three phase voltage and current signals from the line transformers are fed, via isolation transformers and anti-alias filters, into a multiplexer. The output from the multiplexer is then passed through a sample and hold gate and into the analogue to digital converter for digitisation. The resultant digitised signals are stored in a cyclic buffer in the microprocessors random access memory, by the direct memory access unit. The input/output unit is also sampled continuously, until a start signal is received from the line protection equipment (typically a distance relay). Also required are a keypad and alpha numeric display. These are used to display and transfer the modal voltage and current vectors, and to display the final distance to fault result. They are also used to enter the line settings for storage in the microprocessors electrically erasable PROM.

In addition to the above requirements, all inputs and outputs to the equipment must be fully protected for use in the electrically hostile environment of a typical substation. A prototype fault locator equipment is now under development. This will be available in either a panel or rack mounting 19" case. It will include a built in battery backed real time clock to allow time and date tagging of the fault data. Also included will be an RS232 communications port allowing the equipment to be set and interrogated remotely, in addition to locally with the built in keypad and display. Output to a printer will also be supported.

ACKNOWLEDGEMENTS

The authors are grateful for the financial support provided by the Science and Engineering Research Council and GEC Measurements Ltd. The use of

facilities at the City University, London, UK and GEC Measurements Laboratories Stafford are also gratefully acknowledged.

REFERENCES

1. Erikson, L., Saha, M.M. and Rockfeller, G.D., 1985, "An accurate fault locator with compensation for apparent reactance in the fault resistance resulting from remote end infeed", IEEE Trans, PAS-104, 424-435.

2. Takagi, T., Yamakoshi, Y., Yamaura, M., Kondow, R. and Matsushima, T., 1982, "Development of a new type fault locator using the one-terminal voltage and current data", IEEE Trans, PAS-101, 2892-2898.

3. Schweitzer, E.O., III, 1983, "Evaluation and development of transmission line fault locating techniques which use sinusoidal steady-state information", Computers & Elec. Engng USA, 10, (4), 269-278.

4. Cook, V., 1986, "Fundamental aspects of fault location algorithms used in distance protection", Proc. IEE, 133 (6), 354-368.

5. Johns, A.T., Martin, M.A., Barker, A., Walker, E.P. and Crossley, P.A., 1986, "A new approach to ehv directional comparison protection using digital signal processing techniques", IEEE Trans., PWRD-1, (2), 24-34.

6. Wedephol, L.M., 1963, "Application of matrix methods to the solution of travelling-wave phenomena in polyphase systems", Proc. IEE, 110, (12), 2200-2212.

7. Johns, A.T. and Aggarwal, R.K., 1976, "Digital simulation of faulted ehv transmission lines with particular reference to very-high-speed protection", Proc. IEE, 123, (4), 353-359.

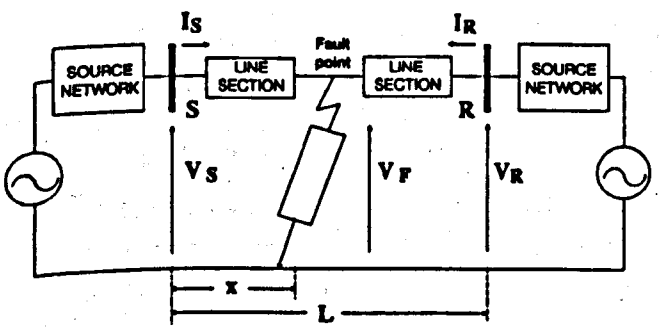

Fig. 1 Single - phase faulted line/source network

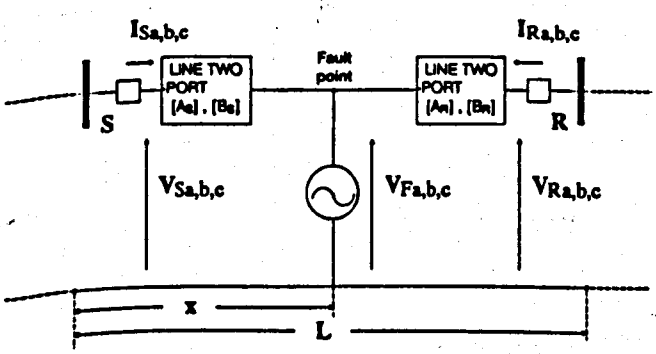

Fig. 2 Single - line diagram of faulted line described by 2 - port matrices

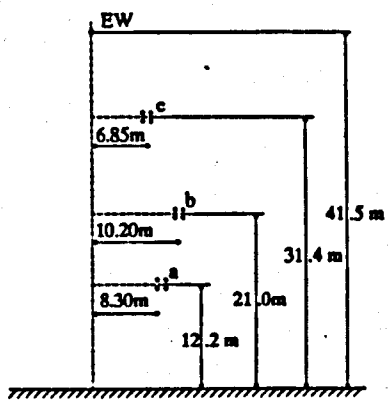

a - Vertical

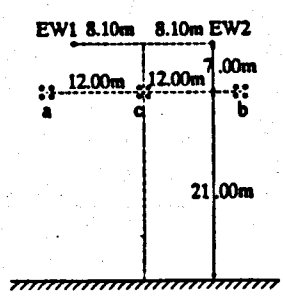

b - Horizontal

Fig. 3 Line configurations

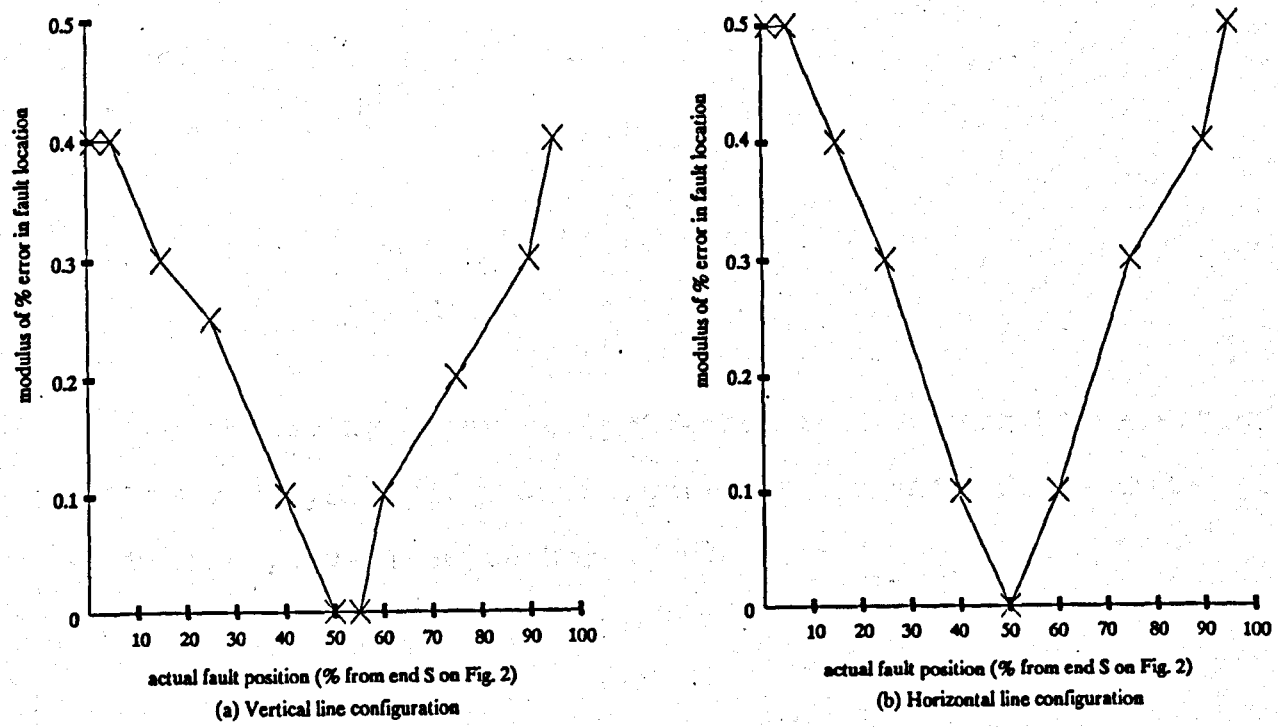

Fig. 4 Measuring accuracy for 100 Km line application

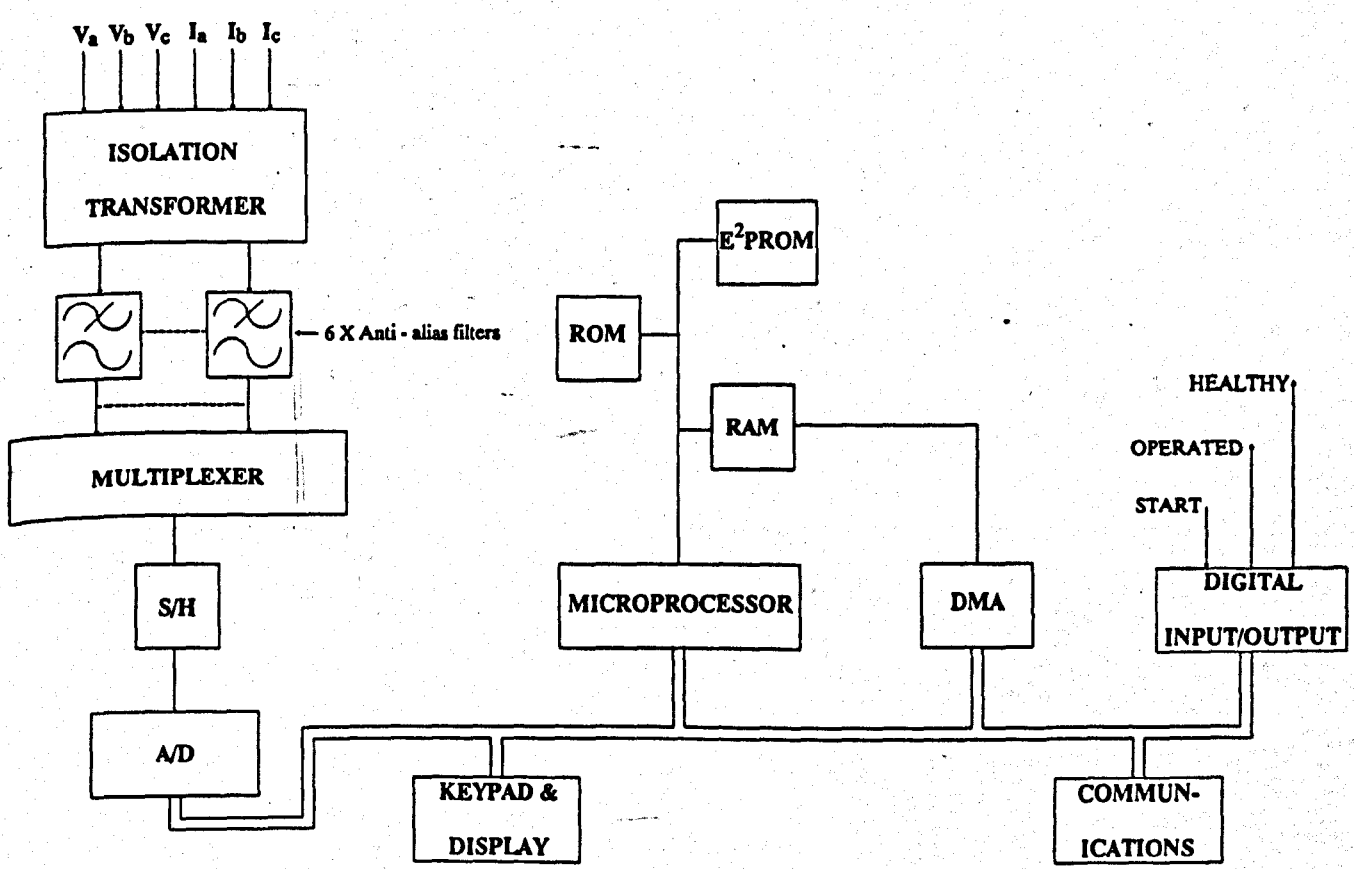

Fig. 5 Hardware block diagram

The following paper was presented to the 24th Universities Power Engineering Conference at Queen's University of Belfast, 19-21 September 1989.

A VERY ACCURATE FAULT LOCATION FOR TRANSMISSION LINES

S. Jamali and A.T. Johns

City University, London , UK.

Abstract- This paper describes a very accurate fault location technique which uses post-fault steady-state voltage and current derived at the line ends. The technique locates the fault independent of fault resistance and source impedances. It maintains its high accuracy for untransposed lines and no fault type identification is required. The paper presents the basic theory of the technique and some results of simulation studies to determine its performance are also given.

INTRODUCTION

The need for very high accuracy in fault location is generally becoming more important because, in ehv systems, there is often little visual evidence of a fault, and post-fault clearnce tests performed at reduced system voltage can be inconclusive. The degree of accuracy is therefore increasing and is much higher than can be obtained using simple conventional impedance to fault measuring techniques; even a small measurement error may require detailed local examination over several kilometres of a typical line.

For a very accurate fault location the following sources of error should be considered:

(a) Line asymmetry: The self and mutual impedance and admittance of each phase of transmission lines is determined by line geometry and are not exactly the same values for all phases. Most previous fault location techniques use symmetrical components which are only applicable to transposed lines (references 1,3 and 4). The fault location technique proposed in reference 2 can be applied to untransposed lines if the impedance for each phase can be set. However in reference 5 it has been reported that when using this technique for untransposed line represented by symmetrical parameters a substantial error will occur due to an asymmetry among phases.

(b) Shunt capacitance: Capacitance current for long line can be comparable with fault current, particularly for high resistance faults. Many of the previously reported algorithms use a lumped model for shunt capacitance which is not an exact representation of line if a very high accuracy in fault location is required.

(c) Fault resistance: Unknown fault resistance and different phase angle of fault current contribution from remote source will introduce error.

(d) Remote source impedance setting: Some previous fault location algorithms require a setting for the remote source impedance. In modern transmission networks, normally several lines and generators are connected to the line terminals. Switching operations often change the source operating configuration from those assumed in setting the fault location equipment which in turn can lead to a large error in fault location.

(e) Capacitve voltage transformer: In the case of wide band type measurement e.g., so called travelling-wave methods, difficulties are often encountered in the use of capacitor voltage transformers,which are generally incapable of passing the necessary higher frequency phenomena.

A fault location technique which considers all the above causes of error is presented and the results of simulation studies to determine the basic accuracy of the methods are given. The technique has also the merit of no requirements for determining the phase(s) involved in a particular fault. Previous techniques use different routines for different types of fault.

The proposed technique requires data from both ends. However, it should be noted that it is only the phasor values that need to be transferred from the remote end and not the entire data set. This can be done either automatically or by voice over a telephone link, for example.

BASIC PRINCIPLES

The voltages and currents measured at each end of a transmission line are filtered so as to produce a measure of the steady-state power frequency voltage and current phasors. The latter are obtained as data described by means of post-fault processing applied to data captured during the fault clearance process.

Simple Single-Phase Line

Consider the relationship applicable to an assumed single-phase line application. With reference to Fig. 1, the post-fault steady-state voltage V_F for a fault at a distance x from ,say, end S is readily expressed in terms of the voltages and currents measured at the ends:

$$V_F=\cosh(\Gamma x)V_S-Z_0\sinh(\Gamma x)I_S \quad 1$$

$$V_F=\cosh(\Gamma(L-x))V_R-Z_0\sinh(\Gamma(L-x))I_R \quad 2$$

In equations 1 and 2, the surge(or characteristic) impedance Z_0 and line propagation constant Γ are given by $Z_0=(Z/Y)^{\frac{1}{2}}$ and $\Gamma=(ZY)^{\frac{1}{2}}$ respectively, where Z is the line series impedance and Y is the line shunt admittance per unit length. Equating equations 1 and 2 eliminates any necessity for defining the fault point network. In practice this is useful due to uncertainties as to the nature of the fault path. Rearrangement of the equations 1 and 2 provides an exact evaluation of the distance to the fault x as given in equation 3.

$$x=\{\tanh^{-1}(-B/A)\}/\Gamma \qquad 3$$

where $A=Z_0\cosh(\Gamma L)I_R-\sinh(\Gamma L)V_R+Z_0I_S$

and $B=\cosh(\Gamma L)V_R-Z_0\sinh(\Gamma L)I_R-V_S$

In the above equation x is complex but has a predominantly real part. The imaginary part of x arises due to computational errors though its magnitude is small relative to the real part which can be taken to represent the fault distance. Equation 3 requires only known line data (Z and Y) and known phasor voltages derived from measurands at the line ends. Any fault location estimate thereby derived is therefore independent of both the fault impedance and the source impedance values, a fact which is of practical importance due to their somewhat indeterminate and variable nature. It is also of interest to note that the equation is valid for both total and superimposed values of voltage and current. Furthermore, the fault location algorithm relates to a distributed line, and inherently includes for the effect of shunt capacitance.

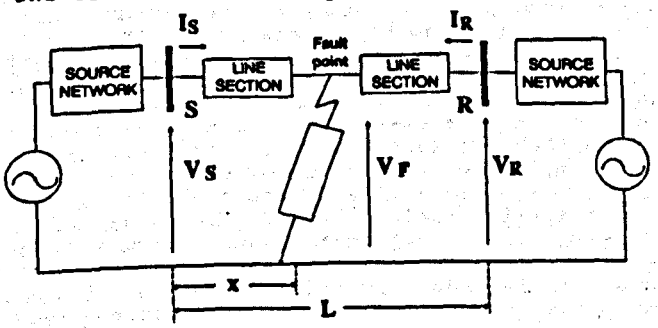

Fig. 1- Single-phase faulted line/source network.

Extension to 3-Phase Power Lines

The method described above cannot be directly applied to a multi-phase power line since a number of phases are involved. For simplicity, consider a single circuit 3-phase transmission line in which the phases are identified by a,b,c as indicated in the single line equivalent of Fig. 2. In this case, the vector of the various voltages and currents ($[V_{Fa,b,c}]$, $[I_{Sa,b,c}]$, etc.) are related using the 2-port matrices $[A_S]$,$[B_S]$,$[A_R]$,$[B_R]$ which in turn are 3x3 matrices defined using the line series impedance matrix [Z] and the line shunt admittance matrix [Y]. With reference to Fig. 2 the multi-conductor equivalent of equations 1 and 2 is :

$$[V_{Fa,b,c}]=[A_S][V_{Sa,b,c}]-[B_S][I_{Sa,b,c}] \qquad 4$$

$$[V_{Fa,b,c}]=[A_R][V_{Ra,b,c}]-[B_R][I_{Ra,b,c}] \qquad 5$$

where $[V_{Fa,b,c}]$,$[V_{Sa,b,c}]$,$[I_{Ra,b,c}]$,etc. are vectors defining voltages and currents for each phase e.g., $[V_{Ra,b,c}]=[V_{Ra},V_{Rb},V_{Rc}]^T$,$[]^T$ denoting a matrix transpose.

It is important to note that the 2-port matrices $[A_S]$,$[B_S]$, etc. can, if necessary, be formed to include any discrete line transposition, which in turn is conductive to maintaining very high levels of measurements accuracy in long line applications. In most cases however it is sufficient to treat each line section as homogeneous.

The key to extending the fault location algorithm for use in actual multi-phase transmission lines lies in de-coupling equations 4 and 5 into uncoupled or independent single-phase networks of the type

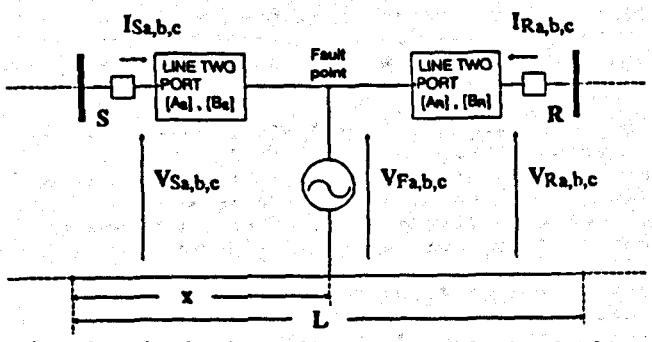

Fig. 2- Single-line diagram of faulted line described by 2-port matrices.

shown in Fig. 1. This is done using the theory of natural modes and matrix function theory (wedepohl (6)) as commonly used in the digital simulation of faulted ehv transmission systems (Johns and Aggarwal (7)). The theory underlying such techniques, though well known to power system analysts, is much too long and involved to explain in a paper of this type; the reader is therefore referred to the latter references for further details. Briefly, the method involves finding the matrix of Eigenvectors of the [Z][Y] product ([Q] say) and the [Y][Z] product ([S] say). In this way, the voltages and currents derived from each phase a,b,c at, say,the sending end would be transformed to corresponding modal voltage quantities 1,2,3 by means of the corresponding [Q] and [S] Eigenvector matrices (7):-

$$\left.\begin{aligned}[V_{sn}]=[V_{s1}\ V_{s2}\ V_{s3}]^T=[Q]^{-1}[V_{sa}\ V_{sb}\ V_{sc}]^T\\ [I_{sn}]=[I_{s1}\ I_{s2}\ I_{s3}]^T=[S]^{-1}[I_{sa}\ I_{sb}\ I_{sc}]^T\end{aligned}\right\} \qquad 6$$

The significance of applying the transformation to modal quantities is that even a multi-conductor line is decomposed into a number of single-phase uncoupled models of the type shown in Fig. 1. For each modal component, there is an equation pair of the form of equations 1 and 2. Thus for a single circuit line, there are three pairs of such equations corresponding to the modes 1,2,3 so that , for mode-2 for example the equation pair used that would form the basis of the fault location in an actual 3-phase line would take the form of equations 7 and 8.

$$V_{F2}=A_{S2}V_{S2}-B_{S2}I_{S2} \qquad 7$$

$$V_{F2}=A_{R2}V_{R2}-B_{R2}I_{R2} \qquad 8$$

The method is general in that, for a double-circuit line for example, six modes are involved which in turn results in six pairs of equations all of the basic form of equations 7 and 8. Any one or more mode pair equations can be used to find a fault location x by equating such equations to obtain for example a mode-2 based evaluaation given by equation 9.

$$x=\{\tanh^{-1}(-B_2/A_2)\}/\Gamma_2 \qquad 9$$

where $A_2=Z_{02}\cosh(\Gamma_2L)I_{R2}-\sinh(\Gamma_2L)V_{R2}+Z_{02}I_{S2}$

and $B_2=\cosh(\Gamma_2L)V_{R2}-Z_{02}\sinh(\Gamma_2L)I_{R2}-V_{S2}$

Equation 9 and its companion equations formed using the other modes is the exact equivalent of equation 3 which was derived for the single phase model in the previous section. The appropriate modal surge impedances

required are readily determined from the matrix product $[Z_{0n}]=[\Gamma]^{-1}[Q]^{-1}[Z][S]$ in which $[\Gamma]$ is a diagonal matrix of so-called modal propagation constants comprising the square root of Eigenvalues of matrix product $[Z][Y]$ (6,7). Matrix $[Z_{0n}]$ thus takes the diagonal form of $[Z_{01}\ Z_{02}\ Z_{03}]$ for a 3-phase line, the individual values being modal surge impedances.

Practical Considerations

The modal surge impedances and propagation constants are pre-computed as indicated in the previous section from the line impedance and shunt admittance matrices ([Z], [Y]). The latter are in turn computed from a knowledge of the line conductor geometry, earth plane resistivity and the conductor parameters. In essence they represent basic parameters set into the algorithm according to the line application involved. However, the algorithm has been found to be so accurate that, even if perfect line transposition is assumed, the resulting accuracy is more than acceptable for most applications. If perfect line transposition is assumed, the calculation of the modal surge impedances and propagation constants is simplified since it is readily shown that, for example, the mode-2 surge impedance for a single-circuit line can be expressed directly in terms of the well known positive phase sequence line impedance (Z_1) and shunt admittance (Y_1) per unit length of line as $Z_{02}=(Z_1/Y_1)^{\frac{1}{2}}$. Similarly $\Gamma_2=(Z_1Y_1)^{\frac{1}{2}}$. Furthermore the assumption of perfect transposition leads to Eigenvector matrices which are equal ($[S]=[Q]$) and which are independent of line geometry. The need to calculate the voltage and current Eigenvector matrices is thereby obviated and in this case they take the special form given in equation 10.

$$[S]=[Q]=\begin{bmatrix}1 & 1 & 1\\ 1 & 0 & -2\\ 1 & -1 & 1\end{bmatrix} \qquad 10$$

Mode Selection

Any type of fault will excite aerial-modes, e.g. mode-2 here, while the earth-mode is excited by earth faults only. Therefore if the line is transposed or the line parameters for untransposed line are available then the aerial-mode can be used for any type of fault and no mode selection is required. It is worth mentioning that by using the aerial-mode, the fault location is evaluated independently of the indeterminate earth path resistivity. However, when transposed line parameters are used for untransposed line as discussed in the previous section it has been found from simulation studies that the earth-mode gives more accurate results for earth faults. Mode selection in this case can easily be done by detecting the presence of residual current at the line ends.

PERFORMANCE EVALUATION

The fundamental characteristics of this fault location algorithm have been determined by testing using a steady-state line simulation programme. This means of testing reveals the inaccuracies in the algorithm itself and does not include any errors introduced by the hardware and/or transducers i.e., it reveals the best can be expected by way of fault location accuracy. The programme uses distributed line parameters in deriving phase variable relationships and thereby gives a more detailed and realistic line representation under operating and fault conditions. The values of voltage and current at the terminating busbars are produced for any fault type and source conditions.

The results presented in this paper relate to one circuit of a typical 400kV vertical constructed line of the type commonly used on the UK supergrid system and to a typical single-circuit 500kV horizontally constructed line as commonly used in longer distance transmission applications in the USA. Details of the line configuration involved are given in Figs. 3a and 3b. A wide range of line lengths and source conditions have been considered but, for reasons of brevity, the results presented are necessarily limited, though they give a clear indication of the accuracy obtained under typical operating earth fault conditions. Relevant parameters used are:-

(a) Phase conductors are 4x54/7/0.33cm s.c.a with 0.305m bundle spacing.
(b) Earthwire is 54/7/0.33cm s.c.a
(c) Earth resistivity, assumed homogeneous = 100Ωm
(d) Source short circuit levels=5GVA and X/R ratio=40 at both ends.
(e) Fault resistance= 100Ω
(f) Line lengths= 100km and 250km.
(g) Prefault line loading is zero.

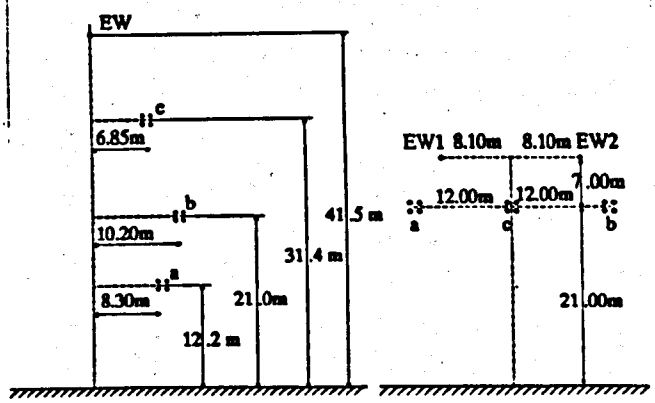

Fig. 3- Line configurations

The lines considered are deliberately untransposed so as to adequately reveal the effect on accuracy of assuming perfect transposition when setting the parameters into the locator. The rasults relate to typical earth faults, fault location estimates being those obtained using mode-1 (earth-mode) quantities.

It will be appreciated from the foregoing that, if the locator is set using the exact parameters derived from the actual Eigenvectors/Eigenvalues for an untransposed line, the only errors that occur are those due to hardware i.e., the algorithmic error is zero. The results presented are for a locator having approximate settings derived on assumption of ideal line transposition. Fig. 4 shows the percentage of error in fault location that occurs for 'a'-earth faults on different line configurations. The error is expressed as a percentage of the total line length. It can be seen from these figures that the locator gives extremely accurate evaluation of fault position that is largely independent of the actual fault point. It can

be seen that the accuracy is not affected by line length; this is a consequence of the fact that the algorithm inherently takes account of shunt capacitance. The consistency of the new algorithm and its relative independence of line configuration is also apparent, the magnitude of error always being less than 0.6% for all fault positions.

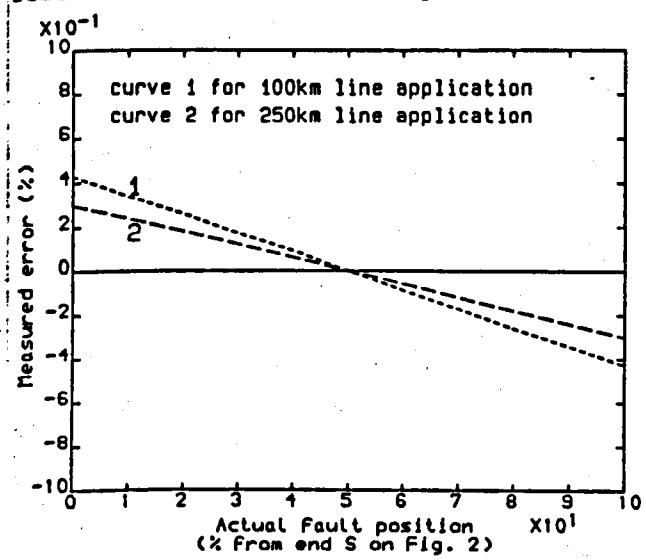

(a)- Horizontal line (see Fig. 3b)

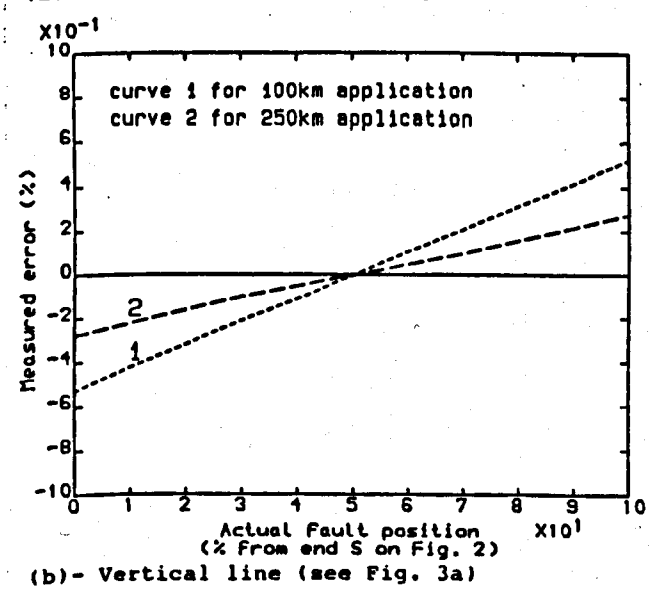

(b)- Vertical line (see Fig. 3a)

Fig. 4- Measuring accuracy for 'a'-earth fault on different line configurations.

Fig. 5 shows the response for double-phase-to-earth (a-b-e) faults involving a 100Ω fault resistance to earth in each faulted phase. The response for the horizontal line subjected to an a-b-e fault is closely similar to 'a'-earth fault shown in Fig. 4a. It can be seen that the error is always less than approximately 1.1% for all fault positions.

The results presented above are typical of those obtained. In all cases studied error was less than approximately 1.5% when the algorithm was assuming perfect line transposition for untransposed line.

CONCLUSION

A very accurate method of fault location for transmission lines has been presented. It has been shown that in spite of simplifying the algorithm by using transposed line parameters for untransposed system it gives a very high accuracy in locating faults irrespective of the fault type, line length and configuration. Moreover the accuracy is not affected by fault resistance and source impedances. The algorithm does not require fault-type identification which avoids possible problems due to incorrect fault-type determination.

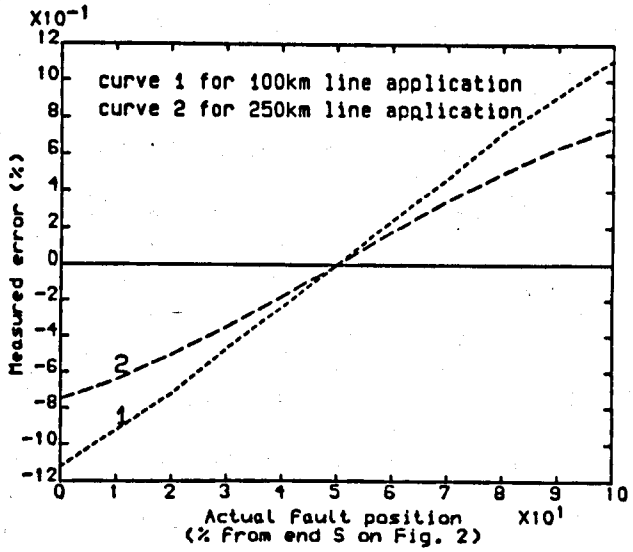

Fig. 5- Measuring accuracy for 'a'-'b'-earth fault on vertical line (see Fig. 3a).

REFERENCES

1. Erikson, L., Saha, M.M. and Rockfeller, G.D., 1985, "An accurate fault locator with compensation for apparent reactance in the fault resistance resulting from remote end infeed", IEEE Trans., PAS-104 pp 424-435.

2. Takagi, T., Yamakoshi, Y., Yamaura, M., Kondow, R. and Matsushima, T., 1982, "Development of a new type fault locator using the one-terminal voltage and current data". IEEE Trans., PAS-101, pp 2892-2898.

3. Schweitzer, E.O., III, 1983, "Evaluation and development of transmission line fault locating techniques which use sinusoidal steady-state information" Computers & Elec. Engng USA, 10, (4), pp 269-278.

4. Cook, V., 1986, "Fundamental aspects of fault location algorithms used in distance protection", Proc. IEE, 133, (6), pp 354-368.

5. Kondow, R., Sugiyama, Y. and Yamada, M., 1985, "Microprocessor-based fault locator", IEE conference publication 249,pp 188-192.

6. Wedepohl, L.M., 1963, "Application of matrix methods to the solution of travelling-wave phenomena in poly-phase systems", Proc. IEE, 110, (12), pp 2200-2212.

7. Johns, A.T. and Aggarwal, R.K., 1976, "Digital simulation of faulted ehv transmission lines with particular reference to very-high-speed protection", Proc. IEE, 123, (4), pp 353-359.